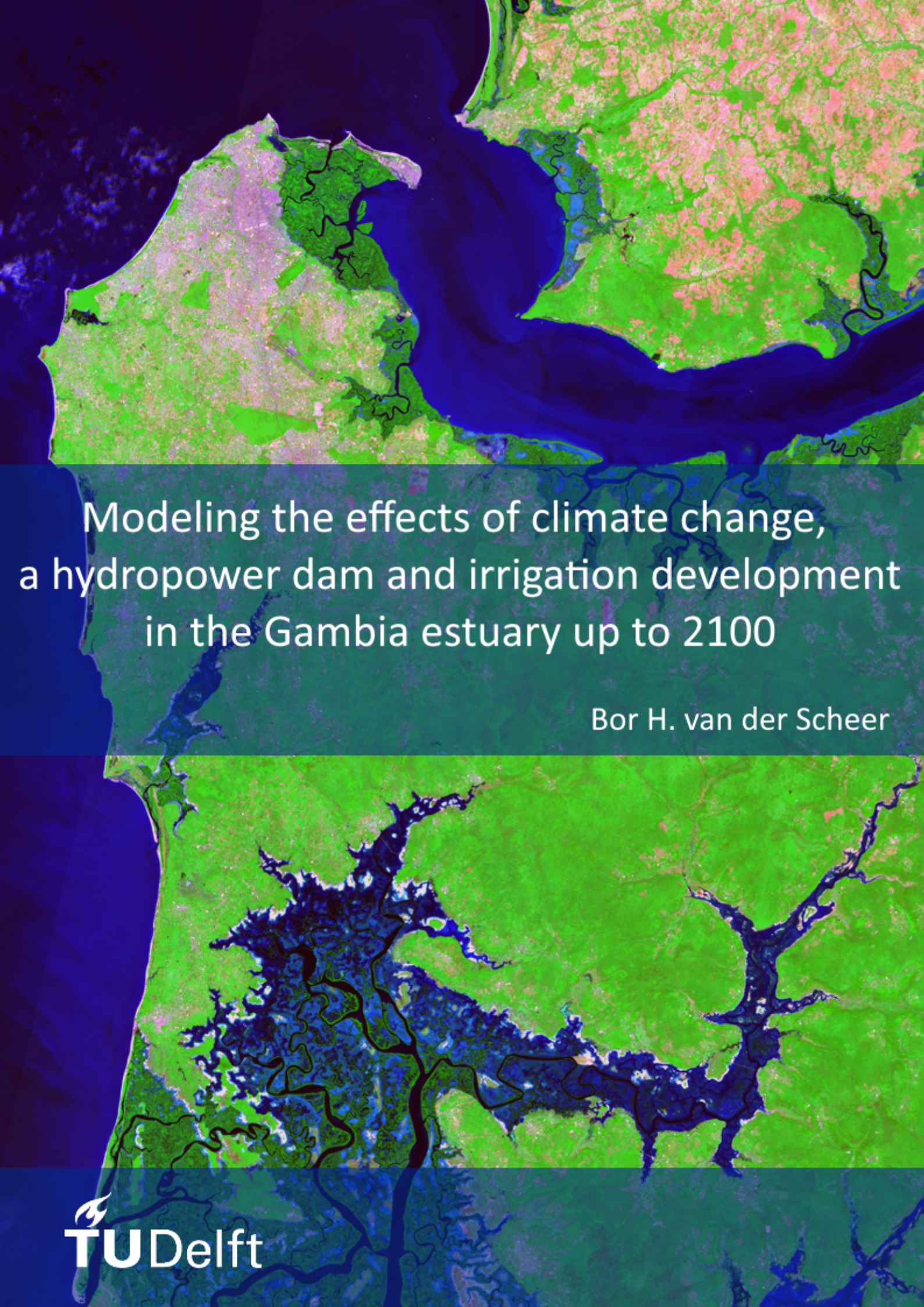

Modeling the effects of climate change, a hydropower dam and irrigation development in the Gambia estuary up to 2100

Bor H. van der Scheer

TU Delft

DETERMINING THE EFFECTS OF HYDROPOWER DAM PLACEMENT AND CLIMATE CHANGE ON SALT INTRUSION IN THE GAMBIA ESTUARY UP TO 2100

Master thesis submitted to Delft University of Technology in partial fulfilment of the requirements for the degree of

Master of Science
in **Civil Engineering**

by

Bor Hadrianus van der Scheer

February 2021

Chairperson & First Supervisor:	Dr. Ir. M.M. Rutten *Water Management*
Second Supervisor:	Ir. W. Luxemburg *Water Management*
Third Supervisor:	Prof. Z.B. Wang *Hydraulic Engineering*
External Supervisor:	B.M. Simpson *Food and Agricultural Organization*

TU Delft

PREFACE

Around December 2019, the study association for the studies Water Management and Environmental Engineering organized their yearly Christmas drinks. Normally a time of celebration, however it was my lucky day. I encountered a friend, Joost Verbart, who had been away for an internship. He had been enquiring possible thesis topics with several professors and told me about the possibility of this study. After applying I was well received since there were no other applicants. This resulted in me being guided by Huub Savenije, an expert in hydrology and in particular salt intrusion, as well as Brent Simpson, another expert from the Food and Agricultural Organization of the United Nations. The knowledge, expertise and experience that I had access to through them helped me excel in this research. I have learned so much more by working together with them, for which I am grateful.

Furthermore, this study could not have been performed without the data that I have received from the Department of Water Resources of The Gambia. I am happy knowing that The Gambia are prepared to share their data for such projects. I would like to thank Landing Bojang for supporting this study and for helping in making important contacts.

Finally, I would like to thank everyone who supported me. To my housemates, Matthijs, René, Sarah and Steven, who were always available for a discussion on programming or analytical issues. To Sarah and Jan who took the effort to proof-read my thesis and comment on it. To my assessment committee, Martine Rutten, Willem Luxemburg en Zheng Bing Wang who gave their feedback in such a way that I always felt motivated to keep on working. To all my friends for their trust in me and their moral support.

SUMMARY

Due to climate change, sea levels rise worldwide, temperatures increase which leads to higher evaporation and possible changes in precipitation patterns. These effects of climate change influence salt intrusion, particularly by affecting the freshwater supply. In The Gambia also a planned hydropower dam and possibly future irrigation development will affect the freshwater supply. The combined effects of climate change, the hydropower dam and irrigation development on salt intrusion are unknown. In the worst-case scenario the estuary could turn hypersaline, such as the Casamance, a river south of The Gambia, which turned hypersaline during the Sahelian drought and never restored. This led to the decay of the entire ecosystem.

The Gambia river is of major importance to the country, the agricultural sector relies on the freshwater it supplies for growing crops, the fishing industry relies on sufficient numbers of fish to catch and the forestry industry makes use of the mangroves growing around the river. All these industries combined account for ±75% of the working force of The Gambia. It can be safely assumed that if the rivers characteristics change severely due to climate change, the hydropower dam or irrigation development, this will have a strong impact on the country.

This thesis aims to clarify the effect that climate change, the hydropower dam and irrigation development have on salt intrusion in the Gambia river. The main research question to answer is:

What are the effects of climate change, a hydropower dam and irrigation development on salt intrusion in the Gambia estuary up to 2100?

To understand the effects of climate change, the hydropower dam and irrigation development, the main research objective is split up into several research questions. Salt intrusion will be analyzed based on the salt intrusion length and salt concentration profiles. Furthermore, the occurrence of hypersalinity and its severity will be analyzed. The remaining questions focus on how undesirable salt intrusion levels can be mitigated and how the aqua- and agricultural sector in The Gambia might be affected.

1. *How does the salt intrusion length develop considering climate change, the hydropower dam and irrigation development in the Gambia estuary?*
2. *How does the salt concentration develop considering climate change, the hydropower dam and irrigation development in the Gambia estuary?*
3. *To what extent can hypersalinity occur and under which circumstances?*
4. *What measures can be taken to mitigate unwanted salt intrusion and how effective are these measures?*

5. *How will aqua- and agriculture in The Gambia be affected by the construction of the hydropower dam?*

A 1D model, SALNST, is used to model salt concentrations over the river length up to the year 2100. To distinguish the effects of climate change, the hydropower dam and irrigation development the following parameters are implemented: sea level rise, climate projections (precipitation and evaporation), hydropower dam operations and irrigation development. Each of these model parameters has multiple values that represent mild and strong changes for the respective parameter. This results in a set of 27 scenarios revealing the individual impact of each parameter.

Analysis of model results reveals a strong impact of climate change related parameters. Projected climate strongly affects the freshwater flow. Sufficiently long alterations in evaporation lead to shifts in salt intrusion lengths and concentrations. The generated projected climate imposes its behavior into the salt intrusion patterns, this shows the sensitivity of the estuary to the projected climate. Sea level rise has a more moderate influence, with increasing sea level it dampens maximum salt intrusion lengths but concurrently causes an inland shift of the minimum salt intrusion lengths. In extreme scenarios where climate change causes severe sea level rise, the river is forced outside of its banks. When this happens, a large evaporative surface arises, in combination with high evaporation this causes the freshwater in the river to evaporate faster which leads to a strongly hypersaline estuary before the end of the century. The hydropower dam has a strong impact as well, although its influence is more regulative. By changing the dam's operations, for example by increasing the amount of flow through the hydropower dam, undesirable salt intrusion can be mitigated. This effect is particularly strong in reducing the maximum salt intrusion lengths and reducing the hyper saline region. Furthermore, independent of how the dam is operated, salt intrusion stabilizes due to a steadier supply of water during the dry season. A reduced flow during the wet season however, results in a land inward shift of the minimum salt intrusion lengths. Contrary to the previous mentioned parameters, the influence of irrigation development on salt intrusion is negligible. It affects freshwater flow too little to have a significant impact. This is due to the relatively small potential irrigation surface.

Salt concentrations are affected similarly, with increasing salt intrusion lengths also increases in the salt concentrations over the estuary can be detected. Measures that reduce salt intrusion lengths also reduce the maximum salt concentrations.

It can be concluded that The Gambia is prone to climate change when considering salt intrusion. Due to the importance of the river, monitoring sea level rise and the development of climate change will be essential for planning and taking counter measures. Understanding the effects that climate change can have regarding salt intrusion can also be used in negotiations to reserve some freedom in the hydropower dam operations. In addition, solutions that limit the increase in evaporative surface for strong sea level rise

(e.g., dikes along a part of the Gambia river) prevent extreme salt intrusion lengths and hypersalinity. The hydropower dam causes a reduced range of salt intrusion lengths, this creates easier to predict salt concentrations which is beneficial for aquaculture. Furthermore, the reduced maximum salt intrusion is also beneficial for irrigation.

CONTENTS

LIST OF FIGURES

LIST OF TABLES

NOMENCLATURE

Constants

s_0	Ocean salinity	M/L^3
g	Gravitational Constant	L/t^2

Variables

A or $A(x)$	Cross-sectional area of the river	L^2
A_add	Additional cross-sectional area due to sea level rise	L^2
A_0	Cross-sectional area at the mouth of the river	L^2
a	Cross-sectional area convergence length	L
B or $B(x)$	Width of the river	L
B_add	Additional width due to sea level rise	L
B_0	Width at the mouth of the river	L
b	Width convergence length	L
B_c	Conveyance width	L
B_s	Storage width	L
C_{ns}	Non steady-state weight	L
D or $D(x)$	Dispersion	L^2/t
D_s or $D_s(x)$	Steady-state dispersion	L^2/t
D_{ns} or $D_{ns}(x)$	Non steady-state dispersion	L^2/t
D_0	Dispersion at the mouth of the river	L^2/t
E	Evaporation	L/t
E_{pot}	Potential evaporation	L/t
E_0	Tidal excursion at the mouth of the river	L
F_d	Dispersion calibration parameter	$-$
F_E	Evaporation calibration parameter	$-$
h	Depth of the river	L
$\bar{h}$	Average depth along the width	L
h_0	Depth at the mouth of the river	L

I	Heat index	T
K	Van der Burgh's parameter	–
L	Average daylight hours per month	t
N	Number of days in the month	–
N_R	Estuarine Richardson number	–
P	Precipitation	L/t
P_n	Net precipitation	L/t
P_t	Tidal prism	L^3
ρ_f	Freshwater density	M/L^3
ρ_s	Salt water density	M/L^3
Q_f or $Q_f(x)$	River discharge	L^3/t
r_S	Cross-sectional storage coefficient	–
s or $s(x)$	Salinity	M/L^3
s_r	River salinity far upstream, uninfluenced by salt intrusion	M/L^3
T	Tidal period	t
Ta	Mean daily air temperature	T
Tai	Mean air temperature for each month in the year	T
v_0	Tidal flow velocity amplitude	L/t
x	Distance from the river mouth	L

1 INTRODUCTION

This chapter introduces the motive behind this study. This is followed up by the presentation of the main research question and several sub questions. Finally, a short, structured overview of this thesis is presented.

1.1 MOTIVE

Climate change
Due to climate change, temperatures and sea levels are rising around the globe (Pörtner et al., 2019). Furthermore, the probability of droughts in the semi-arid region of West Africa increases (Sarr, 2012). For coastal countries with low elevation that have built their economy largely around a prominent river, such as The Gambia, it is essential to understand the potential impact of climate change on their river.

In stable climate conditions, an estuary that is governed by tide and a pronounced dry and wet season, has salt concentrations that vary over the tide and seasons. However, climate change can lead to strong alterations of this process. The river Casamance south of The Gambia turned hypersaline due to droughts in the early 80s (Savenije & Pagès, 1992). Possible increases of salt concentrations in the Gambia river could cause problems for aquaculture which relies on a predictable range of salt concentrations. Increased variations in salt concentrations can result in impaired growing circumstances for aquaculture (Cañedo-Argüelles et al., 2013).

Farmers with plots close to the river make use of tidal irrigation, when the water is forced up by the tide, they open small gates to let water flow onto their plots. After their plots have soaked up the required water for their crops, they open the gates again to let the excess water flow back to the river. An increase in salt intrusion length[1] could therefore cause problems for agriculture when freshwater turns saline. Pump irrigation, which makes use of water upstream of the salt front, can be affected as well if salt intrusion lengths increase significantly.

Hydropower dam & irrigation development
As a solution to power shortages in The Gambia and surrounding countries, a hydropower dam upstream of the Gambia river is being considered as part

1 Salt water intrusion is the movement of saline water into freshwater. Salt intrusion length is the length that salt water of a certain concentration has intruded, seen from the river mouth. This thesis uses a salt concentration of 1 g/L, which has previously been used in the application of this model (Savenije, 2012).

of a sub-regional power sharing program (ECOWAPP, 2012). A dam creates a distinctly different flow pattern from the natural situation by retaining a large volume of water during the wet season and releasing more water in the dry season. In combination with climate change these alterations in flow pose a possible threat to aqua- and agriculture. Furthermore, the area under pump irrigation is expected to increase (FAO, 2007; NRDS, 2014). This further impacts the freshwater supply.

In addition, there is a chance of the estuary turning strongly hypersaline, like the Casamance, resulting in the collapse of the ecosystem (Savenije & Pagès, 1992). This would have a massive impact on the residents and economy of The Gambia, as can be read in Chapter 2. Climate change and the hydropower dam are expected to have a significant influence on the salt distribution in the river. Climate change alters hydrological parameters with increasing sea level and higher evaporation, while the dam alters the flow regime by attenuating the otherwise clear dry- and wet season. To what extent these changes influences the salt intrusion and concentration, and if hypersalinity[2] can occur is unknown. An additional factor that complicates the situation, is that the hydropower dam is not owned and managed by The Gambia. It is therefore crucial to understand what impact the dam will have on the salt intrusion levels in the Gambia river.

1.2 RESEARCH OBJECTIVE

The aim of this study is to clarify what effect climate change and the hydropower dam have on salt intrusion in the Gambia estuary. This will be done by modelling salt intrusion in the Gambia river with four parameters that represent climate change, the hydropower dam and agricultural development. In addition, one of these parameters takes the possible future growth of agricultural surface under pump irrigation into account. For a full overview of methods and materials used see Chapter 4.

1.3 SOCIETAL CONTRIBUTION

This research was under contract with the Food and Agricultural Organization (FAO) of the United Nations (UN) to assist the government of The Gambia in preparing a proposal to the Green Climate Fund. The FAO aims to "lead international efforts to defeat hunger" (FAO, 2020). It is a specialized agency that focuses on reducing hunger around the globe by improving aqua- and agriculture. The research objective of this study is to increase insight in the effect of climate change and a hydropower dam on salt intrusion in the Gambia estuary. This, in turn, contributes to assisting to the FAO's goals and the Sustainable Development Goals (SDGs) of the UN. Specifically, the 13th SGD focuses on taking "urgent action to combat climate

2 According to the Oxford dictionary a hypersaline environment is 'an aquatic environment that is saltier than typical seawater'.

change and its impacts" (UN, n.d.). In addition, the outcome will show The Gambia what possible future scenarios regarding salt intrusion levels they should consider, and to enhance their position in the negotiations regarding the operation freedom of the hydropower dam. Many countries will profit from the produced power (see Chapter 2) however, The Gambia is one of the few which might suffer from negative consequences due to the dam. This research can therefore be used to inform decision makers in The Gambia of the potential harm they might encounter, and to support their position in the negotiations on dam operations.

Furthermore, estuaries worldwide are noticing the effects of climate change on salt intrusion. Salt fronts shift towards deeper inland due to reduced freshwater flow and coastal erosion increases in most cases (Carney et al., 2014; El-Nahry & Doluschitz, 2010; Robins et al., 2016; Vargas et al., 2017). These studies also show that some estuaries are more prone to climate change than others, these estuaries show a stronger response to sea level rise and increasing temperatures. Furthermore, the effects of salt intrusion affecting agriculture negatively are emphasized (Vargas et al., 2017).

1.4 ACADEMIC KNOWLEDGE GAP

In addition to the societal contribution, this research aims to contribute to an existing academic knowledge gap. The applied model, SALNST, will be extended with features to incorporate the effects of sea level rise. Furthermore, an improvement in calculating dispersion will improve the model results. This will be explained more detailed in Chapter 3.

1.5 RESEARCH QUESTIONS

This thesis offers insight into the development of salt concentrations and salt intrusion lengths due to climate change, the hydropower dam and irrigation by answering the research questions below. This is achieved by modeling salt concentrations in the Gambia river until 2100 with a 'non-steady' model, SALNST, which will be explained in detail in Chapter 3. Analyzing the model results gives direct information on salt intrusion lengths and concentrations. Furthermore, the effectiveness of solutions that mitigate salt intrusion can be derived from these results. In total 27 model runs offer insight into the influence of projected climate and sea level rise. In addition, two distinctly different dam operations and three possible developments in agricultural irrigated surface are modeled to show the influence of the hydropower dam and irrigation development. This results in a comparison of the influence of projected climate, sea level rise, dam operations, and irrigation development, predicting their influence on salt concentrations and salt intrusion lengths in the estuary. The results will then be used as a basis for recommendations regarding this complex situation.

1.5.1 Research questions

1. *How does the salt intrusion length develop considering climate change, the hydropower dam and irrigation development in the Gambia estuary?*
2. *How does the salt concentration develop considering climate change, the hydropower dam and irrigation development in the Gambia estuary?*
3. *To what extent can hypersalinity occur and under which circumstances?*
4. *What measures can be taken to mitigate unwanted salt intrusion and how effective are these measures?*
5. *How will aqua- and agriculture in The Gambia be affected by the construction of the hydropower dam?*

1.6 THESIS STRUCTURE

The thesis is organized as follows. Chapter 2 offers a detailed background description of The Gambia, introducing demographics, elevation and social constructs required to understand the sensitivity of The Gambia to climate change and the plans regarding the hydropower dam. Chapter 3 continues with the technical explanation of salt intrusion. A comparison of several models leads to the choice of the model used in this study after which the physics of this model are introduced. Chapter 4 repeats the research questions that have been introduced above. It covers the acquired data and methodology used in this research required to answer the subsequent questions. The chapter finishes by presenting an overview of the scenarios. Chapter 5 entails the results and discusses these for each modeled parameter, followed by a technical summary containing an overview of all parameters. The chapter finishes with an expert interview on morphological changes due to climate change and the hydropower dam. Chapter 6 discusses the limitations of this study after which the conclusion is presented in Chapter 7. The thesis finishes with several recommendations in Chapter 8 regarding future research based on the results of this study as well as regarding certain measures The Gambia should consider.

2 DEMOGRAPHICS AND BACKGROUND INFORMATION OF THE GAMBIA

The Gambia is a small country in west Africa where the Gambia river flows into the Atlantic Ocean. The population of around 2.2 million inhabitants works mainly (± 75% of their labor force) in the agricultural sector, which includes farming, fishing and forestry. Even though the agricultural sector employs such a large percentage of inhabitants, the sector only contributes for 20.4% to the GDP of The Gambia (CIA, 2020). Nonetheless, The Gambia makes effort to attract investors in the agricultural sector (see section 4.2.3). Several predictions about possible increases in irrigated area for the Gambia and Senegal have been made (e.g.(FAO, 2007; NRDS, 2014). These predictions range from no increase in irrigated area to a theoretical scenario in which all irrigatable area is used, increasing the current irrigation by 578%.

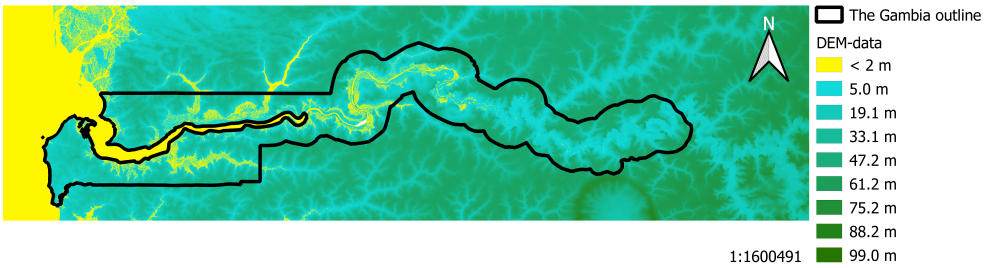

Figure 2.1: Digital elevation map of The Gambia, showing elevation with respect to sea level (source: https://www.diva-gis.org/gdata).

The Gambia is a flat country with a mean elevation of 34 m above sea level. Along the coast and the borders of the Gambia river this is significantly less (see Figure 2.1). Therefore, The Gambia is prone to sea level rise (Amuzu et al., 2018). Due to climate change temperatures are rising worldwide. Several global circulation models (GCMs) give amongst others temperature predictions based on the expected amount of greenhouse gasses in the air (representative concentration pathways or RCPs). One of these GCMs, MIROC, gives the most accurate predictions for The Gambia based on a comparison with historical measurements (see GCM in section 4.2.1 or Appendix A for a detailed description of this process). The predicted increase in temperature leads to higher evaporation. Secondly, also precipitation is predicted by the GCM. Whereas some GCMs predict that the probability of more extreme events increases, this probability does not differ significantly for The Gambia and Senegal, according to the MIROC GCM. Besides the local effects on temperature, evaporation and precipitation, climate change induces sea level rise as well. To what extent the sea level will rise by the end of the century is unclear. Depending on the amount of greenhouse gasses emitted into the atmosphere the Intergovernmental Panel on Climate Change (IPCC)

predicts several ranges of sea level rise. They predict a global mean sea level rise between 0.43 m (0.29-0.59 m) for RCP 2.6 to 0.84 m (0.61-1.10 m) for RCP 8.5 at the end of the century (Pörtner et al., 2019). However, other scientists, such as Spring (2017) and Bamber et al. (2019), anticipate a much larger sea level rise of 2 meters by the end of the century under RCP 8.5.

The Gambia is a member state of the Economic Community of West African states (ECOWAS) and therefore also member of the West African Power Pool (WAPP), which consists of 14 countries (see Figure 2.2b). The goal of ECOWAS is to accelerate the West African economy. They achieve so by promoting economic cooperation as well as regional integration (ECOWAS, 2020). WAPP has a similar goal, to integrate the national power systems of the member states into a unified regional electricity market. Currently the member states of WAPP import power, often in the form of fossil fuels. Ultimately, they want to be able to reliably generate and provide power at competitive cost for this region, decreasing the dependency on imported power. To achieve the goal of the WAPP several projects in the member states of the WAPP are planned. Among all projects a hydropower dam will be built in the Gambia river near the border between Senegal and Guinea (ECOWAPP, 2012). The hydropower dam will create a large reservoir that is mainly located in Guinea. An environmental study commissioned by the Organisation de développement du bassin du fleuve Gambie (OMVG) in 2014 resulted in amongst others preliminary flow requirements to sustain the environment and ecology in the downstream river (OMVG & EIES, 2014). Table 2.1 presents the most important characteristics of the reservoir and dam from this study.

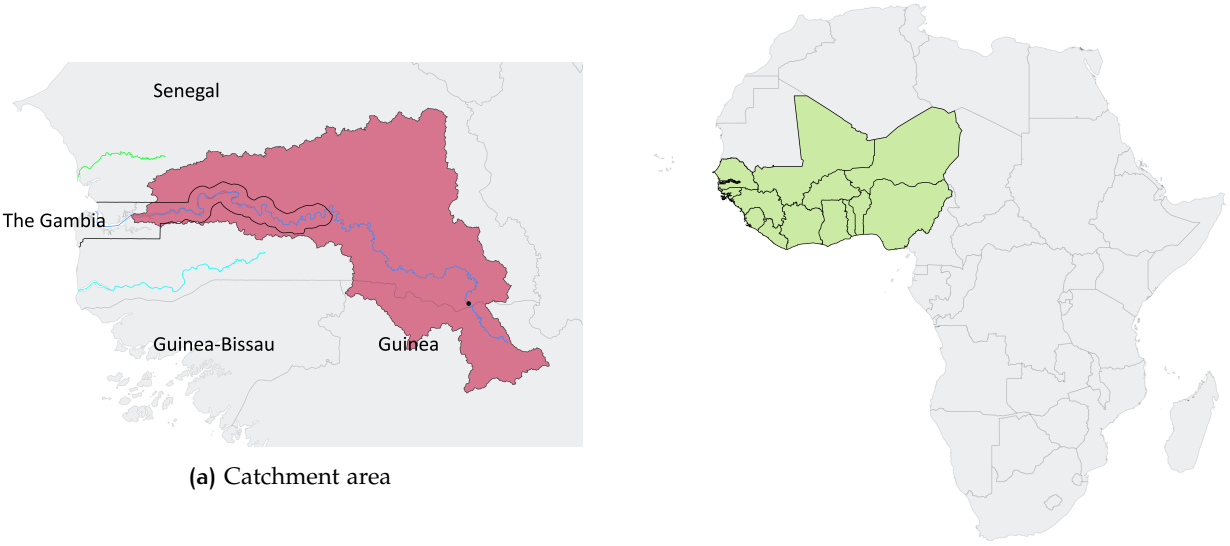

(a) Catchment area

(b) Member states involved with the hydropower dam

Figure 2.2: The Gambia: catchment area and member states of WAPP

Characteristics	Minimum	Maximum
Water level inside reservoir	118 m	200 m
Surface area reservoir	110 km^2	181 km^2
Volume reservoir	2.1 billion m^3	3.8 billion m^3
Useful capacity	-	1.7 billion m^3
Turbine discharge	0 m^3/s	200 m^3/s
Turbine height	75 m	-

Table 2.1: Dam and reservoir characteristics

Figure 2.2a shows the catchment area of the Gambia river, as well as the approximate location of the dam (black dot). This area, bordering the south edge of the Sahara, has a very pronounced dry- and wet season (see Figure 2.3).

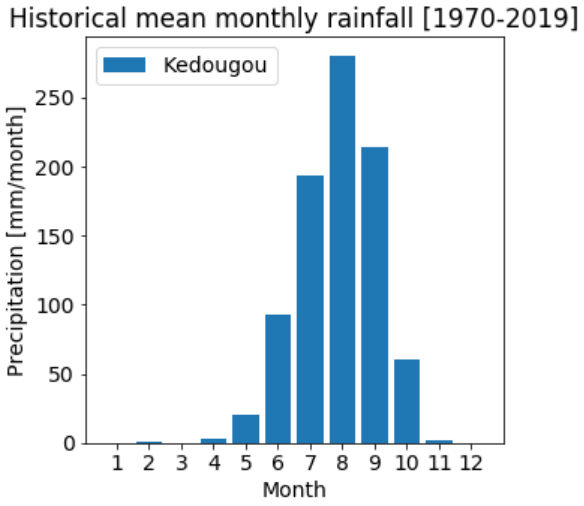

Figure 2.3: Historical mean monthly rainfall in Kedougou, data from personal communication with H.H.G. Savenije and The Gambia Department of Water Resources.

One of the fears is that the estuary of The Gambia turns hypersaline, with salt concentrations far exceeding the ocean salinity. The river south of the Gambia river, the Casamance (see Figure 2.2a), turned hypersaline after the Sahelian drought in the late 1970s and early 1980s (Savenije, 2005). A hypersaline river is of an uninhabitable nature and for The Gambia this would mean that the current ecology would be destroyed. Agri- and aquaculture which depend on sufficient freshwater and salt concentration around or below ocean salinities will not be feasible in strongly hypersaline areas. Since the majority of the population of The Gambia works in this sector this is a large exposure.

3 THEORY ON SALT INTRUSION

To understand how this study deals with salt intrusion in the Gambia river the necessary theory is presented in this chapter. First, several modeling strategies will be discussed to give a balanced overview of methods to calculate salt intrusion, after which the choice for the model used in this study is substantiated. Secondly, the chosen model will be explained, going deeper into the theory of salt intrusion. Starting with the use of geography and followed by the formulas for determining steady state and unsteady state dispersion and salinity the theory and model are explained. The chapter will finish with an explanation of several types of salt intrusion and hypersalinity and its effects.

Before continuing with modeling strategies, it is important to realize that the different models which are discussed below use different solving techniques based on different physics. The details of the physics and solving strategy will be discussed from the second paragraph onward, which contain only the physics of the selected model. These paragraphs will follow the reasoning of Savenije (2012).

3.1 MODELING STRATEGIES

There are several ways of modeling salt intrusion in estuaries. Depending on the estuary, river and tidal characteristics, as well as the available resources and time the approach can differ. There are three different dimensions in which salt intrusion can be modelled. 1D takes only the longitudinal salt distribution into account, 2D adds the vertical salt distribution and 3D also accounts for lateral differences in salinities. The several types of models and modeling strategies will be discussed from a perspective of salt intrusion.

3.1.1 1D models

A predictive model requires numerous input parameters therefore in data-scarce regions, or when time and resources are limited, a 1D analytical model is appropriate to use (Gisen, Savenije & Nijzink, 2015). If an estuary is well-mixed there are little differences in salt concentration in vertical or lateral direction. Therefore, applying a 1D model on well-mixed estuaries is sufficient (Savenije, 2005).

Initial predictive models were based on laboratory experiments and prototype measurements. However, when applying these in practice results were inaccurate due to wrong geometrical assumptions (Cai et al., 2015). In the footsteps of these models, geometrical variations were introduced. Convergent shapes for alluvial estuaries based on the ideal estuary theory from Pillsbury were described by exponentially decreasing width and cross-sectional area (Pillsbury, 1956; Savenije, 1986). These relations were later confirmed to be the most accurate by Parsa and Etemad-Shahidi (2011). Shaha and Cho (2009) compared models based on geometrical measurements with models that used exponentially decreasing relations and concluded the latter performed better. Recently, Zhang (2019) adjusted these relations slightly for estuaries which converge to a large (wide) river.

Data on freshwater discharge, especially in data-scarce regions can be difficult to obtain (Savenije, 2012). To solve this problem Cai et al. (2014) created an analytical model to determine freshwater discharge based on tidal characteristics. Gisen, Savenije and Nijzink (2015) adopted this into the 1D analytical model created by Savenije (1986) improving predictive equations making use of an expanded database. Zhang (2019) provided a theoretical basis for the empirical Van der Burgh coefficient which is applied in the model. The equations used in Savenije's model are based on the 1D steady state salt balance equation. This approach has been used by others albeit with different assumptions elsewhere, mostly regarding dispersion and geography (Aris, 2012; Gay & O'Donnell, 2007; Lewis & Uncles, 2003).

3.1.2 2D & 3D models

When an estuary is not well-mixed but more stratified, a vertical difference in salt concentration can be distinguished. In this situation a 1D model gives a wrong impression of the salt distribution and a 2D model should be used. Similarly, a situation can occur where there are lateral differences in salt concentration, usually in wide waterbodies (e.g. pronounced ebb and flood channels contain different densities of water). If vertical and lateral conditions are combined a 3D model needs to be applied. In practice a single 2- or 3D model can be used for many parameters (e.g. water quality, hydraulics) and the choice of a certain model does not always depend on the salinity characteristics of an estuary. These models are also more complicated than a 1D model and programs have been written which can be adjusted to the required parameters.

2D hydrodynamic models (e.g. ADCIRC, CE-QUAL-W2, RBFVM, TELEMAC-2D, TISAT, WET2D) are widely spread and used. Models like ADCIRC are originally 3D models that can be used in 2D environments. There are little differences between the solving strategies of these models, which make use of either the finite difference method or finite element method (Haddout et al., 2019). The finite difference method has computational superiority while the finite element method has more geographical flexibility. More recently the finite volume method, which incorporates both solving strategies has in-

creased performance in accuracy and lower computational power (C. Chen et al., 2007). Since 2D models assume lateral heterogeneity the model performance is best for narrow waterbodies.

3D hydrodynamic models (e.g. ADCIRC, Delft3D, FVCOM, ICM, SELFE-3D) can account for differences in all directions. These models differ in multiple ways, most often in their computing algorithms. ICM makes use of coarse grid cells while Delft3D has very small ones, this makes ICM a computational efficient model compared to Delft3D while Delft3D has superiority in details (White et al., 2018). SELFE-3D still uses finite element methods for vertical calculations while FVCOM fully incorporated the finite volume method (C. Chen et al., 2007; W. B. Chen et al., 2015; Kuang et al., 2012). Even though large differences can be distinguished in terms of calculation methods and geographical input, most of the 3D hydrodynamic models are based on the Navier Stokes equations (Symonds et al., 2016).

3.1.3 Model choice

The Gambia estuary is a well-mixed estuary which is relatively long compared to its width (see Section 3.3). This allows the use of a 1D model (Savenije, 2005). Secondly, there is little data available and there are no resources available to fill in the gaps that are required for a higher order dimension model. Thirdly, time is of the essence. The hydropower dam will be built and this study is not going to influence this. However, it will offer insight for the government of The Gambia which can then be used in negotiations regarding the dam operations. This reasoning leads to the choice for the 1D SALNST model. This model has been applied, used, improved and proven itself over the years for many estuaries (Gisen, Savenije & Nijzink, 2015; Gisen, Savenije, Nijzink & Abd. Wahab, 2015; Zhang, 2019).

3.2 THE 1D SALNST MODEL

The SALNST model calculates the salt concentration over distance for every timestep. It starts at the river mouth and calculates, for a single timestep, salt concentrations while moving upstream. The solving strategy can be reviewed in Appendix B. The most basic required information to calculate salt concentrations will be mentioned in this section. Starting with the use of geographical relations, followed by advection and dispersion, and ending with salt intrusion.

3.2.1 Geography of the Gambia estuary

The Gambia estuary is a coastal-plain estuary. The bed consists of small sediment that based on the sediment supply and flow can erode or build up. Since an estuary is the transition between river and ocean hydraulics of both play a role. Waves and tides from the ocean transport sediment up and

downstream while the river supplies the estuary with fresh sediment.

The clear shape in The Gambia estuary can be described by the 'ideal estuary theory' of Pillsbury (1956). He relates the often-clear funnel shape in coastal-plain estuaries to the dampening of tidal forces while waves travel upstream. The width and area reduce in such a way, increasing the wave amplitude, that they match the amount of friction that decreases wave amplitude. This results in a constant wave amplitude. In cases where this theory cannot be applied the estuary is often shaped differently, either by bound by geography (e.g. rivers in rocky layers) or by man-made structures such as the Dutch river system.

The funnel shape according to the ideal estuary theory has a clear geometry. It starts wide and converges while following the river upstream. This can be described mathematically (Davies & Woodroffe, 2010; Savenije, 1986) by:

$$B(x) = B_0 \cdot e^{-\frac{x}{b}} \tag{3.1}$$

Where Bo is the width at the mouth, x the distance from the mouth and b the width convergence length. Similarly, the cross-sectional area can be described:

$$A(x) = A_0 \cdot e^{-\frac{x}{a}} \tag{3.2}$$

Where Ao is the cross-sectional area at the mouth and a is the area convergence length. These parameters are dependent on the dominant hydraulics at the location x in the estuary. The hydraulics at the mouth of the river are often dominated by the ocean, although there are cases of steep rivers and rivers with large flows that are dominated by river hydraulics. In the case of ocean dominated hydraulics, a deflection point exists after a distance x1. The distance x1 is the distance in which the energy of ocean waves has been dissipated and riverine hydraulics determine new parameters for the cross-sectional area and width. These describe the further course of the estuary. Therefore, formulas for the width and cross-sectional area become respectively:

$$B(x) = \begin{cases} B_0 \cdot e^{-\frac{x}{b_1}} & x \leq x_1 \\ B_1 \cdot e^{-\frac{x-x_1}{b_2}} & x > x_1 \end{cases} \tag{3.3}$$

$$A(x) = \begin{cases} A_0 \cdot e^{-\frac{x}{a_1}} & x \leq x_1 \\ A_1 \cdot e^{-\frac{x-x_1}{a_2}} & x > x_1 \end{cases} \tag{3.4}$$

If further upstream the riverine hydraulics change significantly again, more deflection points can be determined. Zhilin Zhang [2019] improved these relations for width and cross-sectional area for more riverine estuaries (e.g. the Limpopo Estuary), by letting the area and width converge towards the cross-sectional area and width of the river far upstream. These improved relations have not been used in this study since The Gambia estuary is tidally dominated.

If one assumes the depth to be relatively constant over the width the depth can be determined with the formulas above, resulting in:

$$h(x) = \frac{A(x)}{B(x)} = \frac{A_0}{B_0} \cdot e^{\frac{x(b-a)}{ab}} \tag{3.5}$$

This shows that if the area convergence length is larger than the width convergence length the depth increases and vice versa. However, it has been found by Savenije (1992) that these convergence lengths are often close to each other. In the case of the Gambia estuary they are the same. This results in a more or less constant depth over the estuary.

Figure 3.1 below, shows the shape of the Gambia estuary with two inflections points. A survey in 1971 supervised by H.H.G. Savenije measured the cross-sectional area, the width, the depth and took salinity measures which will be presented later. Since the salt front might move further upstream, the relations for the cross-sectional area and width have been extended to a river lenght of 650 km, making use of aerial imagery. The ratio between the cross-sectional area and width is kept equal.

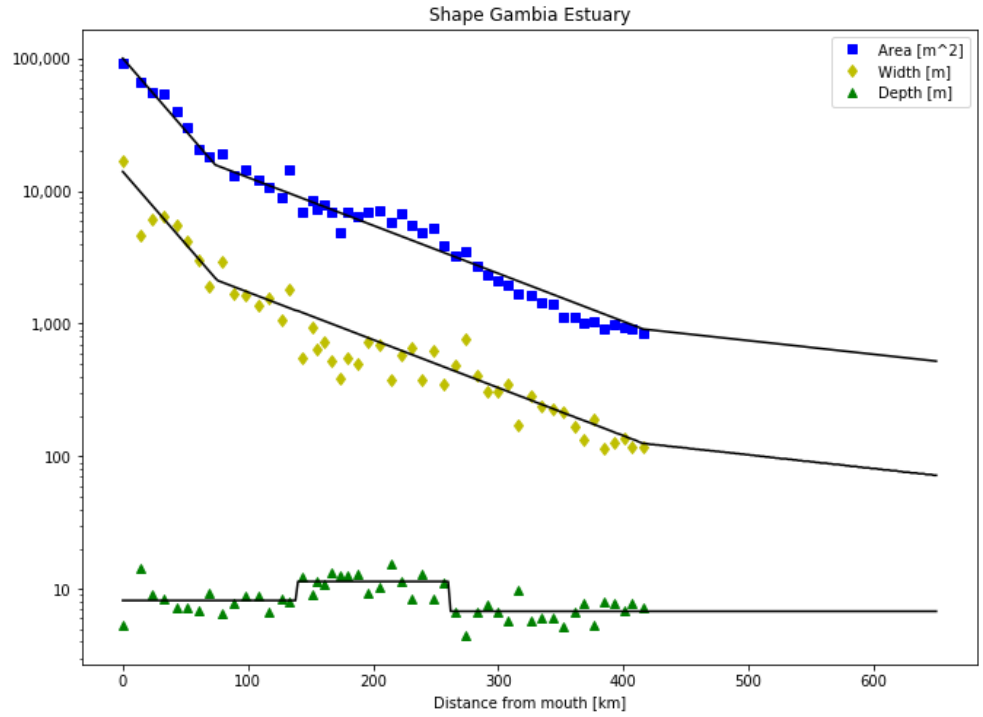

Figure 3.1: Geometrical results from the survey in 1971, the inflection points are clearly visible in the cross-sectional area and width. Furthermore, it can be seen that the depth is more or less constant throughout the estuary. The black lines through the cross-sectional area and width are the relations of Equation 3.3 and Equation 3.4. The black line through the depth follows the measurements more closely but stays nonetheless more or less constant.

Additional geographical changes

The Gambia is a flat country, especially alongside the river. A stroke on both sides of the river of multiple kilometers is close to sea level (see Figure 2.1). This continues up to the border of Senegal where the river banks as well as the surrounding area slowly elevate. Farmers make smart use of these low elevations next to the river. When high tide pushes up freshwater to the level of their fields, they open small gates which allows freshwater to wet their fields. At low tide they open the gates once more to let the excess water escape.

Since the amount of sea level rise this century is unknown a worst-case scenario should be taken into account. Therefore, two stages in the Gambia river can be distinguished. Below a certain threshold value, the river only increases in depth with increasing sea level. Above this threshold value the river also increases in width (Equation 3.6, Equation 3.7). A study of Ettritch et al. (2018) focused on the widening (flooding) due to sea level rise and compared two digital elevation models. This study took place on the Gambia river albeit on a relatively short section. Nonetheless their results have been used to create relations for the additional width and cross-sectional area. Where h_{SLR} is the sea level rise in meters, $h_{threshold}$ the threshold value for sea level rise and c_1 and c_2 constants deducted from the study of Ettritch et al. (2018). These relations have been visualized in Figure 3.2. It can be seen that a small increase in water level above the threshold value accounts for a significant increase in width. This results in a strong increase in surface area once the threshold value is exceeded.

$$B_{add} = \ln\left(\frac{SLR}{c_1}\right) \cdot \frac{1}{c_2} \tag{3.6}$$

$$A_{add} = \frac{h_S LR}{c_2} \cdot \left(\ln\left(\frac{h_S LR}{c_1}\right) - 1\right) - \frac{h_{threshold}}{c_2} \cdot \left(\ln\left(\frac{h_{threshold}}{c_1}\right) - 1\right) \tag{3.7}$$

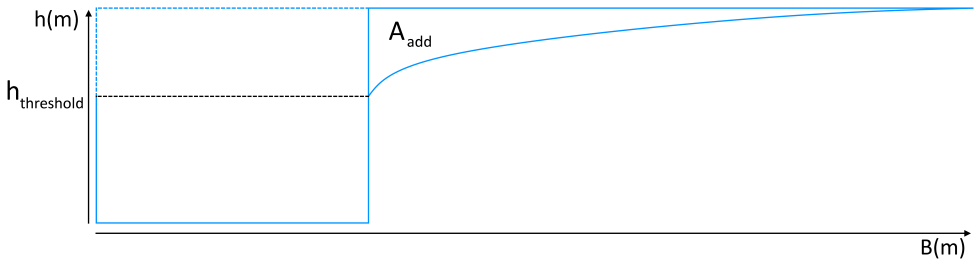

Figure 3.2: Effect of sea level rise. The black dotted line indicates the threshold height. If the water level at a point in the river surpasses this height, the river overflows and an additional cross-sectional area (A_{add}) and width (B_{add}) are added to the river's geometry.

Another change that should not be overlooked is the possible increase in irrigated surface. Agriculture is an important sector in The Gambia and effort is being made to increase the work done in this sector. Studies in The Gambia as well as Senegal determined several scenarios on the possible

development in irrigated surface. Since crops do not like saline water the water extraction is upstream of the saline front. Therefore, an increase in irrigated surface decreases the amount of freshwater discharge in the river. This could potentially have a significant influence on the salt intrusion length and concentration.

3.2.2 Advection and dispersion

Note: Salt concentrations are calculated by solving the salt balance equation. This equation consists of the longitudinal transport of salt along the river which incorporates advection and dispersion. The formulas presented in this section represent the steady- and unsteady-state dispersion, the salt balance equation will be presented in Section 3.2.3.

Salt distribution along the river can be described by two processes: advection and dispersion. Advection, where salt is transported by river flow, is the most effective at distributing salt. This process is predominantly noticeable during the wet season, when large volumes of water flush the salt from upstream towards the mouth of the river. However, also during the dry season advection has a significant role. Due to the high evaporation and limited freshwater availability, there is a point along the river where all freshwater has been evaporated. Further evaporation of water results in seawater being sucked inlands thereby having the opposite effect as the advection during the wet season, where salt is flushed to sea.

Dispersion can be seen as a combination of diffusion and mixing. Diffusion is the process where areas of high salinity diffuse into areas of low salinity. Mixing contains several processes where water fluxes actively bring volumes of higher salinity in contact with areas of lower salinity which are then mixed. The process of dispersion is only dominant during the dry season, when there is little flow. Several types of mixing can be distinguished, here the main processes are described and visualized below.

The three main mixing types are gravitational mixing, trapping and tidal pumping and are visualized in Figure 3.3. Gravitational mixing occurs due to saline water having a higher density than freshwater. To balance water pressures the water level at the freshwater side is slightly higher than at the saline side. The pressures are equal but work on different elevations, therefore creating a flux in which salt water is transported on the bottom of the river in upstream direction while freshwater is transported on top of the river in downstream direction.

Trapping consists of areas that flood when there is high tide. When the tide reverses and water flows back to these small areas a small phase lag compared to the tide in the river is introduced. Therefore, the water that flows back has a different salinity and density than the river water it flows into.

Tidal pumping causes mixing due to the distinctly different inflow and outflow of water out of the estuary. During high tide, when ocean water flows into the estuary, the water comes from all directions (as presented by the red arrows in Figure 3.3). However, during low tide, when the water flows from the estuary to the ocean, a different flow pattern can be distinguished (as presented by the blue arrows), representing more of a water-jet. This difference in inflow- and outflow-pattern result in a different volume of water entering the estuary every time, influencing the salinity of the water.

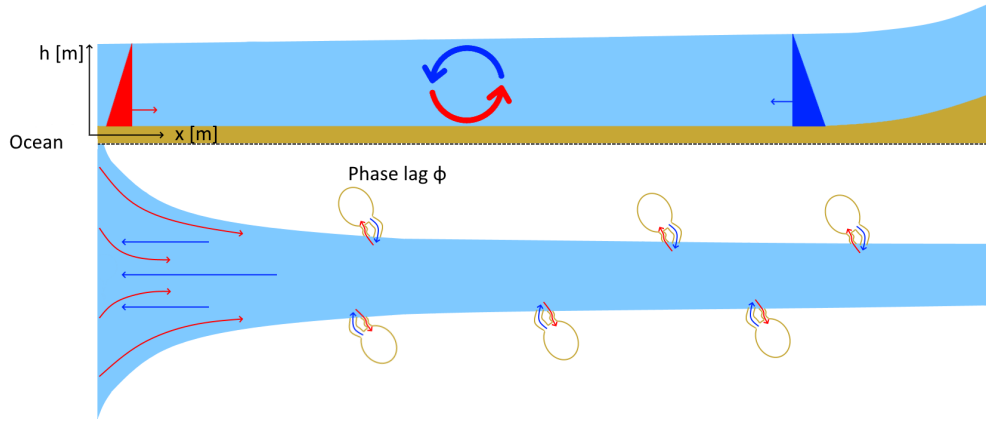

Figure 3.3: The visualization of the main mixing mechanisms; gravitational mixing (upper part of the figure), trapping (enclaves in the estuary) and tidal pumping (difference in inflow- and outflow-patterns), that contribute to dispersion.

Earlier research tried describing individual dispersion components and adding them together but this did not result in a sound relation. There are always processes that are overlooked or overlap. Simultaneously, such a bottom-up approach is sensitive to equifinality (Savenije, 2005; Sivapalan, 2003). Therefore, to counter equifinality all dispersion mechanisms are captured in Van der Burgh's K value. The Van der Burgh K value is an empirical value that links the effective dispersion to the freshwater discharge under steady-state conditions (V.d. Burgh, 1972).

Secondly, two types of dispersion can be distinguished, steady-state dispersion (Equation 3.8, V.d. Burgh, 1972) and unsteady-state dispersion (Equation 3.9, Savenije, 1992). During steady-state conditions the flow in the river does not differ much and Van der Burgh's method for steady-state dispersion can be applied. However, during part of the year the flow in the river varies significantly due to the difference in water availability between the dry and wet season. The system then lags behind the steady-state and an unsteady-state solution needs to be applied. The difference between the two methods is that the steady-state solution solely depends on hydraulic properties while the unsteady-state is dependent on the salinity gradient. In addition, if hyper saline conditions prevail the unsteady-state dispersion takes this into account as well. The formula for unsteady-state dispersion used in the 1D SALNST model was first introduced by Savenije (1992).

Note that the positive x-direction is upstream directed. This means that the discharge Q_f is negative when water is flowing from the river to the ocean.

$$\frac{dD}{dx} = K\frac{Q_f}{A} \tag{3.8}$$

$$\frac{D}{D_0} = (\frac{s}{s_0})^K \tag{3.9}$$

Name	Character	Dimensions
Dispersion	D	L^2/t
Van der Burgh's parameter	K	-
River discharge	Q_f	L^3/t
Cross-sectional area	A	L^2
Dispersion at mouth of the river	D_0	L^2/t
Salinity	s	M/L^3
Salinity at mouth of the river	s_0	M/L^3

To determine the unsteady-state dispersion the dispersion at the mouth of the river is required. The definition of the dispersion at the mouth of a river has been described by Savenije (1993), who based his relation on observations in 13 estuaries over the world. He related several non-dimensional parameters which were known to affect the dispersion. This empirical relation depends on the ratio of the tidal excursion at the mouth of the river (E_0) to the cross-sectional convergence length (a), the tidal flow velocity amplitude ($_0$), the depth at the mouth of the river (h_0) and the Estuarine Richardson number (N_R). The latter being the ratio of potential energy provided to the estuary by the river discharge through buoyancy of fresh water and the kinetic energy provided by the tide during a tidal period (Savenije, 1992). The Estuarine Richardson number depends on amongst others the density of salt water (ocean) and freshwater (ρ_s, ρ_f), the freshwater discharge (Q_f), the tidal period (T) and the tidal prism (P_t). The latter being the volume of water being transported by the tide, which is approximately the tidal excursion at the mouth of the river multiplied by the cross-sectional area at the mouth of the river.

$$\frac{D_0^{HWS}}{v_0 h_0} = 1400\frac{E_0}{a}N_R^{0.5} \tag{3.10}$$

$$N_R = \frac{\Delta\rho}{\rho}\frac{gh}{v_0^2}\frac{Q_f T}{P_t} \tag{3.11}$$

$$\Delta = \frac{\rho_s - \rho_f}{/rho_f} \tag{3.12}$$

$$P_t \approx A_0 E_0 \tag{3.13}$$

Name	Character	Dimensions
Tidal excursion at mouth of the river	E_0	L
Cross-sectional convergence length	a	L
Tidal flow velocity amplitude	v_0	L/t
Depth at mouth of the river	h_0	L
Estuarine Richardson number	N_R	-
Salt water density	ρ_s	M/ L^3
Freshwater density	ρ_f	M/ L^3
Tidal period	T	t
Tidal prism	P_t	L^3
Cross-sectional area at mouth of the river	A_0	L^2

Since the dispersion at the mouth of the river makes use of the depth at the mouth of the river, h equals h_0. Therefore, the dispersion at the mouth of the river can, with the help of the previously introduced formulas, be rewritten to:

$$D_0 = 220\sqrt{g}\frac{E_0}{a}\sqrt{\frac{Q_f T}{P_t}}h_0^{1.5} \tag{3.14}$$

3.2.3 Salt intrusion

Just like dispersion, salt intrusion distinguishes steady-state and unsteady-state. Looking at the formula for steady-state salinity (Equation 3.15, Savenije, 1989), one can see similarities with the formula for unsteady-state dispersion (Equation 3.9). However, steady-state dispersion (Equation 3.8) is applied which makes the steady-state salinity again fully dependent on hydraulic properties. The steady-state salinity is the equilibrium of salt concentration and salt intrusion. Unsteady-state salinity is calculated by solving the salt balance equation (Equation 3.16, Savenije, 2012).

$$s - s_r = \left(\frac{D}{D_0}\right)^{\frac{1}{K}} \tag{3.15}$$

$$r_S\frac{\partial s}{\partial t} - (1-K)\frac{Q_f}{A}\frac{\partial s}{\partial x} - (1-K)r_S\frac{P_n b}{\bar{h}}\frac{\partial s}{\partial x} + \frac{D}{a}\frac{\partial s}{\partial x} - D\frac{\partial^2 s}{\partial x^2} + r_S\frac{P_n}{h_0}s = 0 \tag{3.16}$$

$$r_S = \frac{B_S}{B_c} \tag{3.17}$$

$$P_n = P - E \tag{3.18}$$

Name	Character	Dimensions
River salinity far upstream, uninfluenced by salt intrusion	s_r	M/ L^3
Width convergence length	b	L
Average depth along the width	$\overline{h}$	L
Cross-sectional storage coefficient	R_s	-
Net precipitation	P_n	L/T
Storage width	B_s	L
Conveyance width	B_c	L
Precipitation	P	L/t
Evaporation	E	L/t

3.3 SALT INTRUSION TYPES AND HYPERSALINITY

There are different kinds of salt intrusion. These are distinguished in three types based on how well mixed the salt in a vertical column of water is. The stratified type, the partially mixed type and the well mixed type. Based on the river discharge and tidal flows an estuary has a certain degree of mixing. When the tidal flows dominate it is well mixed and vice versa.

The stratified type is badly mixed, at the ocean side the water is saline and at the river side the water is fresh, in between there is a very short range in which the saline water goes to freshwater. Often a saline wedge is present underneath a layer of freshwater. The partially mixed type and well mixed type have increasingly a more gradual transition. However, the difference between partially mixed and well mixed is not objectively defined. In practice the well-mixed theory can be used up to a stratification of 20-30% (the difference between the salt concentration at the top and bottom of the river divided by their average) (Van Os & Abraham, 1990). The salt measurements that have been taken in the Gambia river in 1971 show barely any stratification, indicating that the Gambia river is well-mixed (Savenije, 2012).

In an estuary of the well mixed type the salinity changes gradually over distance. This can be seen best when measuring the salt concentration while traveling with low water slack, high water slack or the tidal average, the last being very hard to detect. If done correctly a smooth salinity curve shows the gradual change in salinity. There are four types of salt intrusion curves presented in Figure 3.4 below (Savenije, 2012).

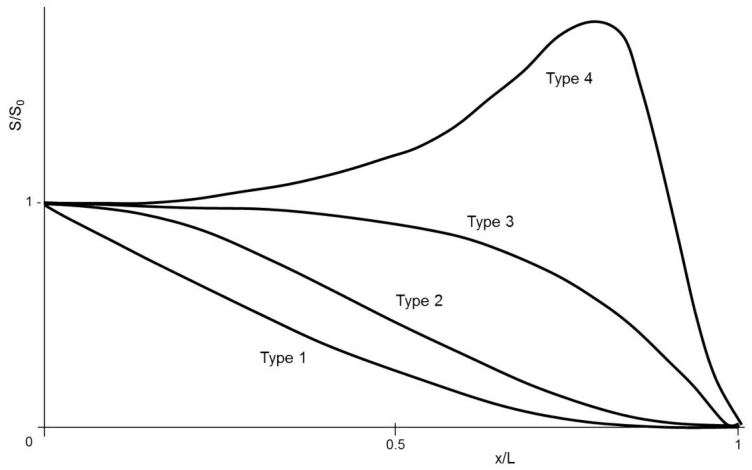

Figure 3.4: The four types of salt intrusion curves (Savenije, 2012).

- Type 1: recession shape
- Type 2: bell shape
- Type 3: dome shape
- Type 4: humpback shape

The first three types are largely linked to the geometric relations. Type 1 occurs in straight and narrow estuaries, such as the Chao Phya in Thailand and the Limpopo in Mozambique. Type 3 are wide channels with a pronounced funnel shape, such as the Gambia river. Type 2 is a mixture of type 1 and type 3, with a narrow river upstream but a strong funnel shape near the ocean. Type 4 however, exists independent of geometric relations. Any of the previously mentioned types can turn into a humpback shape, either when there is a rainfall deficit, evaporation excess or when too much freshwater is removed from the system (e.g. for irrigation purposes). Type 4 is the shape of the salt intrusion curve when an estuary is hypersaline, with a higher salinity than the source.

4 METHODS AND MATERIALS

The aim of this study is to provide insight into the magnitude of salt intrusion change due to climate change and the implications of the construction of a new hydropower dam. This chapter will start by repeating the research questions. Secondly, the required data to answer these questions and where this data comes from is treated followed by the calibration and validation of the model. Afterwards, practical differences between the model and theory are dealt with. Finally, an overview of all scenarios that are used to answer the research questions is presented as well as the method of selecting these scenarios.

4.1 RESEARCH QUESTIONS

The main research objective "What are the effects of climate change and the new hydropower dam on salt intrusion in the Gambia river up to 2100?" will be answered by answering the research questions below. To answer these questions the 1D SALNST model is used (see Section 3.2). Research questions I and II will be answered directly by the model output. Questions III, IV and V will be derived from the results and/or from a qualitative analysis of these results and the model.

1. How does the salt intrusion length develop considering climate change, the hydropower dam and irrigation development in the Gambia estuary?
2. How does the salt concentration develop considering climate change, the hydropower dam and irrigation development in the Gambia estuary?
3. To what extent can hyper salinity occur and under which circumstances?
4. What measures can be taken to mitigate unwanted salt intrusion and how effective are these measures?
5. How will aqua- and agriculture in The Gambia be affected by the construction of the hydropower dam?

4.2 REQUIRED DATA AND COLLECTION

Chapter 3 presented the theory on how the SALNST model used in this study calculates salt intrusion. The dispersion and salt balance equations,

which calculate respectively the dispersion and salt concentration over the length of the river, are composed of the parameters in Table 4.1, below.

Number	Name	Character	Dimensions
1.	Salinity at the mouth of the river	s_0	L^2/t
2.	Gravitational constant	g	L/t^2
3.	Cross-sectional area of the river	A	L^2
4.	Cross-sectional area at the mouth of the river	A_0	L^2
5.	Cross-sectional area convergence length	a	L
6.	Width of the river	B	L
7.	Width convergence length	b	L
8.	Depth at the mouth of the river	h_0	L
9.	Tidal excursion at the mouth of the river	E_0	L
10.	Tidal period	T	t
11.	Van der Burgh's parameter	K	-
12.	Net precipitation	P_n	L/t
13.	River discharge	Q_f	L^3/t
14.	Dispersion at the mouth of the river	D_0	L^2/t
15.	Salinity	s	M/L^3
16.	Dispersion	D	L^2/t

Table 4.1: Required data (1-14) for calculating salt concentrations and dispersion (15-16).

The parameters can be roughly categorized into the following categories: pre-determined parameters (3 – 11), measured and deducted parameters (12 – 13) and parameters to determine (14 – 16). The first two parameters are well-known constants, the ocean salinity (35 g/L) and gravitational constant (9.81 m/s2) and do not need further explanation. The pre-determined values were measured, deducted or optimized during a survey in 1971, led by Savenije. In personal communication with Savenije this data was obtained for this study. The measured and deducted parameters are described below. The values to determine consist of the dispersion at the mouth of the river, which follows from calibrating the model. The dispersion and salt concentration over the length of the river result from solving the formulas for dispersion and the salt balance equation (equations: 3.8, 3.9, 3.15 and 3.16).

4.2.1 Precipitation, evaporation and discharge

The measured and deducted parameters are the net precipitation which is calculated by subtracting evaporation from precipitation, and river discharge which is predicted by the model described in Section 4.2.2 (and in more detail in Appendix C). Evaporation needed for the net precipitation is estimated with Thornthwaite's method which depends on temperature (Thornthwaite, 1948). Temperature and precipitation are projected by a single GCM. The GCM, MIROC-ESM is chosen based on a study performed

by the FAO which can be found in Appendix A (Simpson, 2020). The following paragraph will summarize how the MIROC-ESM GCM was selected, how and why the potential evaporation is determined by Thornthwaite's method and how the model that predicts river discharge works.

GCM

Note: The GCM has been selected, and the data has been retrieved by a climate analist of the FAO. This section is a summary of the full overview which is presented in Appendix A.

To select a good GCM for predicting future precipitation and temperature a comparison between five GCMs was made (Appendix A; Simpson, 2020). The five selected GCMs have all been used in previous climate assessments performed by the FAO. These models are: the GFDL-ESM2M (Geophysical Fluid Dynamics Laboratory – Earth System Model 2M) (Dunne et al., 2012); the MIROC-ESM (Model for Interdisciplinary Research on Climate – Earth System Model) (Watanabe et al., 2011); the IPSL-CM5a-MR (Institut Pierre-Simon Laplace-Climate Model 5a-Mid-Resolution) (Dufresne et al., 2013); the NORESM (Norwegian Earth System Model 1-M) (Bentsen et al., 2013), and the HadGEM2-ES (Hadley Centre Global Environment Model ver.2-Earth System) (Martin et al., 2011). All of these models are part of the Coupled Model Intercomparison Project 5 (CMIP5), used in conducting analysis for the IPCC Fifth Assessment Report (AR5)[1].

To test which of these GCMs performs best in predicting future precipitation and temperature, the model's deviations from observations between 1979 and 2018 for the catchment of the Gambia river were computed. This was compared with a historical dataset: EWEMBI (EartH2Observe, WFDEI and ERA-Interim data Merged and Bias-corrected for ISIMIP) (Dee et al., 2011; Dutra et al., 2015; Lange, 2018; Weedon et al., 2014). The EWEMBI dataset is a robust, global dataset compiled and maintained by the Inter-Sectoral Impact Model Intercomparison Project (ISIMIP) in support of impact assessment teams contributing to the Intergovernmental Panel on Climate Change (IPCC) assessment reports. The dataset provides daily precipitation and temperature data, covering the period from 1979-2018, at a global scale with 0.5° resolution (roughly 55.5 km2 at the equator).

For each GCM the Root Mean Squared Error (RMSE) of the difference between historical values and modelled values for precipitation and temperature were determined (see Figure 4.1). It can be seen that for precipitation and temperature the MIROC-ESM has a relatively low RMSE (although NORESM scores a slightly better on temperature predictions) which is averaged the lowest. Due to the best performance in predicting the historical precipitation and temperature, the MIROC-ESM GCM has been selected as the best GCM to be used in this area.

1 For further details see the IPCC AR5 Chapter 9 "Evaluation of Climate Models" and IPCC Data Distribution Center AR5 Reference snapshot

The output of the MIROC-ESM GCM was further improved through bias correction. This correction is based on the assumption that the predicted data has a systematic error, implying that the output can be corrected and improved. Figure 4.2 shows an example for the minimum temperature at Yundum with the raw model output (raw), the bias corrected output (bc) and observations. As can be seen, the bias corrected output fits much better to the observed data. This is due to a vertical shift in temperature and a change in the speed with which temperature rises.

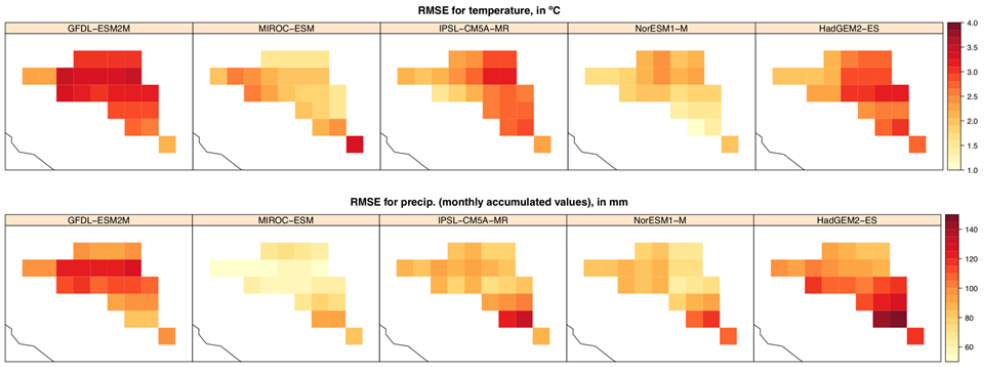

Figure 4.1: GCM to EWEMBI Root Mean Square Error values (1979-2016) for temperature and precipitation across the Gambia River watershed (lighter colors denote smaller RMSEs) (Source: FAO analysis of EWEMBI dataset) (Simpson, 2020).

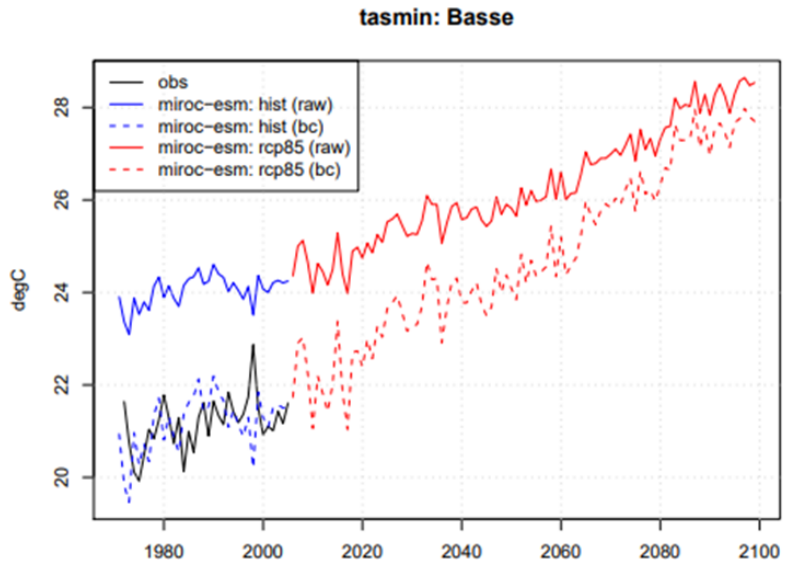

Figure 4.2: GCM raw output (raw), observations (obs) and bias corrected output (bc) for the minimum temperature in Basse (Simpson, 2020).

Evaporation

Potential evaporation is estimated with Thornthwaite's method (Thornthwaite, 1948). This method gives a rough indication of the potential evaporation but

is ideal in terms of required parameters. It only depends on temperature, days in the month and the averaged amount of daylight hours per month. The result is the monthly potential evaporation. Temperature is predicted by the MIROC-ESM GCM and the average amount of daylight hours per month are determined by using the NOAA Solar Calculator. To achieve open water evaporation, which is used on the reservoir surface, a multiplication factor of $\frac{1}{0.85}$ is used. This factor was determined by Verkerk and Van Rens (2005), who compared pan evaporation measurements to Thornthwaite's potential evaporation.

$$E_{pot} = 1.6 \frac{L}{12} \frac{N}{30} \left(\frac{10 \cdot Ta}{I} \right)^{\alpha} \tag{4.1}$$

$$I = \sum \left(\frac{Tai}{5} \right)^{1.514} \tag{4.2}$$

$$\alpha = (6.75 \cdot 10^{-7}) \cdot I^3 - (7.71 \cdot 10^{-5}) \cdot I^2 + (1.792 \cdot 10^{-2}) \cdot I + 0.49239 \tag{4.3}$$

Name	Character	Dimensions
Mean daily air temperature	Ta	T
Number of days in the month	N	-
Average daylight hours per month	L	t
Heat index	I	T
Mean air temperature for each month in the year	Tai	T

Net precipitation

The net precipitation is calculated by subtracting evaporation from precipitation. Subtracting potential evaporation from precipitation would usually give an overestimate of the evaporation and therefore too low net precipitation. However, the evaporation is in the model also adjusted by a calibration parameter (F_E) (see Section 4.3). This justifies the use of potential evaporation, since this calibration parameter can be seen as a correction factor in the determination of the net precipitation.

$$P_{net} = P - E_{pot} F_E \tag{4.4}$$

4.2.2 River discharge

The Gambia river discharge has been recorded at the border of Senegal near Gouloumbou from 1970 until 2005 and for one and a half year starting July 2016 and ending December 2017. The data is not complete throughout the year, with most years lacking measurements in the dry season (December to June). The dataset was provided by Direction de la Gestion et de la Planification des ressources en Eau (DGPRE) through personal communication.

To predict river discharge for future scenarios a simple box model was developed and optimized based on the measured discharge and precipitation in Senegal (Appendix C). A historic monthly measured precipitation dataset for the wet season, from May to October, was made available for this study by the FAO. The dataset starting at January 1981 and ending at January 2017, contains the precipitation data for 6 locations; within The Gambia these are: Basse, Yundum, Janjanbur; within Senegal these are: Kedougou, Goudiry and Saraya. The precipitation data comes from ANACIM, the aviation and meteorology institute of Senegal. Several precipitation stations across Senegal are used to feed the model that ANACIM uses to interpolate precipitation areas where there are no weather stations. The data used in this thesis come from weather stations and was not interpolated.

Geographically there is a distinct difference in precipitation. The north of the catchment receives less precipitation than the south of the catchment (see Figure 4.3). Furthermore, the east side of the catchment is more mountainous and functions as the driving force of the flow in the Gambia river. To create a trustworthy model for predicting river discharge it is important to take these features into account. Since the historical discharge was measured at Gouloumbou part of the catchment that receives rain does not contribute to the river discharge at this point. Therefore, the catchment is split into two parts; a northern and southern part both lying in Senegal. From the several locations that the GCM predicted precipitation and temperature for two were chosen: Kedougou and Goudiry. Figure 4.4 shows a hypothetical split of the eastern side of the catchment, in which the discharge is partly generated by precipitation from Kedougou and partly by precipitation from Goudiry. In practice, the model is optimized by calibrating and validating on the historical measurements, this results in a R-squared value of 86%. The actual contribution of each of the locations is determined by minimizing the error between the estimated discharge and the measured discharge with the scipy.optimize.minimize function in python.

The future predictions of river flow use the predicted precipitation and temperature data, generated by the MIROC-ESM GCM. For more details about the discharge model and its optimization Appendix C.

4.2.3 Sea level rise and irrigation development

The sea level rise values that have been discussed in chapter 2 are split in yearly increments from 2006 to 2099 such that in 2099 the chosen sea level rise is reached. Furthermore, the average sea level rise from 1971 to now, which amounts to 0.16 m, is added (Rahmstorf et al., 2012).

Similarly, the development of irrigation area which was discussed in chapter 2 is implemented. Table 4.2, below shows the change in irrigation area under irrigation for three scenarios.

	2020	2021	2022	2023	2024	2025	2026	2027	2028	2029	2030	2031	2032	2033	2034	2035	2036	2037	2038	2039	2040
Scenario 1 (Current): no changes (i.e., no new land development beyond surface area currently under irrigation); data for The Gambia 2020 baseline from NRDS (2014); data for Senegal 2020 baseline based on a 2001 reference (see also Twente, 2005) to 250ha under production from 600 ha developed (FAO, 2001).																					
A	2300	2300	2300	2300	2300	2300	2300	2300	2300	2300	2300	2300	2300	2300	2300	2300	2300	2300	2300	2300	2300
B	250	250	250	250	250	250	250	250	250	250	250	250	250	250	250	250	250	250	250	250	250
Total	2550	2550	2550	2550	2550	2550	2550	2550	2550	2550	2550	2550	2550	2550	2550	2550	2550	2550	2550	2550	2550
Scenario 2 (Expected): The Gambia has planned new land development between 2021-2024 (e.g., Islamic Development Bank, African Development Bank, financed Regional Rice Value Chain Development Project) gradually adding 2,685 ha; no further changes after 2024; Similarly, Senegal planned development based on assumption of bringing back into production the 350 ha of previous developed pump irrigation land that had been abandoned as referenced in FAO (2001) (see also Twente, 2005).																					
A	2300	2971	3643	4314	4985	4985	4985	4985	4985	4985	4985	4985	4985	4985	4985	4985	4985	4985	4985	4985	4985
B	250	338	425	513	600	600	600	600	600	600	600	600	600	600	600	600	600	600	600	600	600
Total	2550	3309	4068	4826	5585	5585	5585	5585	5585	5585	5585	5585	5585	5585	5585	5585	5585	5585	5585	5585	5585
Scenario 3 (Maximum): Assumptions for The Gambia based on full development of irrigated potential 12,727 ha, based on maximum potential mentioned in NRDS (2014) up to 2024 (roughly 1/2 the 24,000ha targeted in the National Agricultural Investment Plan (2010); Assumption for Senegal based on future targets assumed in the 2005 Twente Study of 2,000 ha (roughly 1/2 of 4,100 potential irrigatable land referenced in FAO, 2001, and Twente, 2005).																					
A	2300	4325	6350	8375	10400	12425	12727	12727	12727	12727	12727	12727	12727	12727	12727	12727	12727	12727	12727	12727	12727
B	250	542	833	1125	1417	1708	2000	2000	2000	2000	2000	2000	2000	2000	2000	2000	2000	2000	2000	2000	2000
Total	2550	4867	7183	9500	11817	14133	14727	14727	14727	14727	14727	14727	14727	14727	14727	14727	14727	14727	14727	14727	14727

Table 4.2: Overview of increase in agricultural surface in the Gambia river catchment. In this table, A and B, in the most right column, stand for respectively The Gambia and Senegal.

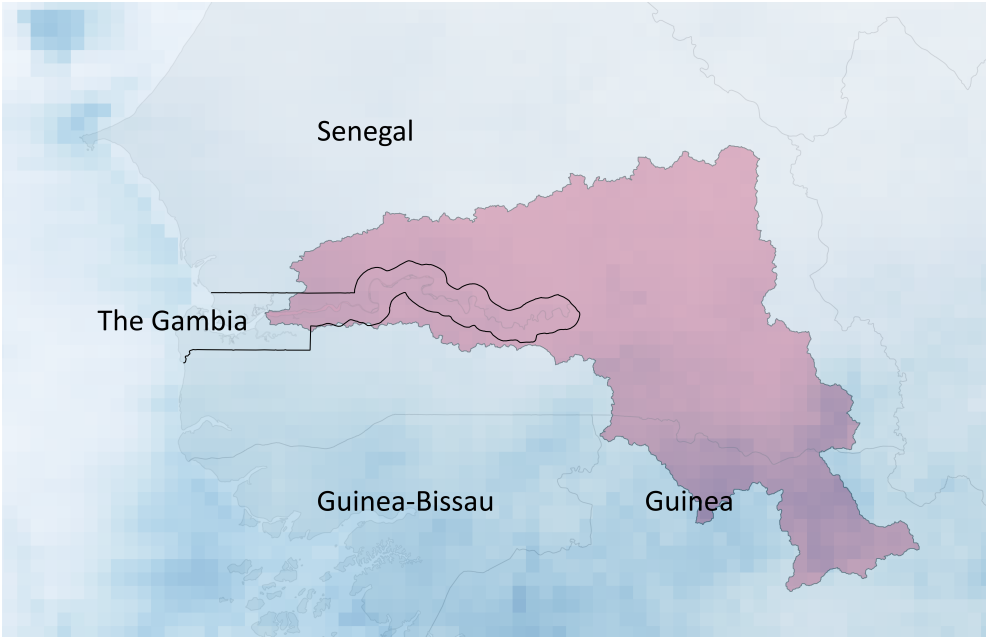

Figure 4.3: A typical month in the rainy season (September 2019), retrieved from NASA: IMERG. The darker blue pixels show precipitation. It is clear that the northern part of the catchment receives less precipitation than the south side.

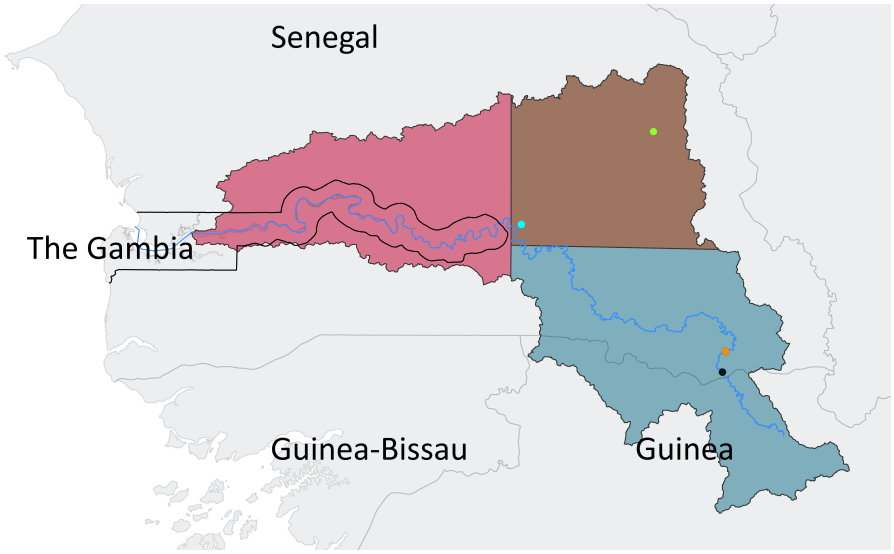

Figure 4.4: Hypothetical split of the catchment. The bright green dot shows Goudiry, the light blue Gouloumbou, the orange dot Kedougou and the black dot the location of the hydropower dam. In blue the Gambia river.

4.3 CALIBRATION AND VALIDATION OF THE MODEL

The calibration of the model makes use of the survey data from 1971. On a boat moving with high water slack multiple measurements along the Gambia river were performed multiple times. This measuring technique yields good salinity data because at high water slack the tidal inflow stocks ($Q_{tidal} =$

0) and therefore at this moment the salt intrusion is at its peak. Calibrating the model is done by changing two factors that scale the dispersion at the mouth (Do) and evaporation: F_d and F_E, presented below. The calibrated model output can be seen in Figure 4.5. This is done manually because due to the steady and unsteady-state nature of the Gambia river a perfect fit is not possible.

$$F_d = 8.64$$
$$F_E = 2.5$$

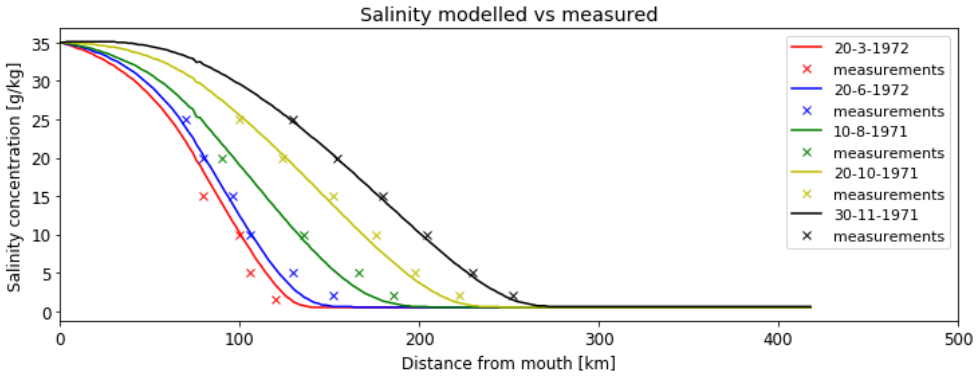

Figure 4.5: Model predictions for salt concentrations over distance, 'x' marks the measurements, the lines are the predictions of the model with the calibration settings mentioned above.

The validation data however, makes use of salinity measurement systems (OTT Ecolog 500 800) installed along the Gambia river. According to the producer of the system these are accurate, trustworthy instruments that after installation are protected against vandalism, their batteries will last 10 years and it automatically sends data. However, in practice this is different. Within a year many of these instruments were reported to be broken, did not send data or needed spare parts that were not available. In the end six instruments measured salinities, however not continually. From these six datasets only four could be used of which the data is disputable. The recordings contain a salinity measured every 15 minutes. The maximum salt concentration of these measurements should coincide with the calibrated model since the maximum salt intrusion occurs during high water slack. By resampling to the monthly maximum concentration of these measurements a small horizontal shift to the right takes place. This shift is caused because the maximum recorded salinity is presented at the end of the month, therefore shifting to the right (see Figure 4.6). The validation of predicted salt concentration 198 km from the mouth of the river can be seen in Figure 4.7.

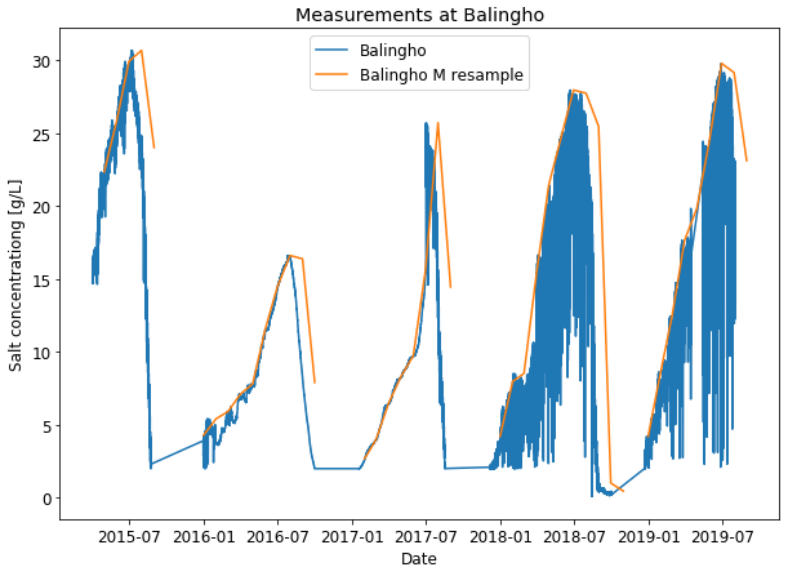

Figure 4.6: The shift that occurs by resampling to the monthly maximum of the salt concentration measurements can be clearly seen for measurements taken near Balingho, The Gambia, 128 km upstream of the river mouth.

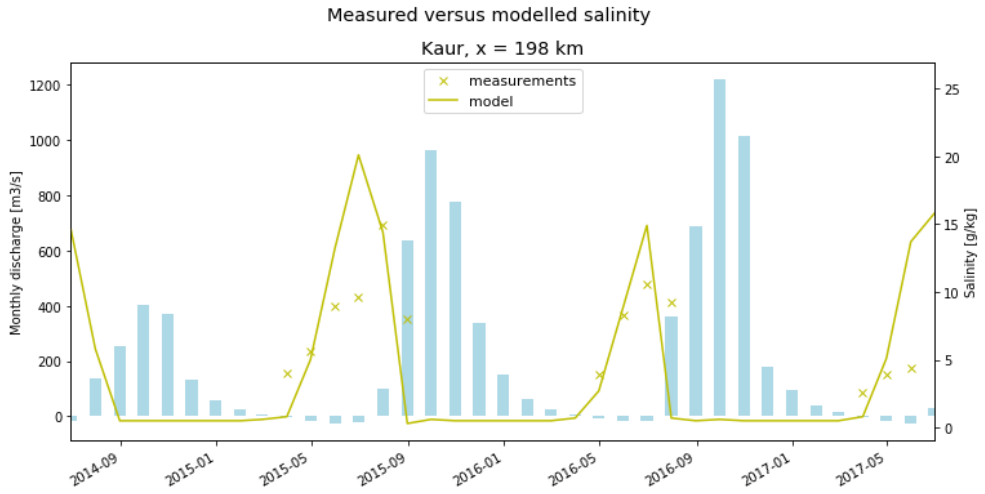

Figure 4.7: Validation of the model by comparison with measurements 198 km upstream of the mouth of the river. The salt concentrations from the measurements and model can be read from the y-axis on the right and are plotted respectively as 'x' and as a continuous line. The left y-axis shows the river discharge (blue bars). Note that due to the coarse temporal resolution of the historic discharge (monthly) the model results are represented coarser as well.

4.4 ANALYSIS OF MODEL OUTPUT AND SELECTION OF KEY FEATURES

Each model run results in a lot of information. Graphical representation of this information gives a clear idea of the effects of certain parameters.

Three graphs will be introduced and their key features explained. These key features will be used when discussing the results.

4.4.1 Cumulative frequency distribution curve

Starting with analyzing Figure 4.8, a cumulative frequency distribution curve (CFD curve). It shows on the y-axis the probability of exceedance or rarity of a certain intrusion length occurring, with 100% always occurring and 0% never occurring. The key features are the minimum and maximum probability of exceedance, these represent the minimum and maximum salt intrusion lengths that occur in the respective time period. In Figure 4.8 the minimum and maximum salt intrusion lengths are depicted by a blue and red arrow. It is important to realize that these intrusion lengths are determined based on a salt concentration of 1 g/L.

Another important key feature is the slope. A steep slope indicates little variation in salt intrusion lengths within the time period while a mild slope indicates stronger varying salt intrusion lengths. In Figure 4.8 the grey lines show how a steepening of the lower slope might look like. The upper slope is defined as the gradient between 90- and 60% probability of exceedance whereas the lower slope is defined as the gradient between 40- and 10% probability of exceedance, to exclude the influence of extremes.

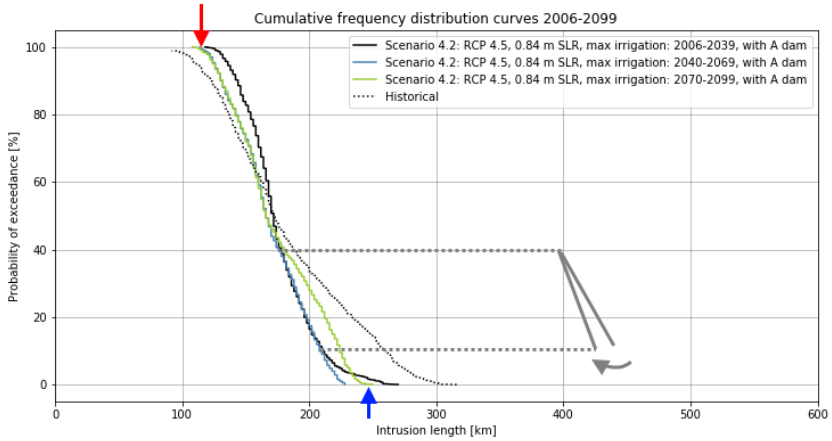

Figure 4.8: Cumulative frequency distribution curve (CFD-curve). The red and blue arrow show respectively the minimum and maximum salt intrusion length. The grey arrow shows how the lower slope of the curve changes.

4.4.2 Median salt intrusion

The second important graph is the median seasonal salt intrusion (Figure 4.9). This graph shows the monthly median salt intrusion length for the same time periods as the previous graph. The intrusion length in km is now represented by the y-axis and the months on the x-axis. The key features of this graph are respectively the peak during the dry season and dip during the

wet season in the median salt intrusion length, visualized by the red and blue arrow. This is again for a salt concentration of 1 g/L. The magnitude of the difference between scenarios is a good indication for the expected shift in salt intrusion lengths because the median is the most occurring salt intrusion length. Furthermore, the median is less affected by extremes which makes it a good representative parameter.

In Figure 4.9 a shift of the wet season dip is visible, marked by the grey arrow. This is another interesting key feature indicating a possible shift of the wet and dry season.

4.4.3 Salt concentration curve

The third graph that contains important information is a plot of all salt concentrations along the length of the estuary at 10-day intervals across the time period indicated. At the mouth of the estuary a constant salinity of 35 g/L is present. Depending on the scenario hypersaline events might occur. The key feature of this graph is the approximate range where hyper salinity occurs, and the magnitude of the hyper salinity (concentration). Figure 4.10 gives an example where the hyper saline region is marked in red and the maximum concentration in blue. In the final overview this graph has also been split into three time periods for easier comparison.

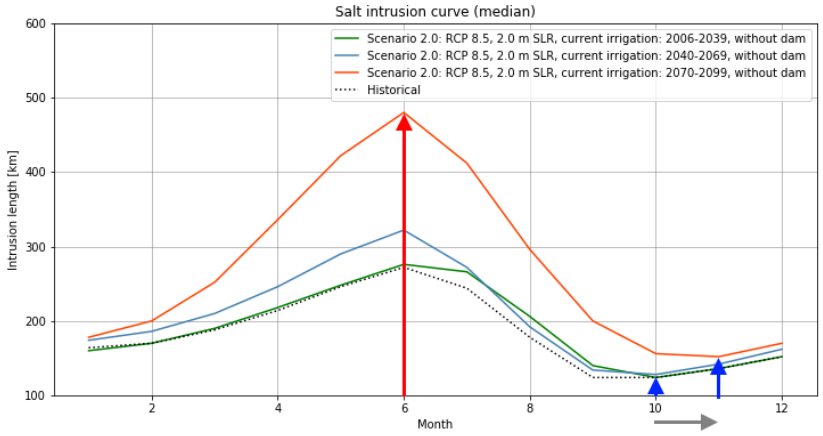

Figure 4.9: Median monthly salt intrusion curve. The red and blue arrows respectively indicate the change of the dry and wet season median salt intrusion length. The grey arrow shows how, in this case the wet season dip, can shift temporaly.

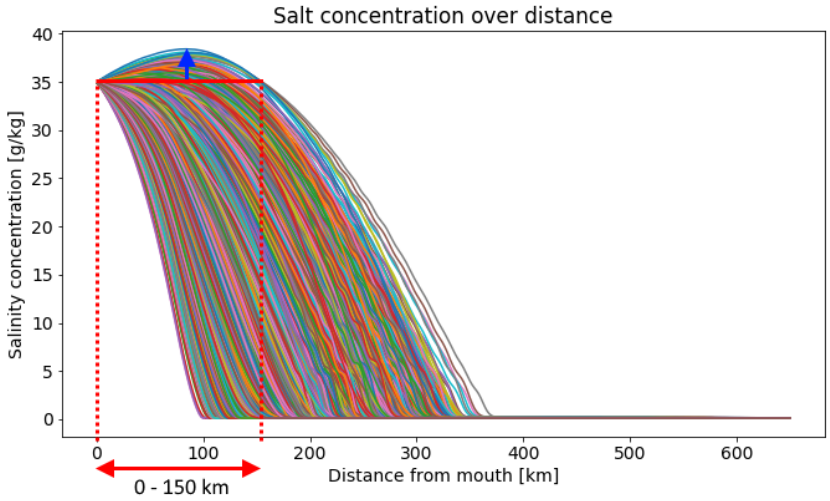

Figure 4.10: Salt concentration curve. Each line represents the salt concentration over distance of a timestep (10-days) in the model. All lines together give an impression of the hypersaline region that occurs during the modelled period. The blue arrow indicates the maximum salt concentration and the red arrow the size of the hypersaline region.

4.4.4 Temporal distribution

The wet- and dry-season climate pattern has a strong effect on salt intrusion lengths and concentrations. During the dry season salt intrudes inland while in the wet season the salt front is pushed back. This is clearly represented in Figure 4.11. This year-to-year pattern with peaks during the dry season and dips during the wet season does not change during model runs. There can be vertical shifts, for example wet season dips that retreat not as much as usual or dry season peaks that are amplified. However, such changes are captured by the key features. The results however, will be used to discuss date ranges which show the maximum and minimum salt intrusion lengths occurring in this period. It is imperative to realize that the presented results do not necessarily occur in the same year within the discussed time period.

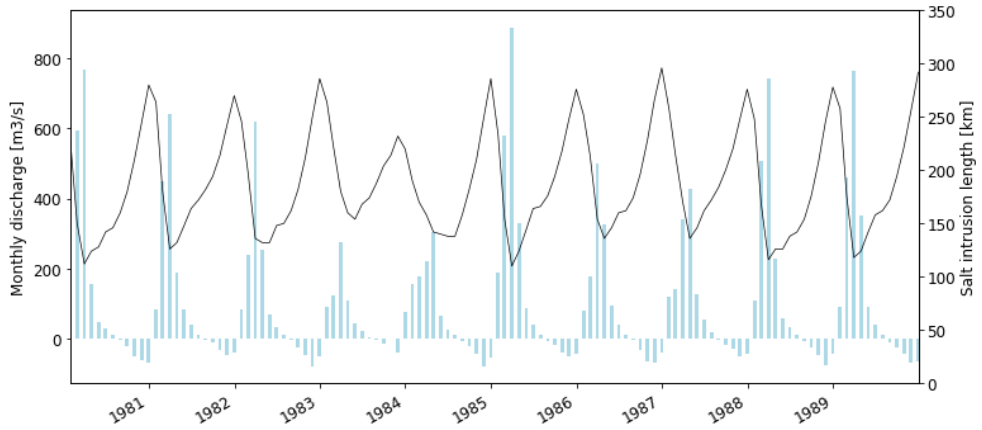

Figure 4.11: Temporal distribution of salt intrusion. This graph shows the discharge (blue bars) and salt intrusion length (salt concentration of 1 g/L as black line) for a small modelled historic time range.

4.5 HISTORICAL SALT INTRUSION

The model results for historical salt intrusion are included in this report because the historic model was calibrated on the only reliable salt measures that have been taken in the Gambia river. These model results were verified and can give an indication of how salt intrusion might change. It is however, absolutely wrong to base conclusions on the differences between these results due to the different datasets that have been used for the historical model results and the current model results (also see Table 4.3 and Figure 4.12 below).

Table 4.3 below gives an overview of the different datasets and their sources. Figure 4.12 visualizes the data used in the historic and current model as well as certain transformations that the data undergoes. This displays how much data related difference there is between the two models. Figure 4.12 only shows the data that is used in both models, in the current model also sea level rise is taken into account which increases the gap between the results of the two models.

Data	Source	Comments	Date range
Historic salt measurements	Survey	Personal communication with H.H.G. Savenije	1971
River geometry	Survey	Personal communication with H.H.G. Savenije	1971
Historic river discharge		Personal communication Direction de la Gestion et de la Planification des ressources en Eau (DGPRE)	1970-2004 2016-2017
Precipitation for calibration of GCM	ANACIM	Dataset acquired by the FAO	1981-2017
Current salt measurements	OTT Ecolog 500 & 800	Personal communication Direction de la Gestion et de la Planification des ressources en Eau (DGPRE)	All within the period 2014-2018
Precipitation & Temperature	MIROC GCM		2006 - 2099
Evaporation	Thornthwaite	Based on temperatures from the MIROC GCM	2006-2099
Freshwater discharge	Block model (see Appendix B)	Based on the precipitation from the MIROC GCM	2006-2099

Table 4.3: Overview of the several datasets and their source, sorted by date range.

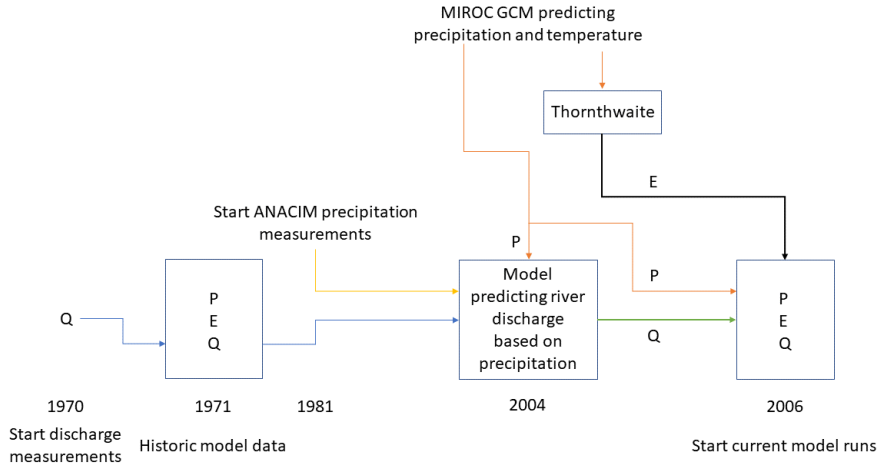

Figure 4.12: Flow chart of precipitation, evaporation and river discharge. The years mentioned at the bottom correspond to the date ranges in Table 3. The colors visualize where data transforms.

4.5.1 Adjustments and simplifications of the model

There are a couple of differences between the theory and how the model applies the theory. These differences are treated in this paragraph together with an adjustment made in the calculations performed by the model.

The SALNST model is a numerical model. In combination with the dependency between the dispersion and salinity calculations this creates a loop in which small numerical errors are propagated and enhanced. This can be seen in the salt concentration plots (see for example the right side of Figure 4.10). If salt intrusion lengths increase the numerical error increases due to the extra amount of calculations and vice versa.

Furthermore, the model can account for unsteady-state dispersion but it does not detect when unsteady-state dispersion needs to be applied. Instead, it makes use of a combination of steady- and unsteady-state calculations for every calculation. This is necessary because the steady-state calculations are used to give direction to the unsteady-state calculations (also see Appendix B.

The implementation of sea level rise is a simplification as well. The several values that are used for sea level rise are split in fractions that are added after each passing year. In addition, the expansion of the river evaporative surface due to sea level rise, which has been discussed in the Figure 3.2.1, is a simplification as well.
An additional adjustment to the model has been made in its calculation. As has been presented in chapter 3 the salt balance equation to be solved is:

$$r_S \frac{\partial s}{\partial t} - q\frac{\partial s}{\partial x} - D\frac{\partial^2 s}{\partial x^2} + r_S \frac{P_n}{h_0} s = 0 \tag{4.5}$$

$$q = (1-K)\frac{Q_f + r_S P_n b \cdot B}{A} - \frac{D}{a} = (1-K)\frac{Q}{A} - \frac{D}{a} \tag{4.6}$$

$$q = \frac{Q_R}{A} - \frac{D}{a} - \frac{dD}{dx} \tag{4.7}$$

The model makes use of a dD/dx that is solely based on steady-state calculations. To account for the non-steady state calculations as well this has to be adjusted. This is implemented as follows. For better understanding of how the model calculates the salt intrusion consult Appendix B.

$$\frac{dD}{dx} = \frac{\frac{dD_s}{dx} + C_{ns}\frac{dD_{ns}}{dx}}{1 + C_{ns}} = \frac{-K \cdot \frac{Q(x)}{A(x)} + C_{ns} D_{ns} K \cdot \frac{\Delta C(x)}{C(x) - C_r}}{1 + C_{ns}} \tag{4.8}$$

Name	Character	Dimensions
Steady-state dispersion	D_s	L^2/t
Non steady-state dispersion	D_{ns}	L^2/t
Non steady-state weight	C_{ns}	-

4.6 SCENARIO OVERVIEW

To answer all research questions numerous scenarios have been modelled. This paragraph treats the parameters used in these scenarios and presents an overview of the modelled scenarios.

4.6.1 Model parameters

Table 4.4 below, presents the parameters that are used in the scenarios. The parameter values are combined according to the created scenarios in Table 4.5. Sea level rise, projected climate and irrigation development have been treated (sea level rise and projected climate in Chapter 2 and irrigation development in Section 4.2.3). Dam operations will consist of two operational schemes, 'DO A' focusing on the flow scheme according to the environmental study in 2014 (OMVG) and 'DO B' focusing solely on power production, maximizing P while keeping it as constant as possible throughout the dry and wet season, see Equation 4.9 below. More detailed information on how the reservoir is modelled and how the operational schemes have been created can be found in Appendix D.

$$P = \rho g \Delta h Q \eta \tag{4.9}$$

$$\Delta h = h_{reservoir} - h_{turbine} \tag{4.10}$$

Abbreviation	Parameter	1	2	3
SLR	Sea level rise	0 m	0.84 m	2 m
PC	Projected climate	RCP 4.5	RCP 8.5	
DO	Dam operations	A	B	
ID	Irrigation development	Current	Expected	Maximum

Table 4.4: Model parameters and their values.

The presented parameters are presented and used as if they are independent of each other. However, obviously the relation between the evolution of climate due to greenhouse gasses and sea level rise is not independent. By assuming an independent relation of these parameters the influence of single parameters on salt intrusion can be extracted. This leads to some improbable or impossible scenarios.

4.6.2 Scenario overview

In Table 4.5 the overview of all the modelled scenarios is presented. The goal of all these scenarios is to determine what the effect is of the individual parameters. Furthermore, the results of all these scenarios give an impression of salt intrusion lengths and salt concentrations that can be expected. They can indicate if or when the estuary turns hypersaline and what The

Gambia can expect in the years up to 2100. However, the model results should not be taken literally (see Section 4.5 and Figure 4.12). In order to determine parameter influence the scenarios are set up to be able to isolate single parameters. This enables the comparison of scenarios where only a single parameter changes, showing the effects on salt intrusion for the respective parameter. The output of each scenario will be presented across three periods, 2006-2039, 2040-2069 and 2070-2099.

Scenario ID:	Sea level rise:	Future weather:	Dam operations	Irrigation development:	Comment:
H	0 m	Historical	No dam	Current	
0.0	0 m	RCP 8.5	No dam	Current	
0.1	0 m	RCP 4.5	No dam	Current	
0.2	0 m	RCP 8.5	No dam	Expected	
1.0	0 m	RCP 8.5	Dam reservoir filling	Expected	2024
1.1	0 m	RCP 8.5	Dam reservoir filling	Expected	2024-2025
2.0	2 m	RCP 8.5	No dam	Current	
2.1	2 m	RCP 8.5	A	Current	
2.2	2 m	RCP 8.5	B	Current	
3.0	0.84 m	RCP 4.5	No dam	Current	
3.1	0.84 m	RCP 8.5	No dam	Current	
3.2	0.84 m	RCP 4.5	A	Current	
3.3	0.84 m	RCP 4.5	B	Current	
3.4	0.84 m	RCP 8.5	A	Current	
3.5	0.84 m	RCP 8.5	B	Current	
4.0	0.84 m	RCP 4.5	A	Expected	
4.1	0.84 m	RCP 4.5	B	Expected	
4.2	0.84 m	RCP 4.5	A	Max	
4.3	0.84 m	RCP 4.5	B	Max	
4.4	0.84 m	RCP 8.5	A	Expected	
4.5	0.84 m	RCP 8.5	B	Expected	
4.6	0.84 m	RCP 8.5	A	Max	
4.7	0.84 m	RCP 8.5	B	Max	
4.8	2 m	RCP 8.5	No dam	Expected	
4.9	2 m	RCP 8.5	No dam	Max	
4.1	2 m	RCP 8.5	A	Expected	
4.11	2 m	RCP 8.5	B	Expected	
4.12	2 m	RCP 8.5	A	Max	
4.13	2 m	RCP 8.5	B	Max	

Table 4.5: Overview of all scenarios.

5 RESULTS AND DISCUSSION

The analysis of results follows the modelled parameters (projected climate, sea level rise, dam operations and irrigation development) and research questions. An analysis is performed for each parameter, split into subsections addressing the relevant research questions. Figures illustrating the most relevant results are presented here for each parameter. These figures are used to illustrate processes and highlight some of the more significant possible outcomes or trends. A complete collection of the results from the analysis can be found in Appendix F. The key features of the analysis, presented in previous chapters, are used here to organize the presentation of results, and are summarized in Table 5.1 below. A summary of the most significant effects of the modelled parameters is presented after the discussion of the last model parameters. The chapter finishes with an expert interview on the morphological changes due to climate change and the hydropower dam.

Furthermore, it is important to keep in mind that to obtain these results small errors have been introduced. Future climate is projected, discharge is modelled based on these projections, estimates on how the river will expand etc. Even if the generation of the input data would be flawless, simplifications have been made to generate results. The combination of all errors, both data and simplifications, result in a range around the model results which can be considered the truth. Therefore, small changes in salt intrusion when comparing scenarios or periods do not necessarily signify any change.

Finally, **it is imperative to understand** that the historical values are the baseline that is used to compare changes to. It is by all means wrong to compare with historical values due to the use of different data. This is explained in section 4.5 and visualized in Figure 4.12.

Key feature	Description
F1	The salt intrusion length for the maximum probability of exceedance. This value is the salt intrusion length that is always exceeded and can be considered the minimum salt intrusion length.
F2	The salt intrusion length for the minimum probability of exceedance. This can be considered the maximum salt intrusion length.
F3	The average gradient of the CFD-curve between 90- and 60% probability of exceedance. The CFD-curve always has a negative gradient (see Figure 4.8) therefore, an increasing negative value indicates a steepening of the slope while a decreasing negative value indicates a flattening of the slope. The gradient represents the variance of the more often occurring salt intrusion lengths.
F4	The average gradient of the CFD-curve between 40- and 10% probability of exceedance. The gradient represents the variance of the less often occurring salt intrusion lengths.
F5	The wet season monthly median salt intrusion length. This gives an indication on how salt intrusion lengths in the wet season evolve. The median gives a good representation what happens to often occurring salt intrusion lengths.
F6	The dry season monthly median salt intrusion length.
F7	The month when the wet season monthly median dip occurs. The dip might shift, if this happens consistently this could indicate a change in seasonality.
F8	The month when the dry season monthly median peak occurs.
F9	The maximum occurring length of the hypersaline region. This region spans from the river mouth until the first moment the salt concentration falls below ocean salinity.
F10	The maximum occurring salt concentration. This is an indicator for the magnitude of hypersalinity.

Table 5.1: Overview and explanation of all key features

5.1 PROJECTED CLIMATE

Projected climate is the first model parameter that will be discussed. Starting with its effects on the minimum and maximum salt intrusion lengths and followed by the effect on probability of exceedance, effect on seasonality and effect on salt concentration. The scenarios and their results for this model parameter are presented in Table 5.2 below. Four combinations have been made with model parameters, only changing the RCP used. To see the influence of projected climate on salt intrusion the differences between RCP 4.5 and 8.5 are analyzed.

scenario ID	Period:	RCP	SLR	ID / DO	CFD-curve				Monthly median min/max				S-x curve	
					F1 [km]	F2 [km]	F3 [-]	F4 [-]	F5 [km]	F6 [km]	F7 [Mos]	F8 [Mos]	F9 [km]	F10 [g/L]
H	1971-2017	N/A	N/A	N/A	92	316	-0.74	-0.41	124	272	9	6	72	35.6
0.1	2006-2039	4.5	0	Current No dam	104	314	-0.94	-0.41	124	280	10	6	98	36.1
	2040-2069				96	308	-0.83	-0.39	112	278	10	6	92	36
	2070-2099				96	328	-0.78	-0.33	110	298	10	6	124	36.6
0.0	2006-2039	8.5	0	Current No dam	104	316	-0.88	-0.42	120	274	10	6	92	36
	2040-2069				92	336	-0.79	-0.37	110	282	10	6	128	36.8
	2070-2099				100	368	-0.87	-0.3	114	308	10	6	168	38.3
3.0	2006-2039	4.5	0.84	Current No dam	108	314	-0.94	-0.41	126	280	10	6	96	36
	2040-2069				100	308	-0.83	-0.41	116	278	10	6	90	35.9
	2070-2099				100	326	-0.78	-0.34	116	298	10	6	116	36.4
3.1	2006-2039	8.5	0.84	Current No dam	106	316	-0.84	-0.42	122	276	10	6	90	35.9
	2040-2069				96	336	-0.79	-0.38	114	284	10	6	122	36.6
	2070-2099				104	366	-0.82	-0.31	120	310	10	6	156	37.4
4.0	2006-2039	4.5	0.84	Expected DO A	118	258	-1.25	-1	142	204	10	7	62	35.6
	2040-2069				112	222	-1	-0.94	128	204	10	6	56	35.5
	2070-2099				108	242	-0.98	-0.7	126	218	10	6	74	35.8
4.4	2006-2039	8.5	0.84	Expected DO A	118	258	-1.07	-1	134	204	10	7	52	35.4
	2040-2069				108	244	-0.94	-0.88	124	206	10	6	76	35.9
	2070-2099				112	264	-1.14	-0.59	130	234	11	6	102	36.7
4.1	2006-2039	4.5	0.84	Expected DO B	116	330	-1	-0.39	134	286	10	7	104	36.2
	2040-2069				108	324	-1	-0.36	122	266	10	6	88	35.9
	2070-2099				108	334	-0.98	-0.3	122	288	10	6	118	36.4
4.5	2006-2039	8.5	0.84	Expected DO B	114	328	-1.07	-0.39	128	282	10	7	92	35.8
	2040-2069				106	342	-1	-0.3	120	264	10	6	128	36.7
	2070-2099				112	366	-1.05	-0.28	126	286	10	7	162	37.5

Table 5.2: Model results for assessing the effects of projected climate on salt intrusion lengths and salt concentrations. Column 3 to 5 show all model parameters that are altered.

5.1.1 Minimum and maximum salt intrusion lengths

Comparing the results of RCP 4.5 to the results of RCP 8.5 for the scenarios in Table 5.2, more or less the same pattern for all scenarios can be detected for the minimum salt intrusion length (F1). The maximum salt intrusion length (F2) shows a clear increase when RCP 8.5 is applied. In the first period the increase is negligible for all scenarios. In the second and third period for the scenarios without dam the difference between RCP 4.5 and RCP 8.5 is respectively 9% and 12%.

The scenarios with a dam implemented show a different course. For the ecological flow operated dam, DO A, the first period shows no difference between RCP 4.5 and RCP 8.5. The second and third period respectively increase with 10% and 9% for RCP 8.5 when comparing these to the same periods for RCP 4.5. For the power production focused operations, DO B, the first period shows a negligible decrease for RCP 8.5 compared to RCP 4.5. In the second and third period this is respectively 6% and 10%.

This is an indication that the dam operations dampen the effect of projected climate on maximum salt intrusion lengths.

5.1.2 Effect on probability of exceedance

For the scenarios without dam the upper slopes of the CFD-curve (F3) the first two periods show a decrease in gradient for RCP 8.5 when comparing with RCP 4.5 this varies between -5% and -11%. This is an indication that for RCP 8.5 more variety in smaller salt intrusions lengths occur. The third period shows an increase between 6% and 12% which indicates less variety in smaller salt intrusion lengths. The lower slopes of the CFD-curve (F4) show the opposite. In the first period a negligible decrease in slope occurs after which the slope steepens between 6% and 8%.

For the scenarios with dam the upper slopes behave differently. For the ecologically operated dam, DO A, a relatively strong decrease of 14% can be seen (Figure 5.1) while for the power production operated dam, DO B this is a steepening of 7% for RCP 8.5 . The second period shows again a decrease of 14% for DO A for RCP 8.5 while for DO B no change is detected. In the third period for both lower slopes an increase in slope is detectable. This is respectively 15% and 7% for DO A and DO B. The upper slopes show a decreasing slope for the second and third period which varies between 6% and 16% for RCP 8.5 compared to RCP 4.5.

Projected climate has a different influence on the salt intrusion lengths in the estuary when a dam is implemented. The variety of salt intrusion lengths is reduced when a dam is implemented. The ecologically operated dam reduces variety the strongest.

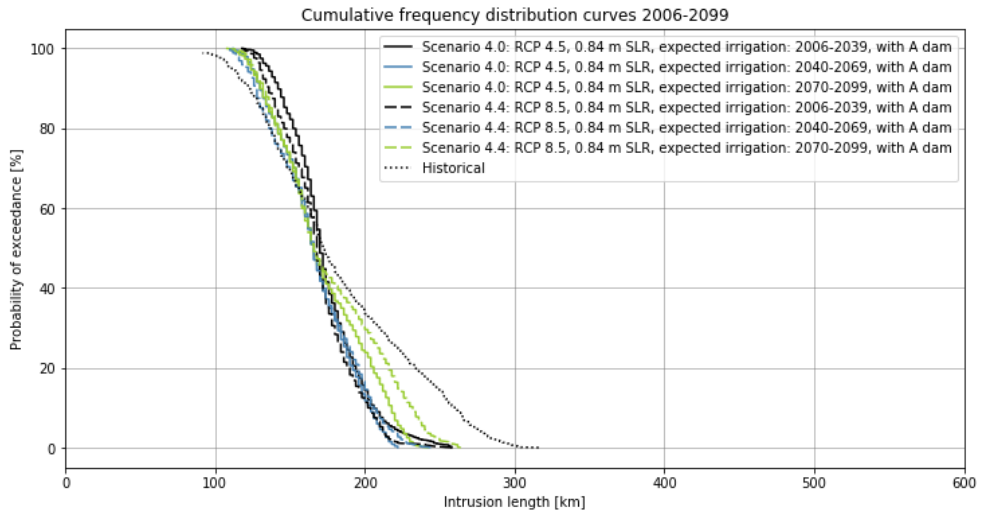

Figure 5.1: CFD curve comparing scenarios 4.0 and 4.4. The differences are most pronounced in the upper slope for the first period while the differences in lower slope are most pronounced in the last period.

5.1.3 Effect on seasonality

The effect of projected climate on the median salt intrusion lengths (F5 and F6) is marginal. A small difference of 6% can be seen in Table 5.2 when comparing RCP 8.5 to RCP 4.5 in the first period for the ecologically operated

dam (DO A). Similarly, only an increase of 7% is noticeable for the third period for the ecologically operated dam when comparing RCP 8.5 to RCP 4.5. The remainder of median wet or dry season peaks change negligible. Furthermore, there is no shift in the dry or wet season peak.

5.1.4 Effect on salt concentration

The effect of the projected climate on the length of the hypersaline region (F9) and the maximum salt concentration (F10) is significant. For all scenarios in the first period RCP 8.5 shows a decrease in the length of the hypersaline region when compared to RCP 4.5. This is -6% for the scenarios without dam and varies between -12% and -16% for the scenarios with dam. In the second and third period a strong increase can be noticed for all scenarios regardless of the dam implementation which varies between 35% and 45%. The absolute change in length range between 10-44 km.

The only increase in salt concentration can be noticed when comparing RCP 8.5 to RCP 4.5 between scenarios 0.0 and 0.1. The remainder of the scenarios shows negligible change. This indicates a dampening effect of sea level rise on the increase of salt concentrations.

5.1.5 Summary

Comparing RCP 8.5 to RCP 4.5 shows increases in maximum salt concentrations varying between 9% to 12%. Dampening effects of the hydropower dam on maximum salt intrusion lengths are visible. The variance of the smaller salt intrusion lengths is larger for RCP 8.5 in the first two periods before the gradient of the CFD-curve steepens. This is true for all scenarios except when DO B is implemented, then the lower slope of the CFD-curve continually steepens. The opposite is true for the variance of the larger salt intrusion lengths, this increases for all scenarios. This is an indication that RCP 8.5 leads to more variance in higher salt intrusion lengths. The median salt intrusion curve shows no significant changes and there is no change in seasonality between RCP 8.5 and RCP 4.5. The hypersaline region is strongly dependent on the projected climate. RCP 8.5 shows increases in the length of the hypersaline region of up to 45% when comparing to RCP 4.5. The salt concentration changes negligible except for the comparison between scenarios 0.0 and 0.1. This is an indication of a dampening effect of increasing sea level rise on projected climate.

5.2 SEA LEVEL RISE

Sea level rise is the second model parameter that will be discussed. Starting with its effects on the minimum and maximum salt intrusion lengths and followed by the effect on probability of exceedance, effect on seasonality and effect on salt concentration. The scenarios and their results for this model parameter are presented in Table 5.3 below.

scenario ID	Period:	SLR	FW	CFD-curve				Monthly median min/max				S-x curve	
				F1 [km]	F2 [km]	F3 [-]	F4 [-]	F5 [km]	F6 [km]	F7 [Mos]	F8 [Mos]	F9 [km]	F10 [g/L]
H	1971-2017	N/A	N/A	92	316	-0.74	-0.41	124	272	9	6	72	35.6
0.1	2006-2039	0	RCP 4.5	104	314	-0.94	-0.41	124	280	10	6	98	36.1
	2040-2069			96	308	-0.83	-0.39	112	278	10	6	92	36
	2070-2099			96	328	-0.78	-0.33	110	298	10	6	124	36.6
3	2006-2039	0.84	RCP 4.5	108	314	-0.94	-0.41	126	280	10	6	96	36
	2040-2069			100	308	-0.83	-0.41	116	278	10	6	90	35.9
	2070-2099			100	326	-0.78	-0.34	116	298	10	6	116	36.4
0	2006-2039	0	RCP 8.5	104	316	-0.88	-0.42	120	274	10	6	92	36
	2040-2069			92	336	-0.79	-0.37	110	282	10	6	128	36.8
	2070-2099			100	368	-0.87	-0.3	114	308	10	6	168	38.3
3.1	2006-2039	0.84	RCP 8.5	106	316	-0.84	-0.42	122	276	10	6	90	35.9
	2040-2069			96	336	-0.79	-0.38	114	284	10	6	122	36.6
	2070-2099			104	366	-0.82	-0.31	120	310	10	6	156	37.4
2	2006-2039	2	RCP 8.5	106	316	-0.84	-0.43	124	276	10	6	86	35.9
	2040-2069			98	452	-0.68	-0.27	128	322	10	6	240	37.7
	2070-2099			122	578	-0.57	-0.18	152	480	11	6	476	62.2

Table 5.3: Model results for assessing the effects of sea level rise on salt intrusion lengths and concentrations. Column 3 and 4 show all model parameters that are altered. The model parameters dam operations and irrigation development are kept constant on respectively 'no dam' and 'current irrigation'.

5.2.1 Minimum and maximum salt intrusion lengths

The minimum salt intrusion length increases for all scenarios negligibly, with the exception of the last two periods of scenario 2.0 which show respectively 7% and 22% increase compared to the scenario without sea level rise. The same pattern repeats for the maximum salt intrusion length, negligible differences between a sea level rise of 0 and 0.84 m. However, scenario 2.0 shows an increase of respectively 35% and 57% when comparing to the 0 m sea level rise scenario. The comparison of Figure 5.2 and Figure 5.3 show the huge differences between 0.84 m and 2.0 m sea level rise. It should be noted that the differences in maximum salt intrusion length for sea level rises of 0.84 m for both climate projections decreased negligibly when comparing to their 0 m sea level rise equivalent. This could indicate a dampening effect of rising sea levels on maximum salt intrusion length.

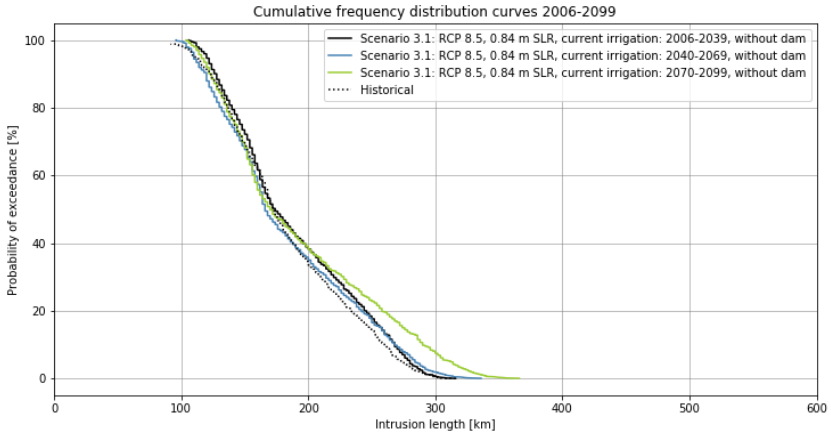

Figure 5.2: CFD-curves for scenario 3.1 of which the values can be read from Table 5.3 above. On the vertical axis shows the probability of exceedance. At 100% the value is always exceeded: the minimum salt intrusion length. Slightly above 0% lies the maximum.

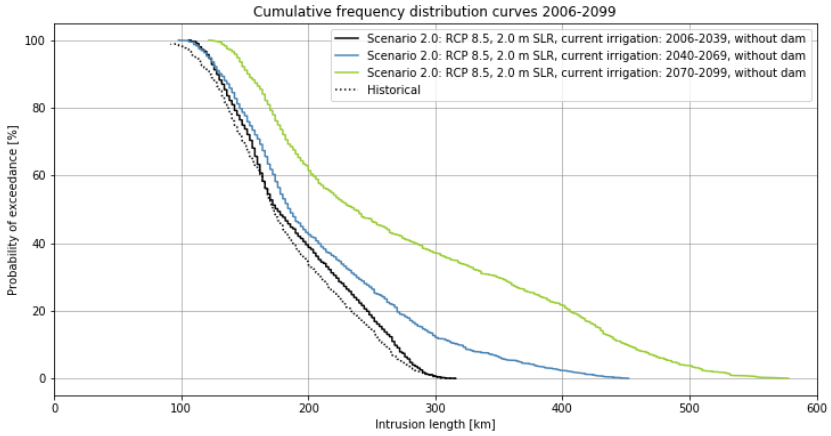

Figure 5.3: CFD-curves for scenario 2.0. When comparing with scenario 3.1 presented in the figure above, it can be seen that for the first period there are barely differences while the 2nd and 3rd period show large differences.

5.2.2 Effect on probability of exceedance

Comparing both 0.84 m sea level rise scenarios with their 0 m sea level rise equivalents no significant differences can be spotted in either lower or upper slopes of their CFD-curves. For the 2.0 m sea level rise a significant decrease in both lower and upper slope can be detected of up to 41% in the third period when comparing to the 0 m equivalent. This is can be seen well in Figure 5.3.

5.2.3 Effect on seasonality

Looking at the wet season median dip (F5) an increase of 5% can be seen for both 0.84 m sea level rise scenarios when comparing with their 0 m sea level rise equivalents in the third period, the remaining periods show negligible change. It should be noted that although negligible the magnitude of the difference grows over time for the 0.84 m sea level rise scenarios. This indicates that rising sea levels cause a deeper inland salt front during the wet season. The dry season median peak (F6) is however not affected by the 0.84 m sea level rise scenarios. This is visualized in Figure 5.4.

The 2.0 m sea level rise shows again a much stronger response. In the second and third period the wet season median increases with respectively 16% and 33% when comparing to the 0 m sea level rise scenario. For the dry season median peak this is respectively 14% and 56%. Further more the wet season dip shifts with one month onto later in the year for the last period. This indicates a longer dry season which can be seen in Figure 5.5.

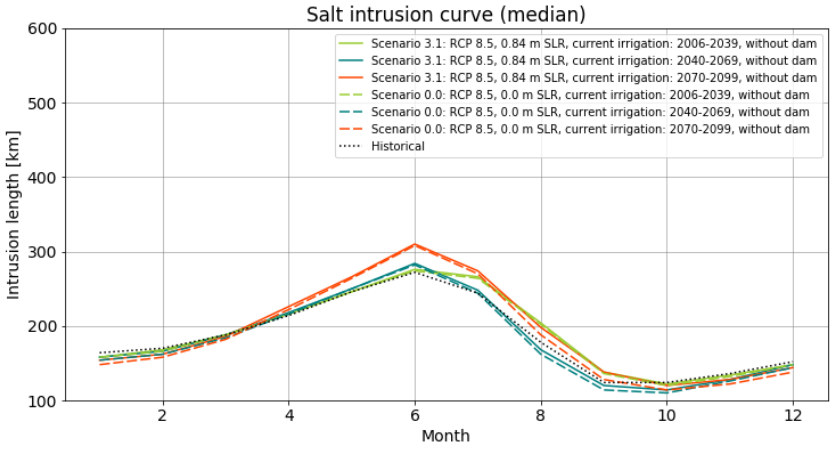

Figure 5.4: Monthly median salt intrusion curves for each time period for scenario 3.1 and reference scenario 0.0. It can be seen that the differences between scenario 3.1 and the reference scenario are very small.

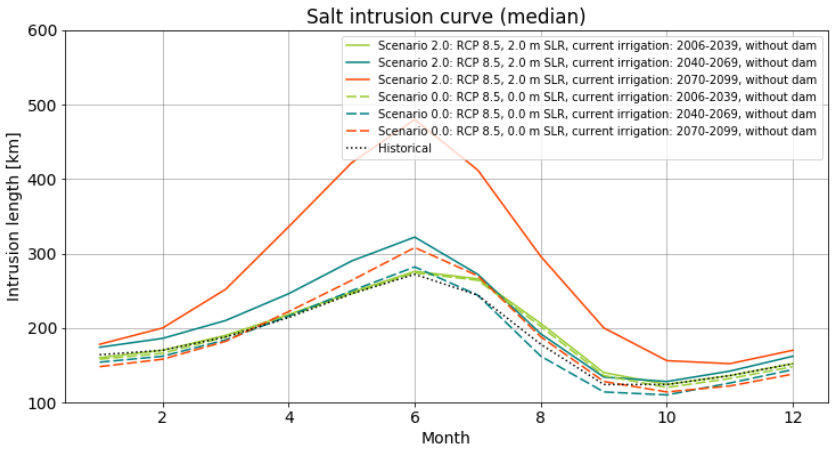

Figure 5.5: Monthly median salt intrusion curves for scenario 2.0 with reference scenario 0.0. Comparing this figure with the figure above; it can be seen that the first period shows more or less the same differences while the second and third period show large differences with the reference scenario.

5.2.4 Effect on salt concentration

Comparing the hypersaline region and salt concentrations, respectively F9 and F10, between the 0.84m sea level rise scenarios and the respective 0 m sea level rise equivalents, show remarkable results. The length of the hypersaline region decreases slightly, up to 7% in the third period. This effect is slightly stronger for the scenario which also applies RCP 8.5 which confirms the somewhat dampening effect of sea level rise on salt intrusion. The maximum salt concentrations decrease negligibly.

2.0 m sea level rise shows a decrease in the length of the hypersaline region of 7% in the first period. The second and third period however, show an increase of respectively 88% and 183% in the size of the hypersaline area. More than doubling the size of the hypersaline area of the 0 m equivalent in the third period. The maximum salt concentration only increases significantly in the third period with 62%, coming close to double the ocean salinity.

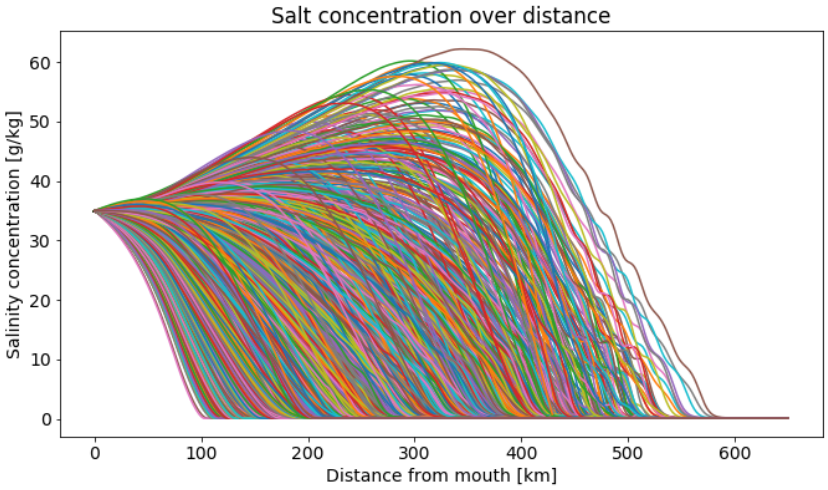

Figure 5.6: Salt concentration plot for scenario 2.0. Each line is a timestep (10 day period) and gives a salinity profile of the Gambia river. The humpback shape of a hypersaline estuary is clearly visible (see Figure 3.4). The temporal aspect of when hypersalinity occurs is not visible in this figure and should instead be read from Table 5.3.

5.2.5 Summary

Sea level rise has little impact on minimum and maximum salt intrusion lengths and the variance of salt intrusion lengths. In addition, no significant impact on the dry season median peak and wet season median dip can be noticed. A 0.84 m increase in sea level does however show a dampening impact on the length of the hypersaline region, reducing it slightly when compared to the 0 m sea level rise equivalents. It has no impact on maximum salt concentrations.

The 2.0 m sea level rise shows different results. There are strong increases in minimum and maximum intrusion lengths and the variance of salt intrusion lengths increase significantly, indicating less predictability of salt intrusion lengths in the estuary. Furthermore, the increase in both wet season and dry season median peaks shows an overall shift of salt intruding further inland. The length of the hypersaline region grows significantly compared to the 0 m sea level rise equivalent from 168 to 476 km. The maximum salt concentration also increases with 62% coming close to double ocean salinity.

5.3 RESERVOIR FILLING

The filling of the reservoir is the third item that will be discussed, it is not a model parameter but a separate model run to see what effect the construction of the dam has on salt intrusion. Furthermore, only one period, from 2006-2039 is included in the model run. This is because the construction is expected to start in 2024 and last for a maximum of two years. The results are discussed starting with the effects on the minimum and maximum salt

intrusion lengths, followed by the effect on probability of exceedance and monthly median. The difference between scenarios 1.0 and 1.1 is the time that the reservoir behind the dam requires to be filled. Scenario 1.0 assumes this takes 1 year and scenario 1.1 assumes this will take 2 years. During this time the amount of flow through the dam is reduced (see 3-64 to 3-71 in OMVG and EIES (2014)). The results of these scenarios can be found in Table 5.4 below.

Scenario ID:			CFD-curve				Monthly median	
	Period:	ID	F1 [km]	F2 [km]	F3 [-]	F4 [-]	F5 [km]	F6 [km]
H	1971-2017	N/A	92	316	-0.41	-0.74	124	272
0	2006-2039	Current	104	316	-0.42	-0.88	120	274
1	2006-2039 [2024]	Expected	104	314	-0.42	-0.92	132	295
1.1	2006-2039 [2024-2025]	Expected	104	324	-0.41	-0.92	132	295

Table 5.4: Model results for assessing the effects of reservoir filling on salt intrusion lengths. The projected climate and sea level rise are constant and respectively RCP 8.5 and 0.0 m sea level rise.

5.3.1 Minimum and maximum salt intrusion lenghts

There is no difference when comparing both scenarios with the minimum salt intrusion lengths to the reference scenario. The maximum intrusion length however shows an increase for the case in which the filling of the reservoir takes two years, while the single year scenario shows a decrease. The increase and decrease in both scenarios are negligibly small.

5.3.2 Effect on probability of exceedance

Similarly, the change in both the upper slope that indicates the variety of the more common salt intrusion lengths as well as the lower slopes which indicates the variety of the less common salt intrusion lengths is negligibly small for both scenarios.

5.3.3 Effect on seasonality

The monthly median salt intrusion peaks change as much for the single year filling as for the two-year filling scenario. The dry season peak increases more indicating a shift to deeper inland salt intrusion lengths during the filling of the reservoir, independent on the duration. The comparison can be seen in Figure 5.7. This indicates a longer period with high salt intrusion lengths for the scenario in which the dam fills for two consecutive years.

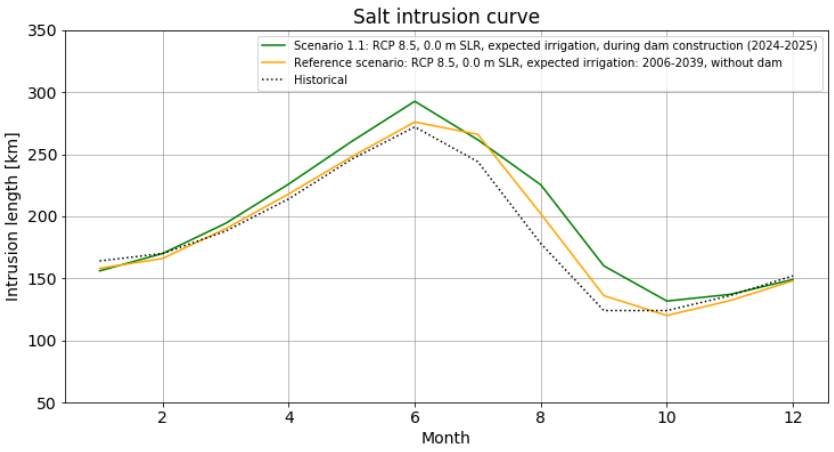

Figure 5.7: Monthly median salt intrusion curve for the 2 year filling scenario compared to the reference scenario.

5.3.4 Summary

The filling of the reservoir has a small impact. Compared to the reference scenario there is a shift in maximum intrusion length. The more common salt intrusion lengths do not change their variance but the less common salt intrusion lengths do, which indicates a less predictable salt intrusion pattern for less likely salt intrusion lengths. Furthermore, an increase of the monthly median dry season peak indicates more often occurring deeper inland salt intrusion lengths.

5.4 DAM OPERATIONS

The dam operational schemes are the third model parameter that will be discussed. The results will be discussed starting with the effects on the minimum and maximum salt intrusion lengths and followed by the effect on probability of exceedance, effect on seasonality and effect on salt concentration. The scenarios and their results for this model parameter are presented in Table 5.5 below. Scenarios 3.0 and 3.1 will be used as reference scenarios since these are the scenarios where no dam has been implemented while the remaining parameters are the same.

scenario ID				CFD-curve				Monthly median min/max				S-x curve	
	Period:	FW	DO	F1 [km]	F2 [km]	F3 [-]	F4 [-]	F5 [km]	F6 [km]	F7 [Mos]	F8 [Mos]	F9 [km]	F10 [g/L]
H	1971-2017	N/A	N/A	92	316	-0.74	-0.41	124	272	9	6	72	35.6
3	2006-2039	RCP 4.5	No dam	108	314	-0.94	-0.41	126	280	10	6	96	36
	2040-2069			100	308	-0.83	-0.41	116	278	10	6	90	35.9
	2070-2099			100	326	-0.78	-0.34	116	298	10	6	116	36.4
3.2	2006-2039	RCP 4.5	A	118	258	-1.25	-1	140	202	11	7	60	35.6
	2040-2069			112	220	-1	-1	128	202	10	6	54	35.5
	2070-2099			108	242	-0.98	-0.74	126	216	10	6	74	35.8
3.3	2006-2039	RCP 4.5	B	116	322	-1	-0.39	134	284	10	7	100	36.1
	2040-2069			108	316	-1	-0.37	122	264	10	6	86	35.8
	2070-2099			108	328	-1.05	-0.3	122	288	10	6	114	36.4
3.1	2006-2039	RCP 8.5	No dam	106	316	-0.84	-0.42	122	276	10	6	90	35.9
	2040-2069			96	336	-0.79	-0.38	114	284	10	6	122	36.6
	2070-2099			104	366	-0.82	-0.31	120	310	10	6	156	37.4
3.4	2006-2039	RCP 8.5	A	118	258	-1.07	-1	134	202	10	7	52	35.4
	2040-2069			108	242	-0.94	-0.94	124	204	10	6	74	35.9
	2070-2099			112	262	-1.05	-0.59	130	232	11	6	102	36.6
3.5	2006-2039	RCP 8.5	B	114	322	-1.07	-0.39	128	282	10	7	88	35.7
	2040-2069			106	338	-1.07	-0.31	120	262	10	6	124	36.7
	2070-2099			112	360	-1.05	-0.28	126	282	10	7	158	37.4

Table 5.5: Model results for assessing the effects of dam operations on salt intrusion lengths and salt concentrations. Sea level rise and irrigation development are constant and respectively 0.84 m sea level rise and 'current' irrigation development.

5.4.1 Minimum and maximum salt intrusion lengths

Table 5.5 shows scenarios with several possible operational schemes for the hydropower dam and both RCPs. In Table 5.5 above 'A' and 'B' respectively stand for the 'ecology focused operations' and 'power production focused operations'.

When comparing the ecology focused operations, DO A, with the reference scenarios it can be seen that the minimum salt intrusion lengths increase significantly ranging between 8% and 13%. However, maximum salt concentrations decrease significantly for these operations ranging between -18% and -29%. The magnitude of these in and decreases range between +10 km and -104 km. When comparing the power production focused operations, DO B, with the reference scenarios a different pattern is visible. Again an increase in minimum salt intrusion lengths of the same magnitude as for DO A can be seen. However, the maximum salt intrusion lengths do not decrease but increase negligibly.

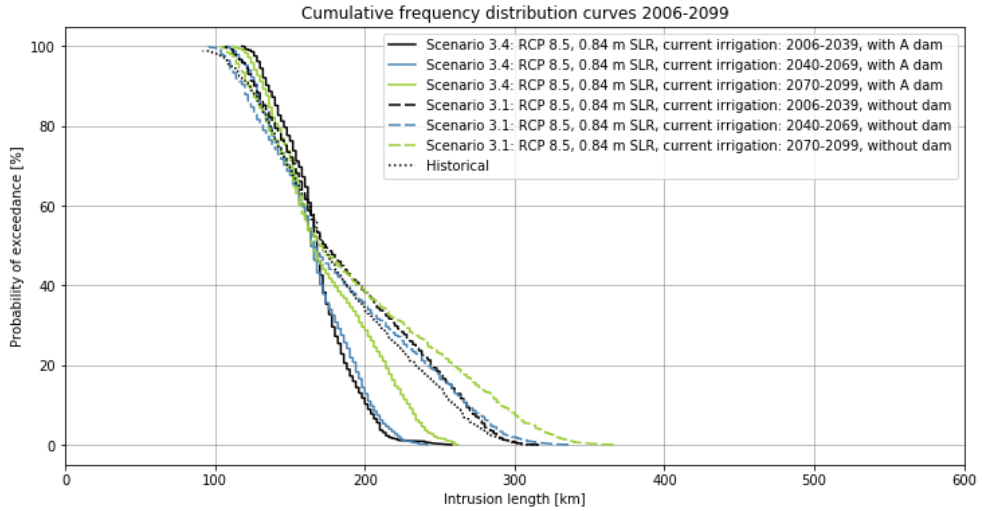

Figure 5.8: CFD-curves for scenario 3.4 and reference scenario 3.1. The increase in minimum salt intrusion length can be seen as well as the decrease in maximum salt intrusion length. The steepening in the slopes is visible as well, indicating a trend of more stabilized salt intrusion lengths.

5.4.2 Effect on probability of exceedance

The comparison of the ecological operations, DO A, show a strong steepening of the gradient of the upper CFD-curve (F3) for DO A compared to the reference scenarios. The increase in slope ranges between 19% and 33%. The increase in the lower CFD-curve is even more substantial which ranges between 88% and 150%. Figure 5.8 visualizes these changes in slope for scenario 3.4 compared to scenario 3.1. The increase in slope of both the upper and lower part of the CFD-curve indicates more predictable salt intrusion lengths with less variation.

When making the same comparison for the power production focused operations, DO B, a similar increase in upper slope can be detected, ranging between 7% and 36%. The lower slope however, decreases between 5% and 17%. This indicates less predictable higher salt intrusion lengths. This is visualized in Figure 5.9.

Comparing Figure 5.8 and Figure 5.9 gives an impression of the differences between the implemented dam operations and the range between dam operations can influence the degree of salt intrusion.

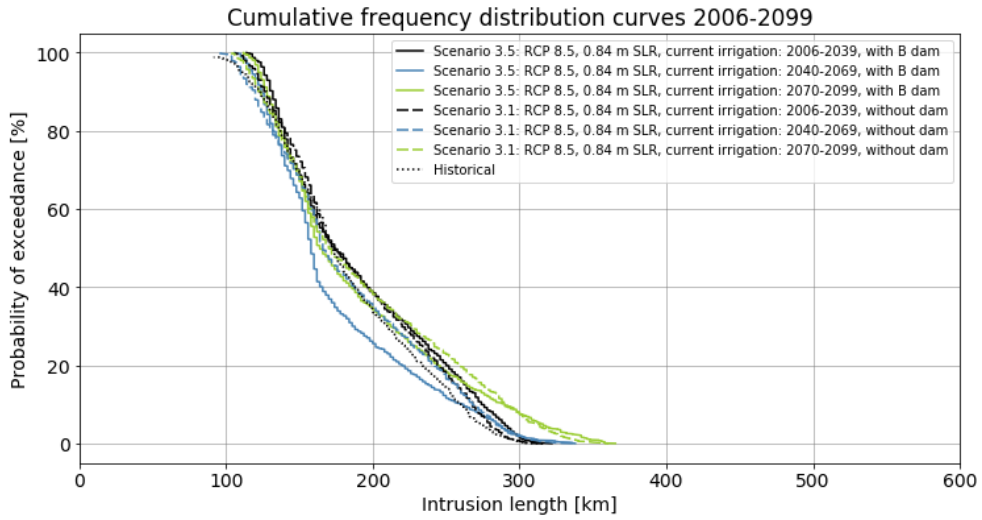

Figure 5.9: CFD-curves for scenario 3.3. The steepening in the upper slopes and afterwards the flattening of the lower slopes can be seen. This indicates less variety in small salt intrusion lengths while the larger salt intrusion lengths show more variety.

5.4.3 Effect on seasonality

Ecological operations can cause a shift in the wet season median peak towards later in the year. This is not the case for power production focused operations. Both dam operations cause during some periods a shift in the dry season peak towards later in the year as well. This can lead for DO A to a shortening of the dry season while for DO B this can lead to a longer dry season.

Comparing Figure 5.10 with Figure 5.11 show the difference between the two operating schemes. The prolonged dry season can be noticed for DO B whereas for DO A only a shift in salt intrusion length occurs.

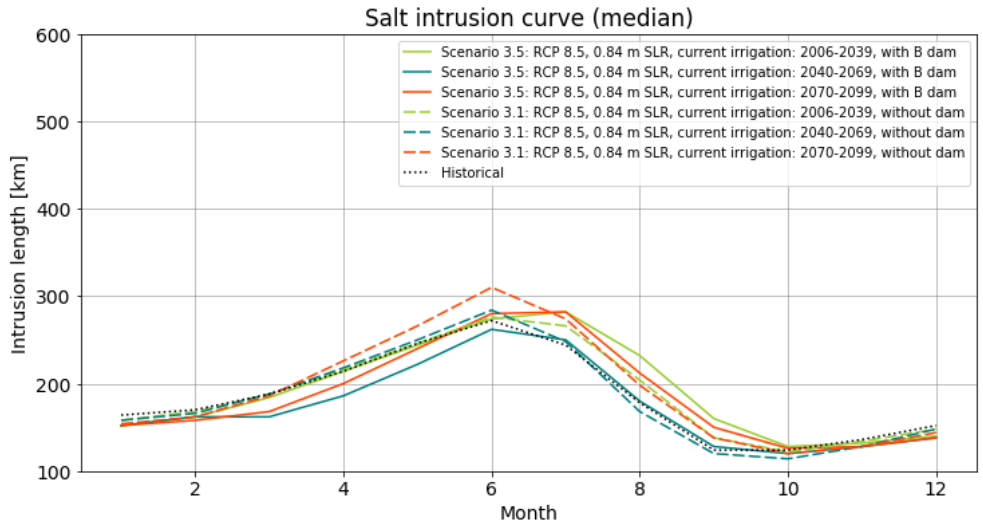

Figure 5.10: Monthly median salt intrusion for scenario 3.5 compared to the reference scenario 3.1. In this case a shift of dry and wet season peaks is visible for the first and third period.

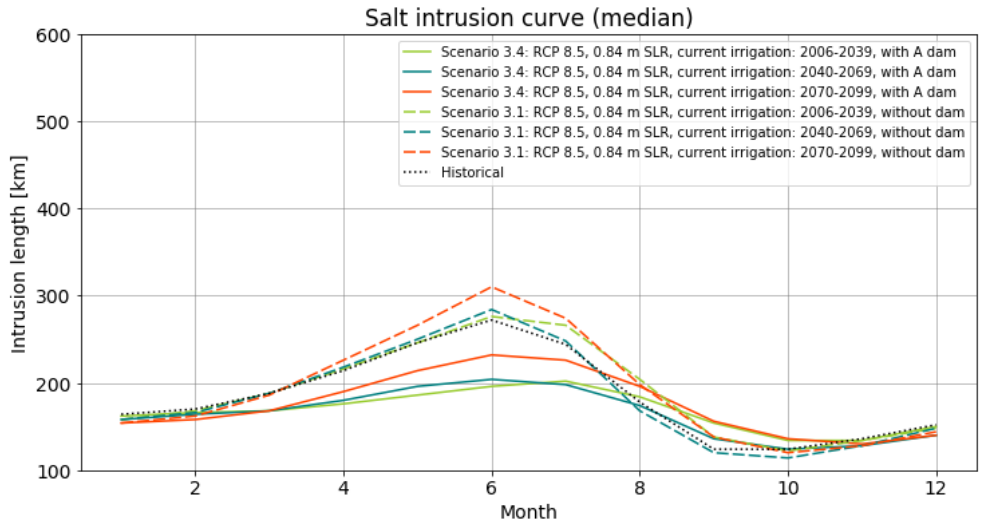

Figure 5.11: Monthly median for scenario 3.4 compared to the reference scenario 3.1. A reduction in dry season median and shift in seasonality are well visible.

5.4.4 Effect on salt concentration

The ecological operated dam has significant influence on the length of the hypersaline region. Reductions between 35% and 42% compared to the scenarios without dam can be seen. The power production focused operations show negligible differences and no trend. For both ways of operating the dam the maximum salt concentration is negligibly impacted.

5.4.5 Summary

Both ways of operating the dam are created to be extremes which is reflected in their impact. This is visualized in the figures above.

The ecological dam operations show an increase in minimum salt intrusion length of up to 13% compared to the situation without dam. The maximum salt intrusion length decreases significantly, up to 29%. This leads to a more stabilized flow which is represented by the steepening of both slopes of the CFD-curve. The monthly median peaks continue with this pattern, slightly increasing the peak during the wet season and decreasing the peak strongly during the dry season. Further more a strong impact on the length of the hypersaline region can be noticed for these dam operations. However, no significant change in salt concentrations can be noticed.

The power production focused operations show a totally different impact. The minimum salt intrusion lengths still increase up to 10% but no reduction of the maximum salt intrusion length can be seen. The lower slope of the CFD-curve flattens which indicates more variation for the rarer salt intrusion lengths. Furthermore, no significant changes in the wet and dry-season peaks can be noticed. The length of the hypersaline region changes negligibly as well as the maximum salt concentrations.

5.5 IRRIGATION DEVELOPMENT

Irrigation development is the final model parameter that will be discussed. Starting with its effects on the minimum and maximum salt intrusion lengths and followed by the effect on probability of exceedance, effect on seasonality and effect on salt concentration. The scenarios and their results for this model parameter are presented in Table 5.6 below. Scenarios 3.2 and 3.4 will be used as reference scenarios since these have the current level of irrigated area.

scenario ID				CFD-curve				Monthly median min/max				S-x curve	
	Period:	FW	ID	F1 [km]	F2 [km]	F3 [-]	F4 [-]	F5 [km]	F6 [km]	F7 [Mos]	F8 [Mos]	F9 [km]	F10 [g/L]
H	1971-2017	N/A	Current	92	316	-0.74	-0.41	124	272	9	6	72	35.6
3.2	2006-2039	RCP 4.5	Current	118	258	-1.25	-1	140	202	11	7	60	35.6
	2040-2069			112	220	-1	-1	128	202	10	6	54	35.5
	2070-2099			108	242	-0.98	-0.74	126	216	10	6	74	35.8
4	2006-2039	RCP 4.5	Expected	118	258	-1.25	-1	142	204	10	7	62	35.6
	2040-2069			112	222	-1	-0.94	128	204	10	6	56	35.5
	2070-2099			108	242	-0.98	-0.7	126	218	10	6	74	35.8
4.2	2006-2039	RCP 4.5	Max	118	270	-1.25	-0.94	142	208	11	7	66	35.7
	2040-2069			114	228	-1	-0.94	128	210	10	6	60	35.5
	2070-2099			108	250	-1.05	-0.67	126	226	10	6	78	35.9
3.4	2006-2039	RCP 8.5	Current	118	258	-1.07	-1	134	202	10	7	52	35.4
	2040-2069			108	242	-0.94	-0.94	124	204	10	6	74	35.9
	2070-2099			112	262	-1.05	-0.59	130	232	11	6	102	36.6
4.4	2006-2039	RCP 8.5	Expected	118	258	-1.07	-1	134	204	10	7	52	35.4
	2040-2069			108	244	-0.94	-0.88	124	206	10	6	76	35.9
	2070-2099			112	264	-1.14	-0.59	130	234	11	6	102	36.7
4.6	2006-2039	RCP 8.5	Max	120	258	-1.07	-0.88	136	208	10	7	56	35.5
	2040-2069			110	250	-0.94	-0.79	124	212	10	6	80	36
	2070-2099			112	272	-1.05	-0.57	132	242	11	6	108	36.8

Table 5.6: Model results for assessing the effects of irrigation development on salt intrusion lengths and salt concentrations. Sea level rise and dam operations are constant and respectively 0.84 m sea level rise and ecological flow, DO A.

5.5.1 Minimum and maximum salt intrusion lengths

Table 5.6 shows six scenarios. These are chosen such that the three agricultural development irrigation areas (current irrigated area, expected irrigated area and maximum irrigated area) are applied. The remaining parameters are kept constant, with a sea level rise of 0.84 m and ecological dam operations, DO A.

Comparing the minimum salt intrusion lengths of the expected and maximum irrigated areas to the current irrigated area shows negligible changes. For the expected irrigated area scenarios, no change is noticeable while for the maximum irrigated area scenarios there is a negligibly small increase.

The maximum salt intrusion lengths do show some differences between the selected scenarios. The expected irrigated area now has negligibly small increases while the maximum irrigated area shows a bigger increase.

5.5.2 Effect on probability of exceedance

When comparing the reference scenarios (3.2 and 3.4) with the other scenarios presented in Table 5.6 it becomes clear that the upper slopes (F3) show no change or a very small steepening (scenario 4.2, p3 and scenario 4.4, p3 show an increase of respectively 7% and 8%). This is visualized in Fig-

ure 5.12.

The lower slopes (F4) show slightly more change. The slopes for the expected irrigated area flatten slightly. This indicates more variation in less common salt intrusions. The slopes for the maximum irrigated area flatten slightly more, especially for RCP 8.5. All variations in the lower slopes point towards a slight flattening of the lower slope with increasing irrigated area. Never the less this is could be considered negligible. Figure 5.12 shows the different CFD-curves for current irrigated area and the maximum increase in irrigated area.

5.5.3 Effect on seasonality

Both dry and wet season peaks vary negligibly due to the change in irrigated area. Furthermore, no shift in seasonality due to the increase in irrigated area can be noticed.

5.5.4 Effect on salt concentration

There is no effect on salt concentrations noticeable due to an increase in irrigation areas.

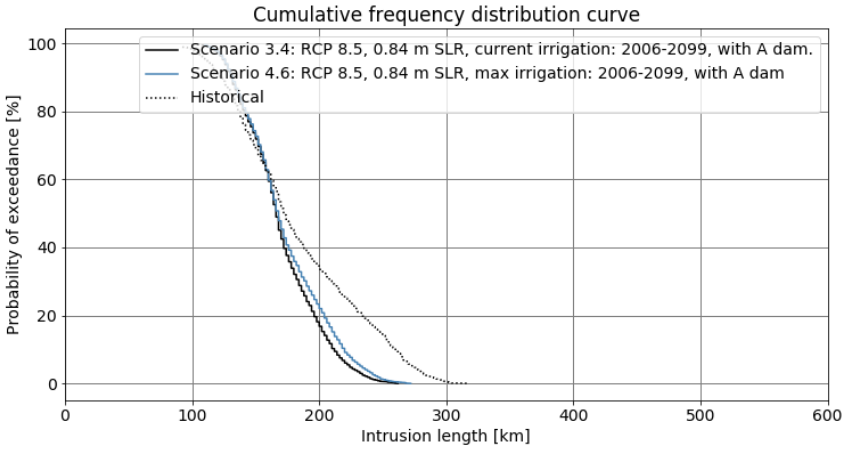

Figure 5.12: Scenario 3.4 which is used as reference scenario to see the influence of change in irrigated area. Scenario 4.6, which has the maximum irrigated area applied shows no change in small salt intrusion lengths but does affect larger salt intrusion lengths.

5.5.5 Summary

Irrigation development does not have an effect on minimum or maximum salt intrusion length. Furthermore, the length of the hypersaline region and maximum salt concentrations within the estuary do not depend on the irrigated area. There is however an increase in the monthly median peak for the dry season when the maximum irrigated area is implemented. This also

shows in the variety of less common salt intrusion lengths which slightly flattens for scenario 4.6 (see Figure 5.12).

5.6 SUMMARY OF MODEL PARAMETERS INFLUENCE

Projected climate has a mediocre impact on the salt intrusion lengths in the Gambia. Small changes in minimum salt intrusion lengths of several kilometres can be seen while relatively large changes of around 40 km can be seen when comparing the maximum salt intrusion length in the last period. The scenarios also reveal a synergy between the hydropower dam and the climate projections, if the hydropower dam is in place it reduces the differences between the climate projections by 50%. Resulting in a difference of about 20 km for the maximum salt intrusion length in the last period.

When RCP 8.5 is applied the salt intrusion lengths become less predictable due to a larger range wherein the salt front can vary. Furthermore, the hypersaline region, the length of the river that is hypersaline grows significantly when comparing RCP 8.5 with RCP 4.5 ($\pm$40%). This shows that the estuary is sensitive to and strongly affected by the evolution of projected climate.

Please note that the projected climate is in this case a model parameter that influences precipitation, discharge and evaporation only. It therefore has effect on the availability of freshwater but not on sea level rise.

When sea level rise is moderate, and the river stays within the river banks, its effects on salt intrusion have a moderate impact. It dampens the effects of strong climate projections (RCP 8.5) on larger salt intrusion lengths. This also results in a more predictable range of salt intrusion lengths (smaller range wherein the salt front moves). The average salt intrusion length shifts inland with increasing sea level rise. Remarkably, a rising sea level also decreases the length of the hypersaline region and salt concentrations, albeit only by a little.

However, when sea level rise is strong, and the river is forced outside of its boundaries, the effects on salt intrusion are entirely different. Due to the river being forced outside of its banks, the freshwater is evaporated quickly. This results in a strong landward shift of salt intrusion lengths. Minimum salt intrusion lengths increase up to 22% before the end of the century, while maximum salt intrusion lengths can intrude up to 57% ($\pm 210 km$) further compared to milder sea level rise scenarios. Furthermore, such extreme sea level rise results in a strongly hypersaline estuary during the dry season. The length of the hypersaline region grows strongly ($\pm$183%) and the maximum salt concentration within the estuary reaches almost double ocean salinities.

The filling of the reservoir has a small impact which is only noticeable in the median salt intrusion during the dry season. This increases to some extent and is slightly stronger in case that the filling will take two years.

The dam operations show large differences in their impact. One being a strong reductor of extreme salt intrusion lengths (ecological flow, DO A), the other increasing them slightly (power production focused, DO B). The ecologically operated dam shows a strongly stabilized estuary in terms of salt intrusion. This makes it easy to predict between what ranges the salt front will be. Furthermore, it has strong decreasing effects on the length of the hypersaline region. The power production focused operations show large similarities with the reference scenarios (scenarios 3.0 and 3.1), it improves the predictability of the salt front at the cost of the salt front being deeper inland. Neither of the dam operations has significant influence on the salt concentrations.

Irrigation development has negligible effects allover. The maximum use of irrigation shifts the occurrence of rarer salt intrusion lengths slightly.

5.7 EXPECTATION AROUND NON-MODELLED PARAMETERS

In this section, the influence that sea level rise and the hydropower dam might have on morphology, and the effect that might have on further salt intrusion will be discussed. Secondly, a small literature review presents the effects that sea level rise and hypersalinity have on the vegetation in and around the estuary.

5.7.1 Morphological effects due to dam and sea level rise

The hydropower dam will trap sediment which lead to a decrease in sediment supply downstream of the dam. This change in sediment supply will affect the river morphology which influences salt intrusion. Besides the dam the rising sea level also affects river morphology. Respectively the hydropower dam and sea level rise can be seen as an upper and lower boundary (see Figure 5.13).

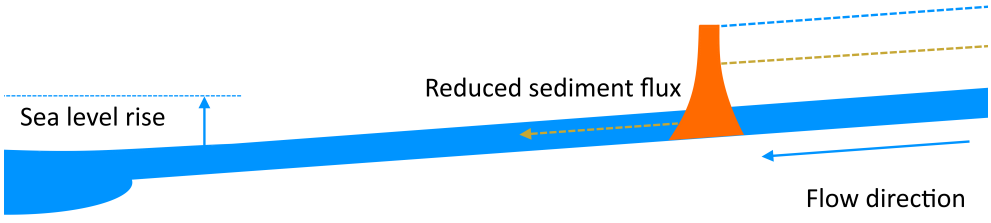

Figure 5.13: Simplified visualization of sea level rise and sediment build up due to the hydropower dam.

It is important to note that the Gambia river is an alluvial river along the entire length of the river. This implies that the river can adjust its slope as

well as its width. Secondly, a variable flow (dry and wet season flow) with an averaged sediment flux is present. The hydropower dam will attenuate the wet season flows and increases the current dry season flows. Since sediment flux is non-linearly related to the flow per meter width the total downstream directed sediment flux presumably will change.

Expert interview

To get an impression of the possible effects on river morphology due to the hydropower dam and sea level rise an interview was conducted with professor C.J. Sloff, an expert on sedimentation processes and sediment management in reservoirs. The interview started with the preliminary statement that it is very hard to say what will happen and that the following possibilities might not happen. As previously described the hydropower dam and sea level rise pose two boundaries which affect the river and estuary.

The hydropower dam can be operated in several ways. This study treats two of them (ecological flow power production) but there is another possibility within the power production category: peaking. Peaking is applied in water scarce regions and it is based on the expected power usage. During the day when power usage peaks energy is produced while during the night, when there is barely any power usage water is saved. If such an operating strategy is applied this creates oscillations in water level between day and night, high and low water. These oscillations cause increased bank erosion compared to when there is a normal, relatively constant flow. The oscillations are strongest near the dam and dampen over distance, however their effect on bank erosion should not be underestimated. Bank erosion is also dependent on the composition and strength of the river banks. If the bank erodes the river widens, this leads to a decrease of depth which can alter the river's characteristics.

Another effect of the hydropower dam is a change in the amount of sediment that is let through. This depends on the type of sediment that is present in the river and the dam and its reservoir's characteristics; how high is the dam; what discharge is let through; what is the size of the reservoir etc. What usually happens is that the heaviest particles such as gravel and sand sink to the bottom of the reservoir. Lighter particles such as clay and silt partially pass through the dam. The amount of sediment that passes through the dam is important for the change in morphology. Just after construction of the hydropower dam the transport capacity of the river is the same as before. If there is a strong sediment reduction this sediment is supplied from the riverbed. However, the riverbed is often covered with larger pieces of sediment, which cannot be transported with such flow. This causes that only the fine sediment entrapped in the riverbed is taken. This leads to a downward migrating wave where the fine sediments are removed from the bed. Due to gravel and sand being trapped in the reservoir the ratio of sediments changes from partially coarse and partially fine to a majority of fine particles. This causes the river to become muddier, especially in the saline parts of the river and in the estuary. Clay interacts with salt, which

creates larger flakes that sediment faster than single clay particles. A strong increase in mud (clay and silts) is to be expected in the downstream regions. In the long term, the slope of the river adjusts to the new sediment load. This is a very slow process. The larger particles at the bottom of the river are not easily transported and protect the underlying sediments. Furthermore, the hydropower dam changes the flow pattern, attenuating the minimum and maximum flows. Since the transport capacity is non-linearly dependent on the flow it is possible the total sediment flux decreases even though the minimum flows increase. If the river becomes wider due to bank erosion it becomes less deep. This can form a new equilibrium based on sediment supply but leads to another threat. Vegetation can grow on parts it could not before. If then a high water event occurs (e.g. upstream storm and lots of water spilled over/through the hydro power dam) the river has higher friction and lower transport capacity which increases the chance on flooding.

On the downstream end of the river sea level increases depth. The tidal influence increases which increase the amount of water flowing in and out of the estuary. If the sediment supply from upstream is large enough, the river bed can grow with the sea level rise. Coastal erosion due to the reduced sand supply should be expected and due to the attenuation of the hydrograph. However, the erosion or sedimentation in the coastal region is very complex and hard to predict.

Apart from the clear positive effects of a hydropower dam there are always unexpected negative consequences. The effects of a change in sediment supply are often underestimated or overlooked. Furthermore, unbalancing the system has clear negative effects for the population. Care has to be taken for them so that they can cope with the change. Besides the morphological changes also ecological and environmental changes should be expected.

5.7.2 Effects of sea level rise and salination on vegetation

Mangrove forests consist of several species of mangrove trees. These can be roughly distinguished into four types by their sensitivity to salt concentration and sensitivity to water depth. Mangrove trees that are in an environment that is too saline will migrate upstream, towards fresher water. Mangrove trees that are in too deep water will migrate towards higher ground. These migratory processes are slow and with too steep increase in either salt concentration or sea level rise (water depth) these mangroves will be threatened (Simpson, 2020).

Fent et al. (2019) confirmed a net increase in mangrove tree cover nationally between 1988 and 2018 after a period of drought in the 1970s and 80s. It shows the sensitivity of mangroves to lack of freshwater and partially the effort that is made in conserving and increasing these areas. Earlier studies confirmed a severe decrease of mangroves (e.g. (Carney et al., 2014)) caused by these droughts. The mangroves have a double function, on one side they are the nursery of many fish and other species and on the other side they

protect coastal regions by reducing their vulnerability (Guannel et al., 2016). However, Ellison (1993) already showed in 1993 that the now thriving mangrove forests will retreat with increased sea level rise. Similarly, Naidoo et al. (2011) showed with their research in 2011 that hypersaline environments are detrimental for mangroves. Under certain scenarios either one or both of these negative impacts will increase the stress on the mangrove forests present in The Gambia. The expected reduction of mangrove forests increases the sensitivity to a reduced sediment flux.

6 LIMITATIONS

This chapter will discuss limitations of this study. First the data and quality of model output will be discussed after which several other limitations will be discussed.

6.1 DIFFERENT DATA SOURCES AND SALT INTRUSION ERROR

The acquired data to model the salt intrusion of the Gambia river consists of many separate sources. Because these sources are often not linked, the quality of the model results can be questioned. The SALNST model used to predict parameter influence is calibrated on historic data. The historic-evaporation, discharge, precipitation and water usage for irrigation are of unknown quality. The methods that were used to obtain these data or some sort of accuracy are not mentioned.

To be able to estimate within what range the model outputs lie an error analysis should be performed. The use of fewer data sources (e.g. projected climate) should lead to an easier estimate of this range. However, this analysis has not been done due to time constraints. Keeping in mind the limitations of the data that have been used in the model lead to a sounder understanding of the quality of the model output. Figure 4.12 contains the overview of the used data in the model. Specifically discharge and evaporation are sensitive parameters.

The discharge is based on the relation between historic measurements of discharge and historic measurements of precipitation a model has been created (Appendix C). This model generates monthly discharge based on projected precipitation. The SALNST model makes use of this monthly data but assumes it to be constant over the month.

Thornthwaite's method has been used to estimate evaporation. This method is ideal because only the daily temperature is required to estimate evaporation for the modelled timescale. Furthermore, the method is not prone increasing errors in time series analysis, such as Hargreaves. However, due to the use of such a basic method the estimates of evaporation might be far off. In addition, the respective average monthly temperature of RCP 4.5 and 8.5 rose between 2.1 and 3.9 degrees between 2006 and 2099, and the average monthly evaporation rose respectively with 112 and 228 mm. Since the precipitation does not vary significantly between the start and end of the

modeling period this increase in evaporation has a relatively high impact. These combinations makes evaporation another sensitive parameter.

6.2 EVAPORATION AND CALIBRATION

Besides the sensitive nature of determining the evaporation, the calibration phase adjusts the evaporation to optimize model results. Afterwards open water evaporation is calculated by adjusting the potential evaporation according to Verkerk and Van Rens (2005). Since the hydropower dam is currently non-existent, the calibration on measured salt concentrations does not take open water evaporation into account.

Similarly, the scenarios where sea level rise forces the river outside of its boundaries, also make use of this calibration parameter. The calibration adjusted the evaporation such that the model results and salt concentration measurements showed a good fit. Furthermore, previously the model had a constant river surface, allowing for the evaporation to be used as a calibration parameter. However, due to the strong expansion of the river and therefore the river's evaporative surface this scaling could lead to an overestimation of the extra evaporated water. Once the threshold value is exceeded and the evaporative surface is significantly increased one can question if the calibration is still correct for this situation and not an overestimation.

6.3 NUMERICAL NATURE

Another limitation that has a strong impact on the model results is the numerical nature of the model (see Appendix B for the solving strategy of the model). Small errors due to rounding lead to increasingly large errors when the amount of calculation steps increase. Therefore the errors are largest for large salt intrusion lengths. The dependency of salinity on dispersion and vice versa (see Chapter 3) increases the amount of calculation steps, this results again in an increasing error. These errors result in oscillations in which salt intrusion is under- and overestimated, as can be seen in Figure 5.6. Due to the numerical error propagation the most interesting results of extreme salt intrusion are at the same time the least accurate. However, trends can still be detected.

6.4 DAM OPERATIONS

Scenario 'DO A' derived from the environmental study (OMVG & EIES, 2014) has unclear relations between water levels in the reservoir and the discharge. These relations could not be verified but have been used nonetheless. Furthermore, the reservoir that will be created once the dam is constructed is based on simple relations of the volume of a frustrum of a cone. This assumption was made for modeling the reservoir. All calculated

parameters that came from this assumption exactly matched the reservoir presented in the study of the OMVG and EIES (2014). This is an indication that the expected characteristics of the reservoir and therefore the water level – discharge relations have not yet been determined accurately.

Scenario 'DO B' optimized the power production only for a single scenario and not for each. This leads to sub-optimal performance of the scenarios which implement DO B. This sub-optimal performance is enlarged by the larger difference in evaporation between RCP 4.5 and RCP 8.5. Secondly, scenario 'DO B' assumes a constant flow for respectively the dry and wet season. The expert interview indicates another possible operating scheme that aims to produce power when its needed. This has not been modelled.

7 CONCLUSION

The presentation of conclusions from this study is organized around the research questions, which are presented below. Each paragraph answers one of these questions by looking qualitatively or quantitatively at the key features and results discussed in Chapter 5. All modelled parameters (projected climate, sea level rise, dam operations, irrigated area) and time periods are included to provide an as complete as possible conclusion. By answering the research questions the research goal of clarifying 'the effects of climate change, a hydropower dam and irrigation development' is reached to some extent. There are no conclusion presented as to what will happen, however the individual effects of these parameters can be used to express the severity of salt intrusion under certain circumstances.

1. *How does the salt intrusion length develop considering climate change, the hydropower dam and irrigation development in the Gambia estuary?*
2. *How does the salt concentration develop considering climate change, the hydropower dam and irrigation development in the Gambia estuary?*
3. *To what extent can hypersalinity occur and under which circumstances?*
4. *What measures can be taken to mitigate unwanted salt intrusion and how effective are these measures?*
5. *How will aqua- and agriculture in The Gambia be affected by the construction of the hydropower dam?*

7.1 SALT INTRUSION LENGTH AND CONCENTRATION

The modelled salt intrusion length and concentration are influenced by projected climate, sea level rise, dam operations and irrigation development. First, the effects that the projected climate and sea level rise have on salt intrusion length and salt concentration will be presented. Afterwards, the effects that the reservoir filling, dam operations and irrigation development have on salt intrusion length and salt concentration will be presented.

7.1.1 The effects of projected climate and sea level rise on salt intrusion length and salt concentration

Projected climate
Projected climate has a significant impact on salt intrusion lengths as can

been seen when comparing RCP 4.5 with RCP 8.5. The maximum salt intrusion length shows increases of up to 12% between RCP 8.5 and RCP 4.5. Furthermore, a strong increase in the size of the hypersaline region, up to 45%, can be seen. Projected climate does not show a significant impact on salt concentrations. Note that this effect is only related to projected climate, in combination with 2.0 m sea level rise the projected evaporation leads to a significant impact in salt concentrations.

Sea level rise
Sea level rise has a limited influence on salt intrusion when it stays below the 1.09 m threshold. Below this threshold sea level rise has no significant impact, except for a counterintuitive decrease in length of hypersaline region. The decrease in length of the hypersaline length can be explained by looking at the formula for salt intrusion that the 1D model uses (see Equation 3.9 and Equation 3.16). Due to sea level rise the depth increases however, only the cross-sectional area increases while the width stays constant. This reduces the gradient of the steady-state dispersion thereby increasing the salt dispersion over the whole estuary. At the same time the increased cross-sectional area increases the effectivity of the advective term in the salt balance equation.

When the sea level rises above the 1.09 m threshold however, the river is forced outside of its banks. Due to the large flat areas around the river, a dramatic expansion of the evaporative surface of the river takes place. Depending on the location in the river the maximum increase in evaporation varies between 17% and 2440%. This results in high levels of freshwater removal due to evaporation. This leads to increases in; salt intrusion lengths of up to 57% ($\pm 200 km$), length of the hypersaline region of up to 183% ($\pm 308 km$), and salt concentrations coming close to double ocean salinity by the end of the century. With the extreme sea level rise projections used the river will likely start overflowing around 2057, however only in the third modelling period (2070-2099) these extreme values are reached.

7.1.2 The effects of reservoir filling, dam operations and irrigation development on salt intrusion length and salt concentration

Reservoir filling
The reservoir filling scenarios have a small impact. There is no significant change noticeable in minimum and maximum salt intrusion lengths when the reservoir is filled in a single year. If this takes two years a minor increase in maximum intrusion length can be noticed. However, the wet season dip in salt intrusion length and dry season peak in salt intrusion length of the monthly median both increase, respectively with 10% and 8%. This is independent of the time it takes to fill the reservoir.

Dam operations
Dam operations have a significant impact on the salt intrusion lengths of the river. The difference between the two dam operation scenarios, DO A and

DO B, is large. DO A, the ecology focused flow operations have a discharge scheme based on the environmental study in 2014 (OMVG & EIES, 2014). DO B, optimizes power production by managing the discharge in such a way that a constant, as high as possible power is produced throughout the wet and dry season.

The ecology focused flow, DO A, shows a strong reducing effect on maximum salt intrusion lengths, up to 29% for RCP 4.5 and up to 28% for RCP 8.5 compared to the scenario without dam. This leads to a more stabilized salt intrusion pattern, where the salt front is contained in a smaller range than without dam. Furthermore, the hypersaline region is strongly decreased, up to 40% for RCP 4.5 and up to 42% for RCP 8.5 when comparing to the scenario without dam.

Power production focused operations shows salt intrusion lengths that are closer to the scenarios without dam. This also leads to a smaller range in which the salt front moves when compared to the situation without dam. However, where the ecology focused operations show a strongly reduction in maximum salt intrusion length and the length of the hypersaline region, the power production focused operations do not.

Irrigation development
Somewhat surprisingly the development of irrigation area does not result in significant impact. Even when maximum irrigated surface is applied this does not lead to significantly different salt intrusion levels. Similarly, the salt concentration levels are barely affected. This is due to the relatively small amount of water necessary for the increased irrigational area ($\pm$2% of flow).

7.2 HYPER SALINITY

Periods of hyper salinity are found in all scenarios, occurring in the dry season where a point is reached when the freshwater flow is depleted and evaporative losses lead to a buildup of salt in the remaining river volume. This can be close to the river mouth or deep inland. Severe hyper salinity (> 40 g/L) only occurs in the 2.0-meter sea level rise scenario.

7.3 MEASURES TO MITIGATE SALT INTRUSION

Depending on the freedom to adjust dam operation, and how sea level rise and the climate develops, the dam operations could be used to limit salt intrusion lengths as well as hyper salinity. The difference between the two modelled ways of operating the dam illustrate the extent to which salt intrusion lengths can be pushed back through changes in the dam discharge rate.

Occasionally supplying the river with fresh sediment that has settled in the reservoir behind the dam could potentially help limit the increase in salt intrusion lengths due to morphological changes. However, this issue was

not included in the present study. Therefore, the effect of the reduced sediment supply on salt intrusion lengths and the potential effectiveness of this strategy are unknown.

Limiting the expansion of the river would make sure that severe hyper salinity and long salt intrusion lengths cannot occur. Comparing the scenarios with 2.0 m sea level rise and those with more moderate sea level rise shows the importance of efforts of efforts aimed at preventing future emissions of greenhouse gasses.

7.4 INFLUENCE OF DAM OPERATIONS ON AGRI- AND AQUACULTURE

It is important to realize this study only looked at the effect the dam operations have on salt intrusion levels. The implementation of the dam shows higher salt intrusion lengths and more occurring higher salt intrusion lengths. However, these increases are not significant enough to harm agri- and aquaculture.

The operation of the dam does not pose a threat to agriculture. Furthermore, the stabilizing effect of the dam on salt intrusion levels leads to less varying salt intrusion lengths and concentrations which would create a better environment for aquaculture.

The magnitude of the shift in seasonality mentioned before can increase when the hydropower dam is solely operated to produce power. This could have implications for agri- and aquaculture.

7.5 ISSUES FOR POLICY MAKERS

The salt intrusion length and salt concentrations in the Gambia river will be heavily affected by climate change. Effort should be made to convince all stakeholders and financers of the dam to leave some room in dam operations. This enables to use the strong effects the dam operation has in decreasing salt concentrations and salt intrusion lengths in periods of need. If this is not possible for whatever reason other solutions ought to be sought, for example an introduction of salt tolerant crops could be a useful adaptation for agriculture.

Banjul lies at the mouth of the Gambia river. The elevation of the city is only slightly more than that of sea level and if sea level rise continues as predicted in the worst-case scenario used in this study (2.0-meter sea level rise) large parts of Banjul will eventually flood. Flooding and other water related problems in Banjul will likely occur before hyper salinity reaches unacceptable levels in the estuary. If Banjul is to be protected this would require substantial financial means. This leads to the question: if financial

resources are used to protect Banjul, will there be enough to protect the estuary as well? For example by limiting the expansion of the river due to sea level rise.

8 RECOMMENDATIONS

There are several recommendations, these can be split in two categories. Recommendations to improve this study and its results and recommendations to monitor and attenuate unwanted salt intrusion lengths and concentrations.

8.1 IMPROVING THIS STUDY

8.1.1 Reducing amount of data sources and/or error determination

As has been mentioned in the limitations reducing the numerous different sources of data should be a priority. Figure 4.12 gives a good impression for the key data used by the model but there is more data which could lead to significant improvements of this study.

- New salt measurements, by moving boat method, would enable a more accurate calibration and validation. Since new salt measurements would be performed the whole calibration on historical data will be unnecessary.
- A geometrical relation between sea level rise and the increase in river surface area and how this relation varies along the river would lead to a significant improvement. Looking at the impact this region has on hyper salinity this relation would be crucial when looking deeper into scenarios with more pronounced sea level rise.
- A better understanding of how the dam will be operated is of great value. The extreme differences between the two ways of operating the dam show a significant impact on salt intrusion in the estuary. However, it is likely that stakeholders of the dam have certain requirements in mind and that the freedom shown in this study is in reality not given. An update on dam and reservoir characteristics and the expected type of operations would give more realistic results.

8.1.2 Evaporation effect on calibration

The calibration of the model is performed by adjusting the dispersion at the mouth of the estuary and a factor that is multiplied with the evaporation. When the river expands this increase in river evaporative surface also applies the scaled evaporation. The calibration process that sets this calibration factor for the evaporation might therefore introduce an error in the

scenarios where sea level rise surpasses the threshold value and the evaporative surface increases. Knowing if this has an impact and if so, changing the calibration strategy could be useful, especially if the impact is large.

8.1.3 Numerical nature

The numerical nature of the model, especially for large intrusion lengths, introduces oscillations which become larger when salt intrudes further inland (increased number of calculations needed). These errors still show the trends that are happening, however for more detailed and precise analysis these numerical errors should be limited as much as possible. Numerical optimization, reducing the numerical errors as much as possible is highly recommended for analysis of extremes (deep inland salt intrusion fronts). If extremes are not of the essence, an error analysis would give an impression within what range the predicted salt concentrations are.

8.1.4 Temporal analysis

Only a very basic analysis of the seasonality of the dry and wet season has been performed. This might lead to misinterpretation of the results regarding seasonality. The shift in the wet season dip and dry season peak do not necessarily represent the length of the respective seasons. This can be clearly seen in Figure 5.7, where both scenarios have the same month in which the wet season dip and dry season peak occur. It would be useful to analyze the data more in depth to have a better understanding of the parameters effects on seasonality.

8.1.5 Historic dataset

As has been explained in Section 4.5.1 comparison with historic modeled salt intrusion is wrong. However, being able to compare to historic values would give a much better impression of how salt intrusion is likely to evolve. This could have been solved by including the GCM estimates for historic precipitation and temperature, and calibrate the model on these settings instead of unrelated historic parameters.

8.2 MEASURES FOR THE GAMBIA

Even if sea level rise is moderate in this century it is likely to continue for a long time, also after global temperatures stabilize. According Nauels et al. (2019) a 1.0 m sea level rise will still happen in the year 2300 even if the Paris Agreement is honored. Because the threshold value is close to a meter (1.09 m) this could mean that the river will be forced outside of its banks at some point in the future. Monitoring at which rate the sea level rises is a tool to set deadlines for potential measures. Furthermore, since Banjul's elevation is close to sea level, monitoring sea level rise would help with planning measures in and around the capital. The monitoring can be done cheaply by

making use of the new NASA satellites.

In unfavorable conditions large areas will be flooded due to sea level rise. Assuming that effort will be made to save Banjul and solely focusing on the estuary a choice has to be made. Either the salt intrudes far upstream and hypersaline conditions become so extreme that large parts of the estuary will deteriorate, or an investment has to be made to limit the expansion of the river due to sea level rise. The deterioration of the estuary will cause large economic and ecologic destruction. However, limiting the expansion of the river by for example dikes would also cause the loss of large areas of agricultural lands that are currently irrigated by the tide. Ideally a measure could be designed that keeps the farmlands but limits the rivers expansion.

BIBLIOGRAPHY

Amuzu, J., Jallow, B., Kabo-Bah, A. & Yaffa, S. (2018). The Climate Change Vulnerability and Risk Management Matrix for the Coastal Zone of The Gambia. *Hydrology*, *5*(1), 14. https://doi.org/10.3390/hydrology5010014

Aris, N. A. (2012). *Modeling of salt water intrusions into Langat River Estuary, Malaysia* (tech. rep.).

Bamber, J. L., Oppenheimer, M., Kopp, R. E., Aspinall, W. P. & Cooke, R. M. (2019). Ice sheet contributions to future sea-level rise from structured expert judgment. *Proceedings of the National Academy of Sciences of the United States of America*, *166*(23), 11195–11200. https://doi.org/10.1073/pnas.1817205116

Bentsen, M., Bethke, I., Debernard, J. B., Iversen, T., Kirkevåg, A., Seland, Ø., Drange, H., Roelandt, C., Seierstad, I. A., Hoose, C. & Kristjánsson, J. E. (2013). The Norwegian Earth System Model, NorESM1-M – Part 1: Description and basic evaluation of the physical climate. *Geoscientific Model Development*, *6*(3), 687–720. https://doi.org/10.5194/gmd-6-687-2013

Cai, H., Savenije, H. H. G. & Jiang, C. (2014). Analytical approach for predicting fresh water discharge in an estuary based on tidal water level observations. *Hydrol. Earth Syst. Sci*, *18*, 4153–4168. https://doi.org/10.5194/hess-18-4153-2014

Cai, H., Savenije, H. H. G., Zuo, S., Jiang, C. & Chua, V. P. (2015). A predictive model for salt intrusion in estuaries applied to the Yangtze estuary. *Journal of Hydrology*, *529*, 1336–1349. https://doi.org/10.1016/j.jhydrol.2015.08.050

Cañedo-Argüelles, M., Kefford, B. J., Piscart, C., Prat, N., Schäfer, R. B. & Schulz, C. J. (2013). Salinisation of rivers: An urgent ecological issue. https://doi.org/10.1016/j.envpol.2012.10.011

Carnahan, B. & Wilkes, J. O. (1973). Numerical Methods for Chemical Engineering. https://doi.org/10.1017/cbo9780511812194

Carney, J., Gillespie, T. W. & Rosomoff, R. (2014). Assessing forest change in a priority West African mangrove ecosystem: 1986-2010. *Geoforum*, *53*, 126–135. https://doi.org/10.1016/j.geoforum.2014.02.013

Chen, C., Huang, H., Beardsley, R. C., Liu, H., Xu, Q. & Cowles, G. (2007). A finite volume numerical approach for coastal ocean circulation studies: Comparisons with finite difference models. *Journal of Geophysical Research: Oceans*, *112*(3). https://doi.org/10.1029/2006JC003485

Chen, W. B., Liu, W. C. & Hsu, M. H. (2015). Modeling assessment of a saltwater intrusion and a transport time scale response to sea-level rise in a tidal estuary. *Environmental Fluid Mechanics*, *15*(3), 491–514. https://doi.org/10.1007/s10652-014-9367-y

CIA. (2020). Gambia, The - The World Factbook. https://www.cia.gov/the-world-factbook/countries/gambia-the/#people-and-society

Davies, G. & Woodroffe, C. D. (2010). Tidal estuary width convergence: Theory and form in North Australian estuaries. *Earth Surface Processes and Landforms*, *35*(7), n/a–n/a. https://doi.org/10.1002/esp.1864

Dee, D. P., Uppala, S. M., Simmons, A. J., Berrisford, P., Poli, P., Kobayashi, S., Andrae, U., Balmaseda, M. A., Balsamo, G., Bauer, P., Bechtold, P., Beljaars, A. C. M., van de Berg, L., Bidlot, J., Bormann, N., Delsol, C., Dragani, R., Fuentes, M., Geer, A. J., … Vitart, F. (2011). The ERA-Interim reanalysis: configuration and performance of the data assimilation system. *Quarterly Journal of the Royal Meteorological Society*, *137*(656), 553–597. https://doi.org/10.1002/qj.828

Dufresne, J. L., Foujols, M. A., Denvil, S., Caubel, A., Marti, O., Aumont, O., Balkanski, Y., Bekki, S., Bellenger, H., Benshila, R., Bony, S., Bopp, L., Braconnot, P., Brockmann, P., Cadule, P., Cheruy, F., Codron, F., Cozic, A., Cugnet, D., … Vuichard, N. (2013). Climate change projections using the IPSL-CM5 Earth System Model: From CMIP3 to CMIP5. *Climate Dynamics*, *40*(9-10), 2123–2165. https://doi.org/10.1007/s00382-012-1636-1

Dunne, J. P., John, J. G., Adcroft, A. J., Griffies, S. M., Hallberg, R. W., Shevliakova, E., Stouffer, R. J., Cooke, W., Dunne, K. A., Harrison, M. J., Krasting, J. P., Malyshev, S. L., Milly, P. C., Phillipps, P. J., Sentman, L. T., Samuels, B. L., Spelman, M. J., Winton, M., Wittenberg, A. T. & Zadeh, N. (2012). GFDL's ESM2 global coupled climate-carbon earth system models. Part I: Physical formulation and baseline simulation characteristics. *Journal of Climate*, *25*(19), 6646–6665. https://doi.org/10.1175/JCLI-D-11-00560.1

Dutra, E., Balsamo, G., Calvet, J.-C., Minvielle, M., Eisner, S., Fink, G., Pessenteiner, S., Orth, R., Burke, S., van Dijk, A., Polcher, J., Beck, H., de La Torre, A. M. & Sterk, G. (2015). Global Earth Observation for integrated water resource assessment Report on the current state - of - the - art Water Resources Reanalysis. (March). http://earth2observe.eu/files/Public%0ADeliverables/D5.1_Report%0Aon%0Athe%0AWRR1%0Atier1.pdf%0Ahttp://earth2observe.eu/files/Public%20Deliverables/D5.1_Report%20on%20the%20WRR1%20tier1.pdf

ECOWAPP. (2012). 128 MW Sambangalou Hydopower plant. http://pipes.ecowapp.org/en/project/implementation/128-mw-sambangalou-hydopower-plant

ECOWAS. (2020). Economic Community of West African States | Vision 2020. https://www.ecowas.int/about-ecowas/vision-2020/

Ellison, J. C. (1993). Mangrove Retreat with Rising Sea-level, Bermuda. *Estuarine, Coastal and Shelf Science*, *37*(1), 75–87. https://doi.org/10.1006/ecss.1993.1042

El-Nahry, A. H. & Doluschitz, R. (2010). Climate change and its impacts on the coastal zone of the Nile Delta, Egypt. *Environmental Earth Sciences*, *59*(7), 1497–1506. https://doi.org/10.1007/s12665-009-0135-0

Ettritch, G., Hardy, A., Bojang, L., Cross, D., Bunting, P. & Brewer, P. (2018). Enhancing digital elevation models for hydraulic modelling using flood frequency detection. *Remote Sensing of Environment*, *217*, 506–522. https://doi.org/10.1016/j.rse.2018.08.029

FAO. (2007). *Caracterisation des systemes de production agricole au Senegal* (tech. rep.). http://www.ntiposoft.com/domaine_200/pdf/caractspasenegal.pdf

FAO. (2020). About FAO | Food and Agriculture Organization of the United Nations. http://www.fao.org/about/en/

Fent, A., Bardou, R., Carney, J. & Cavanaugh, K. (2019). Transborder political ecology of mangroves in Senegal and The Gambia. *Global Environmental Change*, *54*, 214–226. https://doi.org/10.1016/j.gloenvcha.2019.01.003

Fischer, H. B., List, J. E., Koh, C. R., Imberger, J. & Brooks, N. (2013). *Mixing in Inland and Coastal Waters*. Elsevier. https://books.google.nl/books?hl=nl&lr=&id=8QoBBQAAQBAJ&oi=fnd&pg=PP1&dq=fischer+1979+mixing+inland+and+coastal+waters&ots=BS-FGHaPy5&sig=5zMU--4VwccDwora5l4KR6cLaps#v=onepage&q=fischer%201979%20mixing%20inland%20and%20coastal%20waters&f=false

Gay, P. S. & O'Donnell, J. (2007). A simple advection-dispersion model for the salt distribution in linearly tapered estuaries. *Journal of Geophysical Research*, *112*(C7), C07021. https://doi.org/10.1029/2006JC003840

Gisen, J., Savenije, H. H. G. & Nijzink, R. (2015). Revised predictive equations for salt intrusion modeling in estuaries. *Hydrol. Earth Syst. Sci. Discuss*, *12*, 739–770. https://doi.org/10.5194/hessd-12-739-2015

Gisen, J., Savenije, H. H. G., Nijzink, R. & Abd. Wahab, A. (2015). Testing a 1-D analytical salt intrusion model and its predictive equations in Malaysian estuaries. *Hydrological Sciences Journal*, *60*(1), 156–172. https://doi.org/10.1080/02626667.2014.889832

Guannel, G., Arkema, K., Ruggiero, P. & Verutes, G. (2016). The Power of Three: Coral Reefs, Seagrasses and Mangroves Protect Coastal Regions and Increase Their Resilience (C. N. Bianchi, Ed.). *PLOS ONE*, *11*(7), e0158094. https://doi.org/10.1371/journal.pone.0158094

Haddout, S., Maslouhi, A., Baimik, I., Igouzal, M. & Marah, H. (2019). Two-dimensional modeling of the vertical circulation of salt intrusion in the Sebou estuary under different hydrological conditions. *ISH Journal of Hydraulic Engineering*, *25*(2), 170–187. https://doi.org/10.1080/09715010.2017.1391134

Kuang, C., Huang, J., Cheng, S. & Liu, S. (2012). A saltwater intrusion model based on semi-implicit Eulerian-Lagrangian finite-volume method. *Journal of Tongji University. Natural Science*, *40*, 38–44. http://en.cnki.com.cn/Article_en/CJFDTotal-TJDZ201201006.htm

Lange, S. (2018). Bias correction of surface downwelling longwave and shortwave radiation for the EWEMBI dataset. *Earth System Dynamics*, *9*(2), 627–645. https://doi.org/10.5194/esd-9-627-2018

Lewis, R. E. & Uncles, R. J. (2003). Factors affecting longitudinal dispersion in estuaries of different scale. *Ocean Dynamics*, *53*(3), 197–207. https://doi.org/10.1007/s10236-003-0030-2

Martin, G. M., Bellouin, N., Collins, W. J., Culverwell, I. D., Halloran, P. R., Hardiman, S. C., Hinton, T. J., Jones, C. D., McDonald, R. E., McLaren, A. J., O'Connor, F. M., Roberts, M. J., Rodriguez, J. M., Woodward, S., Best, M. J., Brooks, M. E., Brown, A. R., Butchart, N., Dearden, C., … Wiltshire, A. (2011). The HadGEM2 family of Met Office Unified

Model climate configurations. *Geoscientific Model Development*, *4*(3), 723–757. https://doi.org/10.5194/gmd-4-723-2011

Naidoo, G., Hiralal, O. & Naidoo, Y. (2011). Hypersalinity effects on leaf ultrastructure and physiology in the mangrove Avicennia marina. *Flora: Morphology, Distribution, Functional Ecology of Plants*, *206*(9), 814–820. https://doi.org/10.1016/j.flora.2011.04.009

Nauels, A., Gütschow, J., Mengel, M., Meinshausen, M., Clark, P. U. & Schleussner, C. F. (2019). Attributing long-term sea-level rise to Paris Agreement emission pledges. *Proceedings of the National Academy of Sciences of the United States of America*, *116*(47), 23487–23492. https://doi.org/10.1073/pnas.1907461116

NRDS. (2014). *National Rice Development Strategy (NRDS) - The Gambia* (tech. rep.).

OMVG & EIES. (2014). *Mission d'appui conseil a l'OMVG pour la realisation de son projet energie* (tech. rep.).

Parsa, J. & Etemad-Shahidi, A. (2011). An empirical model for salinity intrusion in alluvial estuaries. *Ocean Dynamics*, *61*(10), 1619–1628. https://doi.org/10.1007/s10236-011-0457-9

Pillsbury, G. B. (1956). *Tidal Hydraulics* (Vol. 34). Corps of Engineers, US Army. https://books.google.nl/books?hl=nl&lr=&id=FAEIAQAAIAAJ&oi=fnd&pg=PP11&dq=Pillsbury,+G.+B.+(1956).+Tidal+hydraulics+(Vol.+34).+Corps+of+Engineers,+US+Army.&ots=vAl9djoDOV&sig=kCO8R45LFoNkr1DGlCZXqDDFSVA#v=onepage&q&f=false

Pörtner, H.-O., Roberts, D., Masson-Delmotte, V., Zhai, P., Tignor, M., Poloczanska, E., Mintenbeck, K., Alegría, A., Nicolai, M., Okem, A., Petzold, J., Rama, B. & Weyer, N. (2019). Summary for Policymakers. In: IPCC Special Report on the Ocean and Cryosphere in a Changing Climate. *Ipcc*, 36. https://www.ipcc.ch/site/assets/uploads/sites/3/2019/11/03_SROCC_SPM_FINAL.pdf

Rahmstorf, S., Foster, G. & Cazenave, A. (2012). Comparing climate projections to observations up to 2011. *Environmental Research Letters*, *7*(4), 044035. https://doi.org/10.1088/1748-9326/7/4/044035

Robins, P. E., Skov, M. W., Lewis, M. J., Giménez, L., Davies, A. G., Malham, S. K., Neill, S. P., McDonald, J. E., Whitton, T. A., Jackson, S. E. & Jago, C. F. (2016). Impact of climate change on UK estuaries: A review of past trends and potential projections. https://doi.org/10.1016/j.ecss.2015.12.016

Sarr, B. (2012). Present and future climate change in the semi-arid region of West Africa: a crucial input for practical adaptation in agriculture. *Atmospheric Science Letters*, *13*(2), 108–112. https://doi.org/10.1002/asl.368

Savenije, H. H. G. (1986). A one-dimensional model for salinity intrusion in alluvial estuaries. *Journal of Hydrology*, *85*(1-2), 87–109. https://doi.org/10.1016/0022-1694(86)90078-8

Savenije, H. H. G. (1989). Salt intrusion model for high-water slack, low-water slack, and mean tide on spread sheet. *Journal of Hydrology*, *107*(1-4), 9–18. https://doi.org/10.1016/0022-1694(89)90046-2

Savenije, H. H. G. (1992). *Rapid assessment technique for salt intrusion in alluvial estuaries* (Doctoral dissertation). Delft University of Technology. IHE

Report series 27. https://repository.tudelft.nl/islandora/object/uuid%3A1b350a99-b85d-4193-8f1b-29891366a34a

Savenije, H. H. G. (1993). Predictive model for salt intrusion in estuaries. *Journal of Hydrology*, *148*(1-4), 203–218. https://doi.org/10.1016/0022-1694(93)90260-G

Savenije, H. H. G. (2005). *Salinity and Tides in Alluvial Estuaries*. Gulf Professional Publishing. https://books.google.nl/books?hl=nl&lr=&id=PLn2XkMp8fAC&oi=fnd&pg=PP15&dq=Savenije,+H.H.G.,+(2005).+Salinity+and+tides+in+alluvial+estuaries.+Gulf+Professional+Publishing.&ots=p1LnhgB9Ge&sig=yk4OB9dlMx-PeHThlAT2Bfs1qyo#v=onepage&q=Savenije%2C%20H.H.G.%2C%20(2

Savenije, H. H. G. (2012). Salinity and tides in alluvial estuaries; Second completely revised edition. *Open Access*, 163. http://hubertsavenije.files.wordpress.com/2014/01/salinityandtides2_21.pdf

Savenije, H. H. G. & Pagès, J. (1992). Hypersalinity: a dramatic change in the hydrology of Sahelian estuaries. *Journal of Hydrology*, *135*(1-4), 157–174. https://doi.org/10.1016/0022-1694(92)90087-C

Shaha, D. C. & Cho, Y.-K. (2009). *Comparison of empirical models with intensively observed data for prediction of salt intrusion in the Sumjin River estuary, Korea* (tech. rep.). www.hydrol-earth-syst-sci.net/13/923/2009/

Sivapalan, M. (2003). Process complexity at hillslope scale, process simplicity at watershed scale: Is there a connection? *EAEJA*, 7973. https://ui.adsabs.harvard.edu/abs/2003EAEJA.....7973S/abstract

Spring, S. (2017). NOAA Technical Report NOS CO-OPS 083 noaa National Oceanic and Atmospheric Administration National Ocean Service Center for Operational Oceanographic Products and Services GLOBAL AND REGIONAL SEA LEVEL RISE SCENARIOS FOR THE UNITED STATES. https://doi.org/10.7289/V5/TR-NOS-COOPS-083

Symonds, A. M., Vijverberg, T., Post, S., Van Der Spek, B.-J., Henrotte, J. & Sokolewicz, M. (2016). *Comparison between MIKE 21 FM, DELFT3D and DELFT3D FM flow models of Western Port Bay, Australia.* (tech. rep.).

Thornthwaite, C. W. (1948). An Approach toward a Rational Classification of Climate. *Geographical Review*, *38*(1), 55. https://doi.org/10.2307/210739

UN. (n.d.). Goal 13 | Department of Economic and Social Affairs. https://sdgs.un.org/goals/goal13

Van Os, A. & Abraham, G. (1990). Density Currents and Salt Intrusion.

Vargas, C. I., Vaz, N. & Dias, J. M. (2017). An evaluation of climate change effects in estuarine salinity patterns: Application to Ria de Aveiro shallow water system. *Estuarine, Coastal and Shelf Science*, *189*, 33–45. https://doi.org/10.1016/j.ecss.2017.03.001

V.d. Burgh, P. (1972). *Ontwikkeling van een methode voor het voorspellen van zoutverdelingen in estuaria, kanalen en zeeën* (tech. rep.). Rijkswaterstaat, Deltadienst. https://repository.tudelft.nl/islandora/object/uuid%3A5aea8938-4179-4958-8d60-0a806f95409d

Verkerk, M. & Van Rens, C. (2005). *Saline intrusion in Gambia River after dam construction* (tech. rep.).

Watanabe, S., Hajima, T., Sudo, K., Nagashima, T., Takemura, T., Okajima, H., Nozawa, T., Kawase, H., Abe, M., Yokohata, T., Ise, T., Sato, H., Kato, E., Takata, K., Emori, S. & Kawamiya, M. (2011). MIROC-ESM 2010: Model

description and basic results of CMIP5-20c3m experiments. *Geoscientific Model Development*, *4*(4), 845–872. https://doi.org/10.5194/gmd-4-845-2011

Weedon, G. P., Balsamo, G., Bellouin, N., Gomes, S., Best, M. J. & Viterbo, P. (2014). The WFDEI meteorological forcing data set: WATCH Forcing Data methodology applied to ERA-Interim reanalysis data. *Water Resources Research*, *50*(9), 7505–7514. https://doi.org/10.1002/2014WR015638

White, E., Messina, F., Moss, L. & Meselhe, E. (2018). Salinity and Marine Mammal Dynamics in Barataria Basin: Historic Patterns and Modeled Diversion Scenarios. *Water*, *10*(8), 1015. https://doi.org/10.3390/w10081015

Zhang, Z. (2019). A theoretical basis for salinity intrusion in estuaries. https://doi.org/10.4233/uuid:d95a29ff-8865-4484-864a-74fd75028292

A GLOBAL CIRCULATION MODEL

This appendix contains a chapter of the proposal mentioned in Section 1.3, written by B.M. Simpson. This chapter has been incorporated in this appendix since it contains a detailed description of how the GCM has been selected and the projected climate data has been produced.

Climate trend analysis and projected climate change in The Gambia and over the Gambia river watershed.

Author: Simpson, B.M. 2020, United Nations Food and Agriculture Organization.

As part of the global hydrologic system, the Gambia River3 is directly affected by changes occurring in the principal drivers of climate change. From the global to national scales, changes in temperature and rainfall regimes, and associated changes in moisture loss through evaporation, are altering the movement of water within the river and watershed, and subsequently impacting key ecological segments along the river and Gambian fisheries. To understand the magnitude and rate of current and future changes, it is necessary to interrogate appropriate datasets for the presence of important trends, historically, as well as those that are reasonable to anticipate in the coming decades. This chapter presents a summary of a detailed analysis undertaken to identify the underlaying physical attributes of historical and projected changes of temperature and precipitation within the watershed. This analysis was further used to inform the assessment of climate change impacts on the ocean environment and river ecologies, and in modelling the impact of climate change on the saline intrusion into the Gambia River, presented in the following chapters. These additional chapters, together and separately, are used in assessing the likely biological impacts of climate change on the various fisheries, and individual species, as well as aiding in the physical location of specific adaptive activities.

Data

Over two-thirds of the Gambia River watershed is located within Senegal, with the remaining portion split near evenly between The Gambia and Guinea.[4] Due to the cross-border nature of the watershed, in order to undertake a trend analysis of possible changes in historical weather patterns that might be affecting the basin's hydrology, as well as projecting future trends, it is necessary to rely on weather records at a commensurate spatial scale, above national level. The EWEMBI (EartH2Observe, WFDEI and ERA-Interim data Merged and Bias-corrected for ISIMIP) dataset was selected for this purpose (Lange, 2018; Dee et al., 2011; Weedon et al., 2014; Dutra, 2015). The EWEMBI dataset is a robust, global dataset compiled and maintained by the Inter-Sectoral Impact Model Intercomparison Project (ISIMIP) in support of impact assessment teams contributing to the Intergovernmental Panel on Climate Change (IPCC) assessment reports. The dataset provides daily precipitation and temperature data, covering the period from 1979-2018, at a global scale with 0.5° resolution (roughly 55.5 km2 at the equator).

In assessing climate trends in the Gambia River watershed, daily temperature (maximum, minimum and average) and precipitation values were reconstructed as monthly averages. This reconstruction was carried out for two reasons. First, it simplified the dataset for use in trend detection, where seasonal changes in magnitude and spatial distribution of precipitation within the watershed is the primary concern. Secondly, use of monthly timescale was commiserate with the data inputs needs of

3

[4] 14 percent of the watershed lays in The Gambia, 71 percent in Senegal and 15 percent in Guinea (Oréade-Brèche and ISL Ingénierie, 2014). The shape file for the Gambia Watershed was obtained from the HydroSHEDS database (https://hydrosheds.org/page/overview). The watershed includes those areas upstream from the extent of permanent saltwater intrusion into the river at KP 64.

the SALNST salinity model being used to project changes in the saltwater intrusion into the Gambia River (see Chapter 3). For this later purpose, in additional to precipitation data, daily maximum and minimum temperatures were used to calculate potential evapotranspiration values using Thornthwaite's equation, which is based on temperature (Thornthwaite, 1948).

For future climate projections, five global circulation models (GCMs) used by FAO in other national assessments were selected. The selected models are: the GFDL-ESM2M (Geophysical Fluid Dynamics Laboratory – Earth System Model 2M)(Dunne et al., 2012); the MIROC-ESM (Model for Interdisciplinary Research on Climate – Earth System Model)(Watanabe et al., 2011); the IPSL-CM5a-MR (Institut Pierre-Simon Laplace-Climate Model 5a-Mid-Resolution)(Dufresne et al., 2013); the NORESM (Norwegian Earth System Model 1-M)(Bentsen et al., 2013), and the HadGEM2-ES (Hadley Centre Global Environment Model ver.2-Earth System)(Martin et al., 2011). All of these models are part of the Coupled Model Intercomparison Project 5 (CMIP5), used in conducting analysis for the IPCC Fifth Assessment Report (AR5).[5]

To assess the correlation between the different GCMs and the EWEMBI dataset, a quality control check was performed. The Root Mean Square Error (RMSE) was used to determine the best fit between each of the models' re-creation of historical daily precipitation and temperature values for the period 1979 to 2016 covered by the EWEMBI dataset. Figure A shows the RMSE by geographic location for each of the models, and Figure B shows the RMSE by months. The MIROC-ESM, developed by the University of Tokyo, the National Institute for Environmental Studies (NIES) and the Japanese Agency for Marine-Earth Science and Technology (JAMSTEC), had the lowest RMSE values for precipitation and close to lowest for temperature. Based on the low RMSE, the MIROC-ESM was selected for use in generating the projected weather for use in the SALNST salinity assessment.[6]

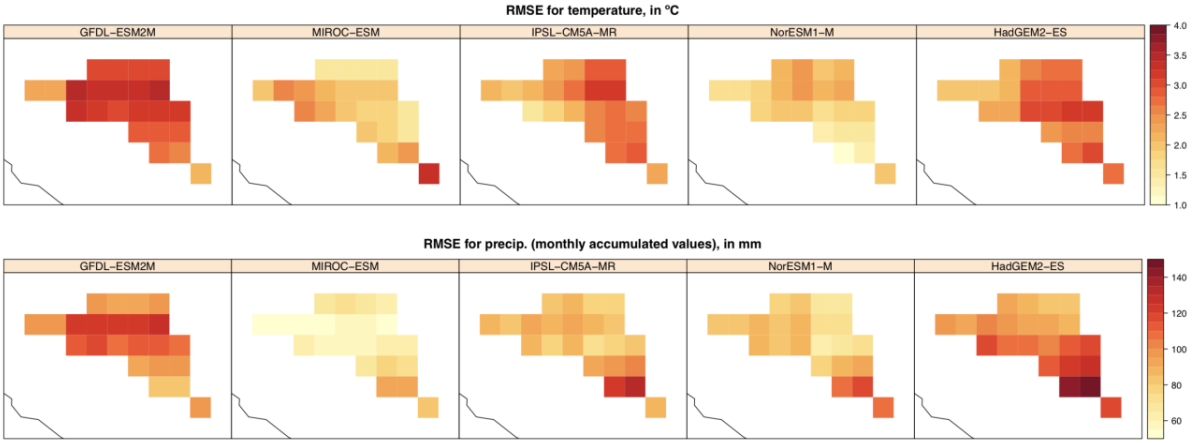

Figure A. *GCM to EWEMBI Root Mean Square Error values (1979-2016) for temperature and precipitation across the Gambia River watershed (lighter colors denote smaller RMSEs)(Source: FAO analysis of EWEMBI dataset).*

[5] For further details see the IPCC AR5 Chapter 9 "Evaluation of Climate Models" (https://www.ipcc.ch/site/assets/uploads/2018/02/WG1AR5_Chapter09_FINAL.pdf) and IPCC Data Distribution Center AR5 Reference snapshot http://www.ipcc-data.org/sim/gcm_monthly/AR5/Reference-Archive.html

[6] For further details on data processing for the SALNST assessment, see chapter 3.

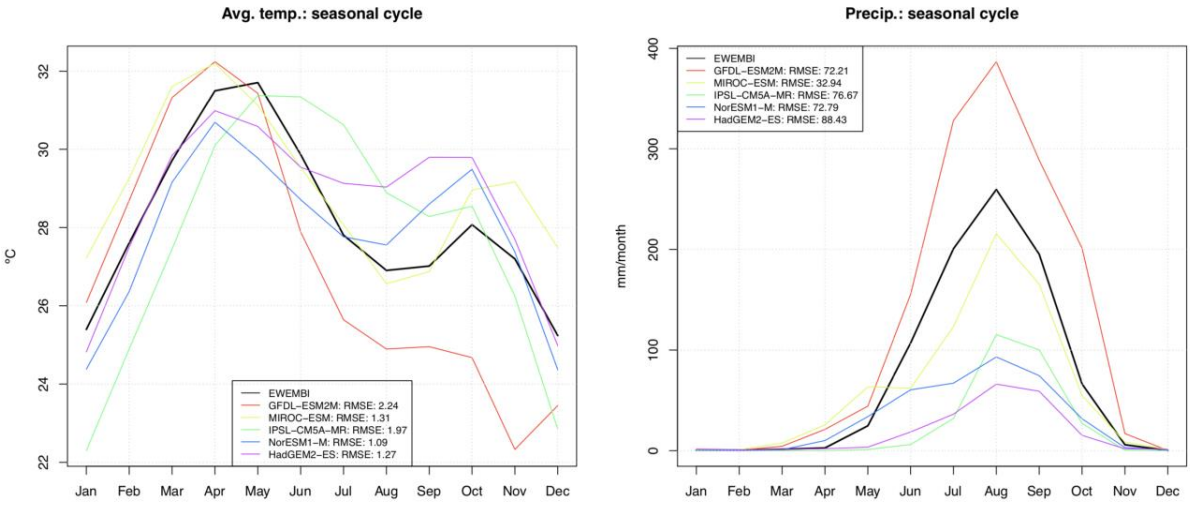

Figure B. *GCM to EWEMBI Root Mean Square Error values for monthly temperature and precipitation (1979-2016) in the Gambia River watershed (Source: FAO analysis of EWEMBI dataset).*

Analysis: Historical trends

Considering the whole of the Gambia River watershed over the period 1979-2016, average annual precipitation has shown a non-significant increase of about 1 mm per year, while temperatures have increased on average 0.02 °C per year, or about 0.74 °C in total over the period (statistically significant at the 95 percent confidence interval) (see Figure C). This rate of warming is approximately 40 percent less than the average rate of temperature increase for Africa, which warmed at the rate of 0.028 C/yr over the same time period, or 1.06 °C total (NOAA, 2020). Geographically, temperatures have increased uniformly over the entire watershed, while precipitation has declined slightly in the central watershed, with slight increases seen in the upper reaches of the watershed, and along the coast (see Figure D).

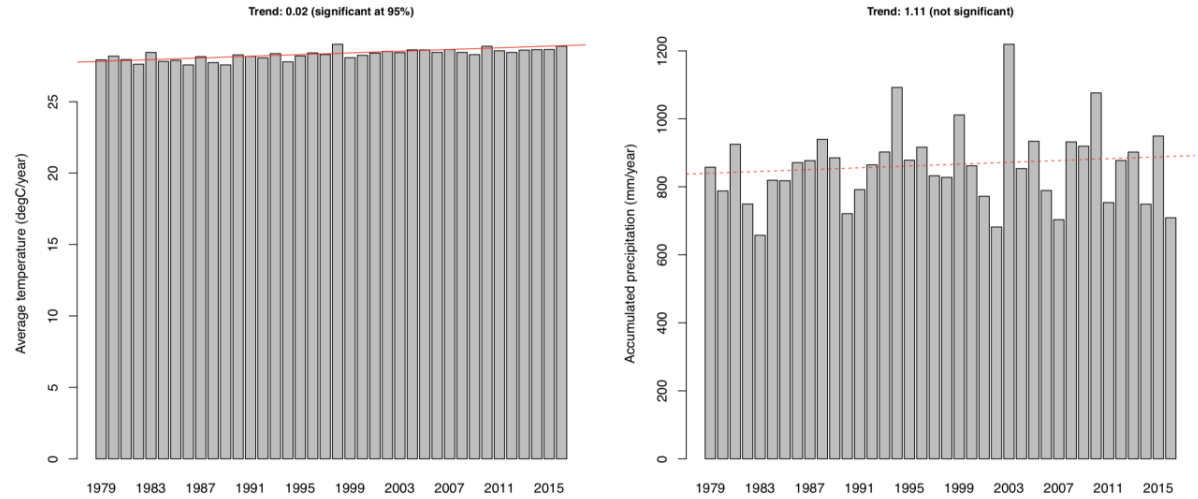

Figure C. *Annual changes in temperature and precipitation within the watershed, 1979-2016 (the solid line indicates a statistically significant trend)(Source: FAO analysis of EWEMBI dataset).*

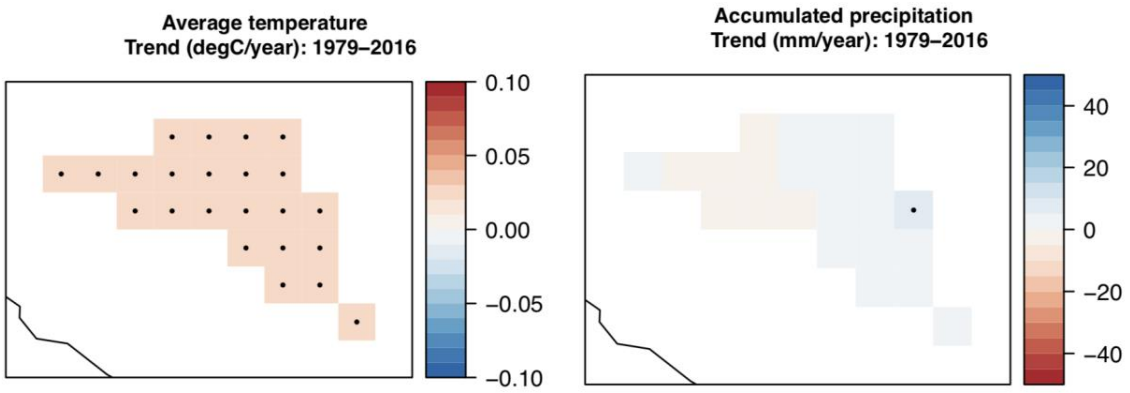

Figure D. *Average annual change in temperature and precipitation, 1979-2016 (grid cells with black dots indicate statistically significant trends)(Source: FAO analysis of EWEMBI dataset).*

When viewed at decadal time intervals between 1979 and 2016 (1979-1988; 1989-1998; 1999-2008; 2009-2016), the data show a strong evolution in spatial trends in both precipitation and temperature. As seen in Figure E, the general cooler and relatively wet decade of the 1980s is followed by consecutive decades of sustained warming and an initial shifting and subsequent decades of decline in precipitation. Of particular importance with regards to precipitation is the shift from increases in the 1979-1988/1989-1998 period, to declines in 1999-2008/2009-2016 period. The plans for the Sambangalou dam used historical rainfall patterns (1970 - 2001)(ISL, 2014) for modelling future hydrology of the watershed. The lower current and potential future rainfall may, therefore, lead not only to an under performance of the dam in generating hydroelectric power but also hold significant implications for the hydrologic dynamics and biological communities downstream within The Gambia (more details on this issue area presented in Chapter XX on saline intrusion).

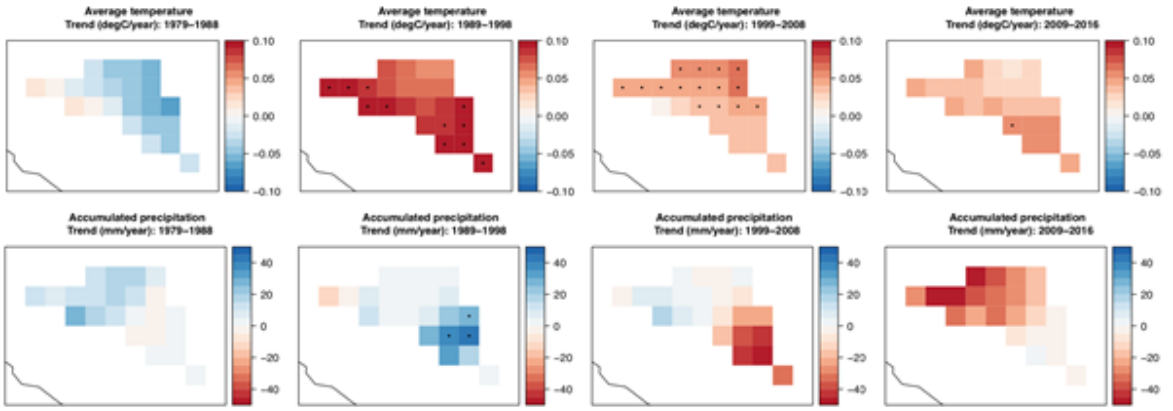

Figure E. *Decadal average temperature and rainfall within the Gambia River watershed (grid cells with black dots indicate statistically significant trends)(Source: FAO analysis of EMEMBI dataset).*

From a temporal perspective, Figure F shows a general increase in temperature and slight shifting in timing for precipitation by decade. The slight delay in onset of the rainy season and lengthening in

the peak rainfall period in the most recent decade (2009-2016), suggests a somewhat later, but longer wet season flood, delaying the entry of saline water into the upper reaches of the estuary.

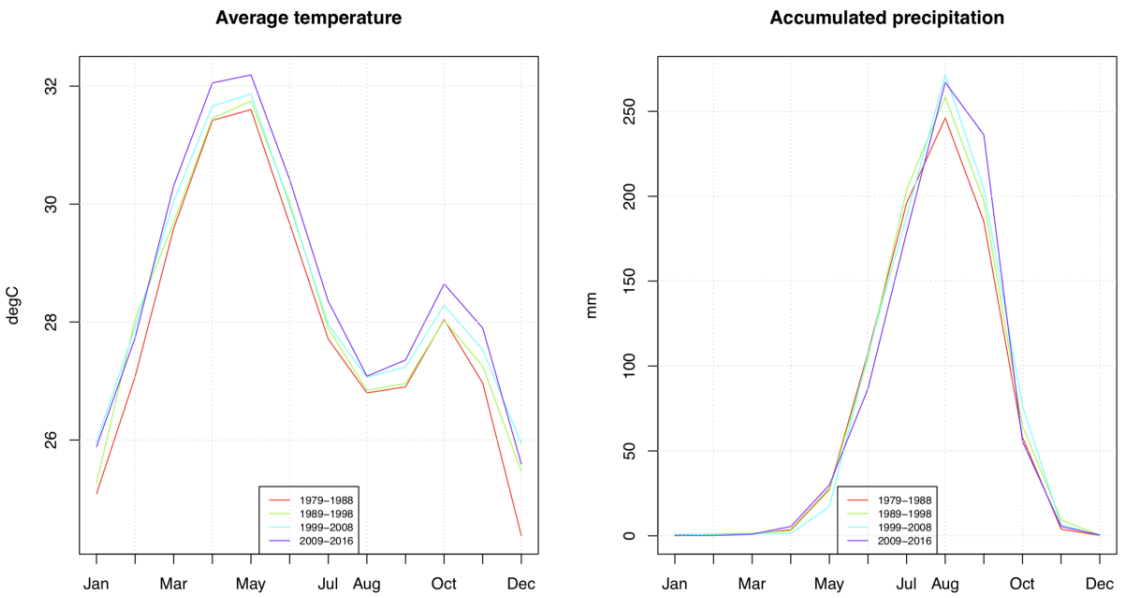

Figure F. *Decadal average monthly temperature and precipitation (1979-2016) in the Gambia River watershed (Source: FAO analysis of EWEMBI dataset).*

Analysis: Future projections

Each of the five GCMs were used to generate future downscaled temperature and precipitation projections for the watershed, reported here at three future time intervals, near (2011-2040), medium (2041-2070) and far (2071-2099) future. For this study, we include only references to projected impacts resulting from Representative Concentration Pathway (RCP) 8.5, a high emissions business as usual scenario resulting in 8.5 watts/m^2 of additional energy being retained within the earth's atmosphere. Projections under the more moderate emission scenarios, e.g., RCP 4.5, can be assumed to be similar in sign with possible modest variance in intensity, geographic and temporal distribution. The decision to use RCP 8.5 for projecting possible future climate is based on the metrics presented in Figure G.

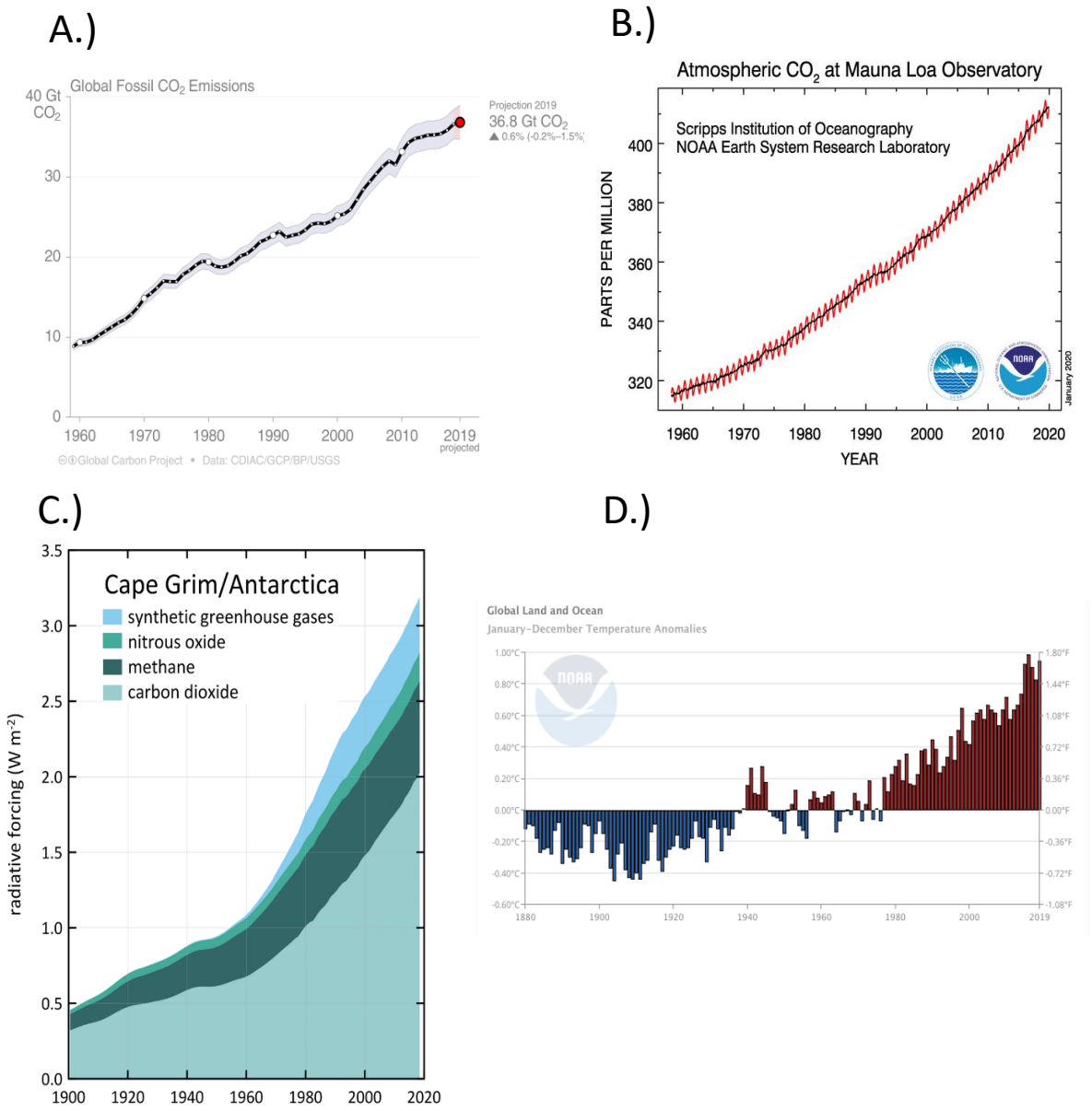

Figure G. *A.) Rates of emissions have continue to increase (Global Carbon Project, 2019); B.) Observed atmospheric concentrations of CO_2 continue to rise (NOAAa, 2020); C.) Radiative forcing of the global climate system, from all greenhouse gases, continues to rise (CISRO, 2019); D.) Global air and sea surface temperatures (SST) continue to rise – 2019 witnessed the second highest average global temperature, and the highest sea surface temperatures – the past five years are the hottest five years on record (air and sea surface temperatures), and the past decade the hottest decade ever recorded (air and sea surface temperatures)(NOAAb, 2020; Cheng, et al., 2020).*

Currently, global warming is at 1.1 C° above pre-industrial times (range among the five global datasets 1.05 – 1.2 C°) (WMO, 2020), and on-track for 2.3 – 4.7 C° of warming by 2060 (90 percent confidence

interval)(Sherwood et al., 2020). The voluntary nationally determined commitments to reduce greenhouse gas emissions under the Paris Agreement, if implement to 100 percent effectiveness, are assessed to allow global temperatures to rise to 2.8 – 3.5 C° by 2100 (Climate Action Tracker, 2019), consistent with an RCP8.5 trajectory. The vast majority of countries are assessed to be lagging behind in implementing their current national commitments (FEU-US and ACT, 2019). Evidence emerging from the new generation of global circulation models (CMIP6) being used in preparing the upcoming IPCC 6th assessment report suggest that climate sensitivity may have been seriously underestimated, by over 30 percent, with the potential warming equilibrium (and rate of warming) from a doubling of CO_2 over 2 degrees warmer than previously thought (e.g., Zelinka et al., 2020). In sum, based upon the evidence, there is currently no empirical basis for anticipating anything other than the projected impacts associated with an RCP 8.5 future. Should future progress be made in reducing greenhouse gas emissions, various projected impacts can be assumed to somewhat less, but consistent in sign, to those indicated in this study.

Below, Figure H shows the generally mixed projections for precipitation, with both mixed results between the models at each time interval, and within each model across the three periods. Only one model projects a consistent, through slight, declining trend in precipitation across all three time periods, while most models show a decline in precipitation in the medium and far future time periods. This divergence in model output is consistent with studies focusing on projected precipitation within the Sahelian zone, where models general split between those predicting precipitation increases and decreases (Giannini, 2016). Figure I, shows the various projected changes in the seasonal distribution of precipitation across the different time periods, with three models indicating an increasingly later start to the rainy season, and two showing a slight lengthening of the rainy period. Again, variance in model output and the seasonal shifting in precipitation is high, and is to be expected.

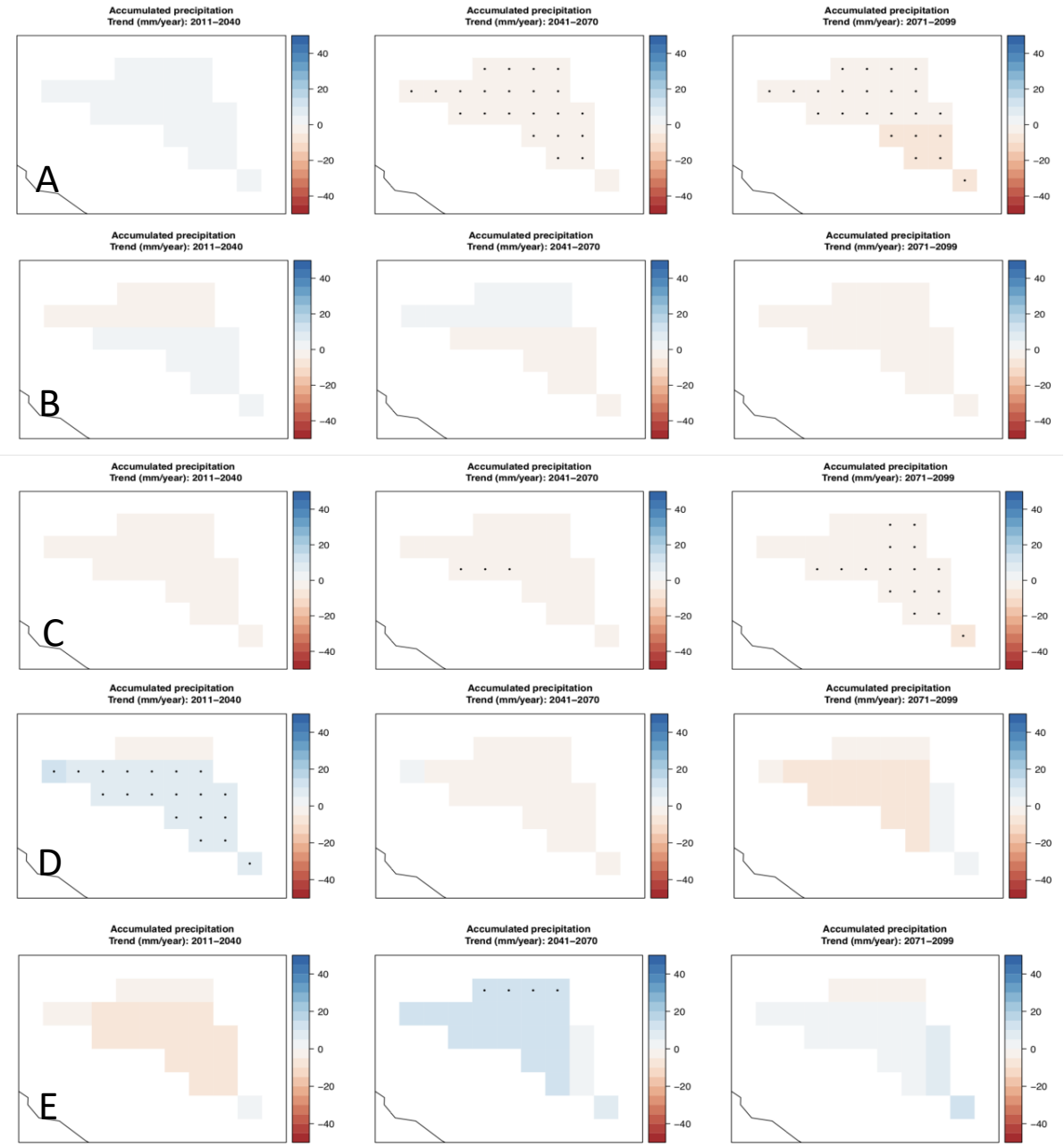

Figure H. *Projected geographic trend in precipitation for RCP 8.5 across three time periods (near (2011-2040), medium (2041-2070) and far (2071-2099) future) for five GCMs – (A) HADGEM2-ES; (B) NORESM1-M; (C) IPSL-CM5a; (D) MIROC-ESM; (E) GFDL-ESM2M)(grid cells with black dots indicate statistically significant trends)(Source: FAO analysis).*

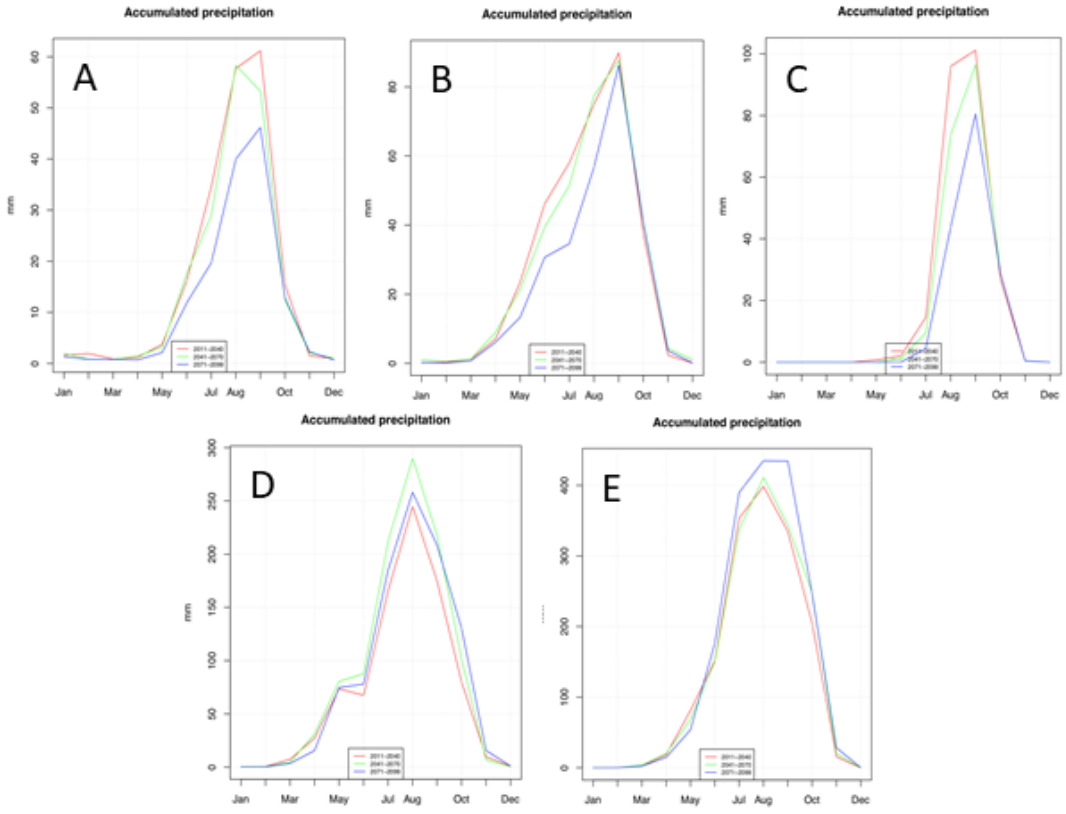

Figure I. *Projected trend in seasonal precipitation for RCP 8.5 across three time periods (near (2011-2040), medium (2041-2070) and far (2071-2099) future) for five GCMs – (A) HADGEM2-ES; (B) NORESM1-M; (C) IPSL-CM5a; (D) MIROC-ESM; (E) GFDL-ESM2M)(Source: FAO analysis).*

In contrast to the projected trends for precipitation, the trends for temperature change show a much higher degree of consistency across both the different models and time periods (Fig. J). All models, across all time periods, show a sustained upward trend in mean temperatures, consistent with what is known about the future of global climate change, with mean minimum temperatures rising at roughly twice the rate as mean maximum temperatures. The output from all models is statistically significant at a 95 percent confidence interval. There do not appear to be any important trends in terms of the temporal distribution of rising temperatures as shown in Figure K.

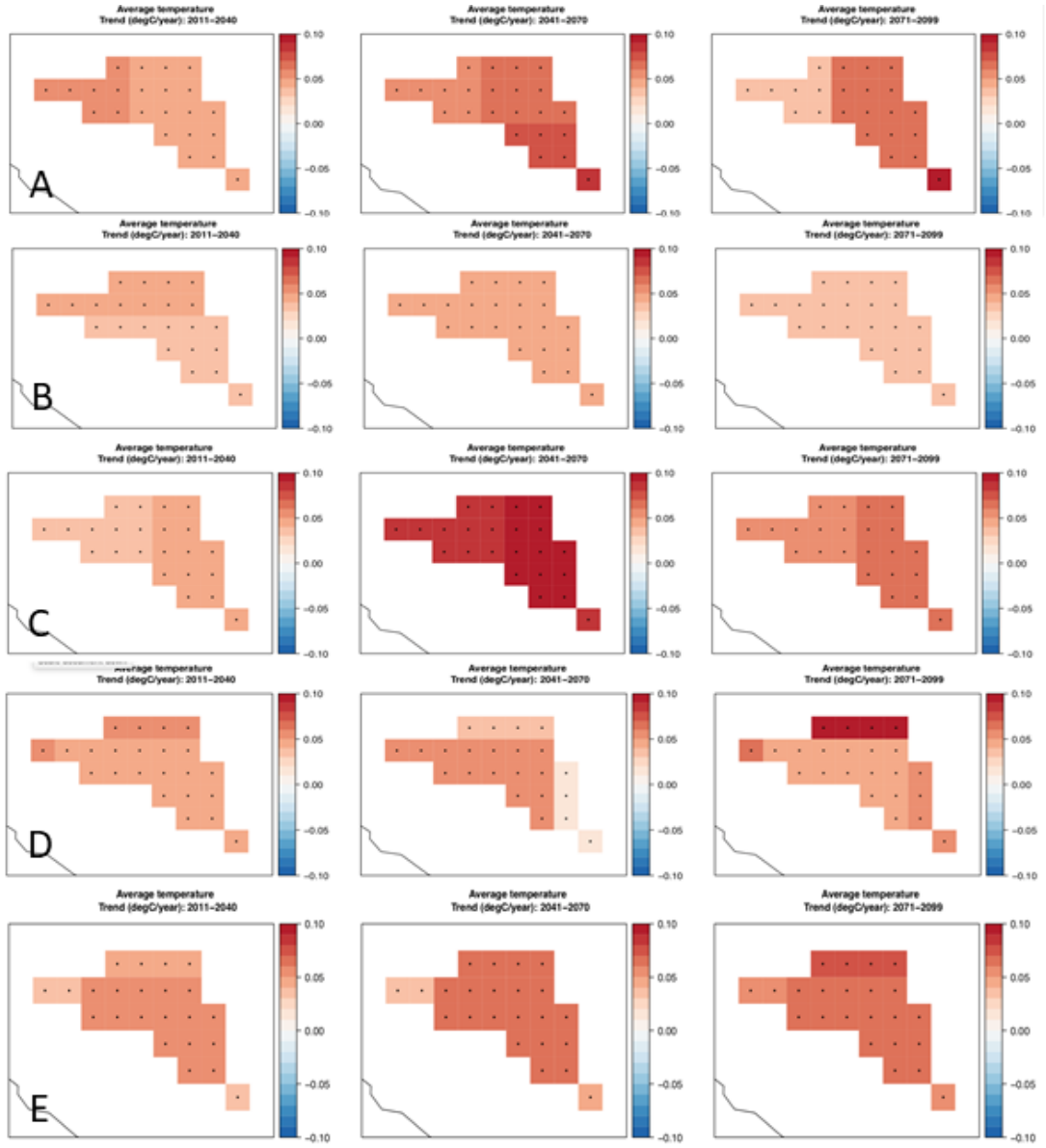

Figure J. *Projected geographic trend in temperature for RCP 8.5 across three time periods (near (2011-2040), medium (2041-2070) and far (2071-2099) future) for five GCMs – (A) HADGEM2-ES; (B) NORESM1-M; (C) IPSL-CM5a; (D) MIROC-ESM; (E) GFDL-ESM2M)(grid cells with black dots indicate statistically significant trends) (Source: FAO analysis).*

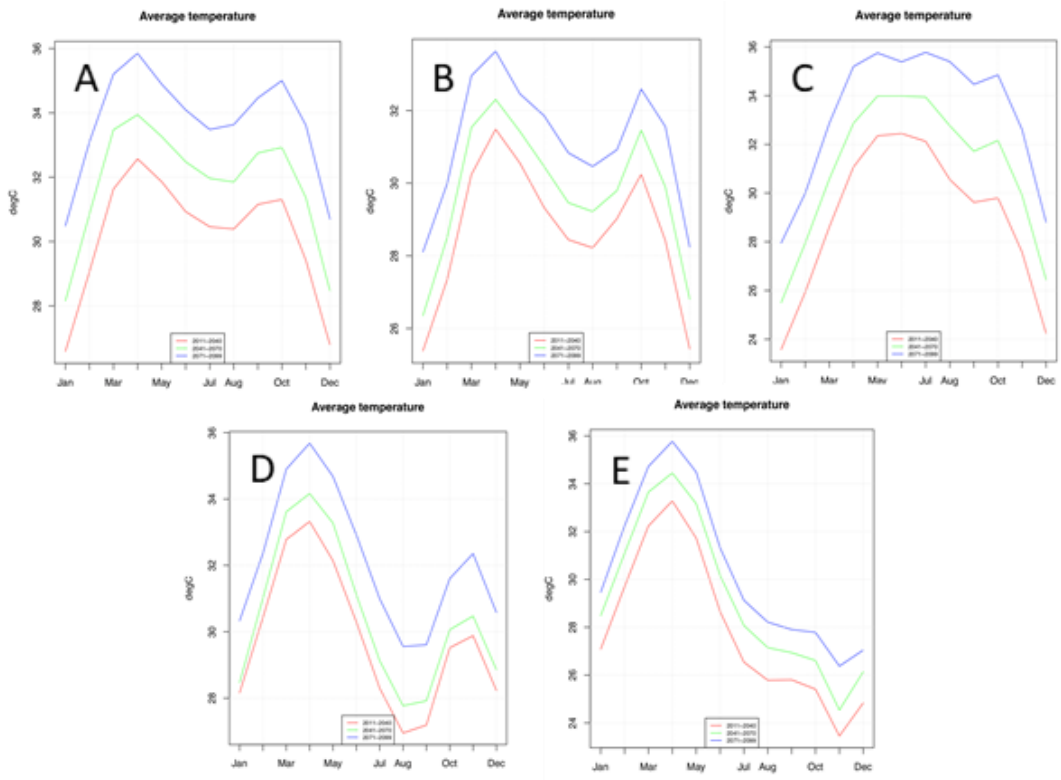

Figure K. *Projected trend in temperature for RCP 8.5 across three time periods (near (2011-2040), medium (2041-2070) and far (2071-2099) future) for five GCMs – (A) HADGEM2-ES; (B) NORESM1-M; (C) IPSL-CM5a; (D) MIROC-ESM; (E) GFDL-ESM2M)(Source: FAO analysis).*

Conclusions

Overall, across the model projections there is a mixed through general agreement in the potential of declines in future precipitation, albeit modest, towards the end of the century. Given the historical trend and virtual certainty of continued increases in temperature across all locations and time periods, resulting in greater rates of evaporation, one conclusion to be gained from this analysis is the likelihood of there being a decline in streamflow within the Gambia River in the decades ahead. Such a conclusion is consistent with a meta-analysis done on studies on river basin runoff in West Africa, which found that for the Gambia River basin future streamflow will likely decline by 4.5 percent (Roudier et al., 2014). Human activities that contribute to greater removal of water from the river (e.g., irrigation) and increased evaporation (e.g., from irrigated surfaces and dam reservoir), will accelerate the process of climate change driven moisture loss. For example, Gambia's National Water Management Strategy estimates a 7 percent reduction in stream flow in the Gambia River at Kedougou, immediately downstream from the Sambangalou dam under construction in Senegal, due to evaporation from the dam's reservoir (GoTG, 2015). This volume of moisture loss translates roughly into a 3.5 percent reduction in stream flow as the river enters The Gambia.[7]

From the perspective of ecological niches and the life cycle of individual species, the potential shifting in the seasonality (timing and length) of the annual flood/recession cycle, within a context of

[7] Stream flow in the Gambia River at Sambangalou has been measured as 48 percent of the volume at Gouloumbou, Senegal, 32 km upstream from where the river enters The Gambia (Oréade-Brèche and ISL Ingénierie, 2008).

declining overall streamflow, may have even greater effect. Such trends, when combined with the offtake of water for irrigation in the freshwater portions of the river, increased evaporation and further alterations in the flood cycle imposed by the water retention and release schedule of the Sambangalou dam, will greatly amplify the impacts of climate change alone (these issues are explored in greater detail in Chapters xx-xx – to be published).

References

Bentsen, M., et al. 2013. The Norwegian Earth System Model, NorESM1-M – Part 1: Description and basic evaluation of the physical climate, Geosci. Model Dev., 6, 687-720.

Bruyère C.L., et al. 2014. Bias corrections of global models for regional climate simulations of high-impact weather. Climate Dynamics 43(7-8):1847–1856.

Cheng, L., et al. 2020. Record-Setting Ocean Warmth Continued in 2019. Advances in Atmospheric Sciences Vol. 37: 137-142.

Climate Action Tracker. 2019. https://climateactiontracker.org/documents/698/CAT_2019-12-10_BriefingCOP25_WarmingProjectionsGlobalUpdate_Dec2019.pdf. (accessed 29/01/2020).

CSIRO (Commonwealth Scientific and Industrial Research Organization). 2019. https://blog.csiro.au/more-greenhouse-gas-in-atmosphere-than-you-may-have-realised/. (accessed 29/01/2020).

Dee, D.P., et al. 2011. The era-Interim Reanalysis: Configuration and performance of the data assimilation system. Quarterly Journal of the Royal Meteorological Society, 137(656, Part a), 553–597.

Dufresne, J., et al. 2013. Climate change projections using the IPSL-CM5 Earth System Model: from CMIP3 to CMIP5. Clim Dyn 40, 2123–2165.

Dunne, J.P., et al. 2012. GFDL's ESM2 global coupled climate–carbon Earth System Models. Part I: Physical formulation and baseline simulation characteristics. Journal of Climate 25:6646–6665.

Dutra, E. 2015. Report on the current state-of-the-art Water Resources Reanalysis. Deliverable 5.1 of the project Global Earth Observation for integrated water resource assessment (eartH2Observe). Available at https://earth2observe.eu/files/PublicDeliverables.

Frieler, K., et al. 2017. Assessing the impacts of 1.5oC global warming—Simulation protocol of the Inter- Sectoral Impact Model Intercomparison Project (ISIMIP2b). Geoscientific Model Development, 10(12), 4321–4345.

FEU-U and ACT (Fundación Ecológica Universal FEU-US and Acting on Climate Together). 2019. https://drive.google.com/file/d/1nFx8UKTyjEteYO87-x06mVEkTs6RSPBi/view. (accessed 29/01/2020).

Giannini, A. 2016. 40 Years of climate modelling: The causes of late-20th century drought in the Sahel. In: Behnke R. and Mortimore M. (eds.) The End of Desertification? Disputing Environmental Change in the Drylands. Springer Earth System Sciences. Berlin Heidelberg: Springer-Verlag.

Global Carbon Project. 2019. https://www.globalcarbonproject.org/carbonbudget/ (accessed 29/01/2020).

Government of The Gambia. 2015. National Water Resources Assessment and Management Strategy. Prepared by, NIRAS. Consulting Services for the National Water Sector Reforms Studies for The Gambia. Banjul: Ministry of Environment, Climate Change, Water Resources, Parks and Wildlife.

Gutiérrez, J.M., et al. 2019: An intercomparison of a large ensemble of statistical downscaling methods over Europe: Results from the VALUE perfect predictor cross-validation experiment. International Journal of Climatology, Vol. 39(9): 3750-3785.

Lange, S. 2018. Bias correction of surface downwelling longwave and shortwave radiation for the EWEMBI dataset. Earth System Dynamics, 9(2), 627–645.

Martin, G.M., et al. 2011. The HadGEM2 family of Met Office Unified Model climate configurations, Geosci. Model Dev., 4, 723–757.

NOAA (National Oceanic and Atmospheric Administration). 2020a. Mouna Loa CO_2 Record. https://www.esrl.noaa.gov/gmd/ccgg/trends/full.html. (accessed 29/01/2020).

NOAA (National Oceanic and Atmospheric Administration). 2020b. Global Land and Sea Surface Temperature Record. https://www.ncdc.noaa.gov/cag/global/time-series/globe/land_ocean/ytd/12/1880-2019. (accessed 29/01/2020).

Oréade-Brèche and ISL Ingénierie (ISL). 2014. Etude d'Impact Environnemental et Social du Projet Energie (Revue du rapport COTECO 2008). Mission d'Appui Conseil a l'OMVG pour la Realisation de son Projet Energie. Projet de Rapport Final. Dakar: OMVG.

Roudier, P., A. Ducharne and L. Feyen. 2014. Climate Change Impacts on Runoff in West Africa: A review. Hydrology and Earth System Sciences Vol. 18: 2789-2801.

Sherwood et al., 2020. An Assessment of Earth's Climate Sensitivity Using Multiple Lines of Evidence. Review of Geophysics doi: 10.1029/2019RG000678

Themessl, M.J., et al. 2012: Empirical-statistical downscaling and error correction of regional climate models and its impact on the climate change signal. Climatic Change 112(2):449–468.

Thornthwaite, C. W. (1948). "An approach toward a rational classification of climate". Geographical Review 38(1): 55–94.

Watanabe, S., et al. 2011. MIROC-ESM 2010: Model description and basic results of CMIP5-20c3m experiments. Geoscientific Model Development 4(4):845-872.

Weedon, G.P., et al. 2014. Watch forcing data methodology applied to ERA-Interim reanalysis data. Water Resources Research, 50, 7505–7514.

WMO, 2020. WMO Confirms 2019 as Second Hottest Year on Record. https://public.wmo.int/en/media/press-release/wmo-confirms-2019-second-hottest-year-record. (accessed 29/01/2020).

Zelinka, M.D., A.M. Myers, D.T. McCoy, S. Po-Ghedley, P.M. Cadwell, P. Ceppi, S.A. Klein and E. Taylor. 2020. Causes of Higher Climate Sensitivity in CMIP6 Models. Geophysical Research Letters Vol. 47(1).

B NUMERICAL SOLUTION OF THE UNSTEADY STATE EQUATION

This appendix is almost an exact copy from the dissertation of Savenije (1992), however formulas B.8 to B.13 are slightly adjusted. The adjustments have been made by H.H.G. Savenije after a discussion with prof. Stelling.

B.1 can be solved numerically by using a six-point implicit finite differences scheme as proposed by Fischer et al. (2013). Therefore, B.1 is written in the following format:

$$\frac{\Delta s}{\Delta t} + q\frac{\Delta s}{\Delta x} - D\frac{\Delta^2 s}{\Delta x^2} + \frac{r}{h_0}s = 0 \tag{B.1}$$

where:

$$q = (1-K)\frac{Q_r - Brb}{A} + \frac{D}{a} \tag{B.2}$$

The six-point implicit finite differences scheme is shown in figure B.1. The known salinities at three consecutive grid points in space, at time t_0, are: s_1, s_2 and s_3. The unknown salinities at the same grid points, at time $t_1 = t_0 + \Delta t$, are s_4, s_5, and s_6. THe distance between two consecutive grid points is Δx.

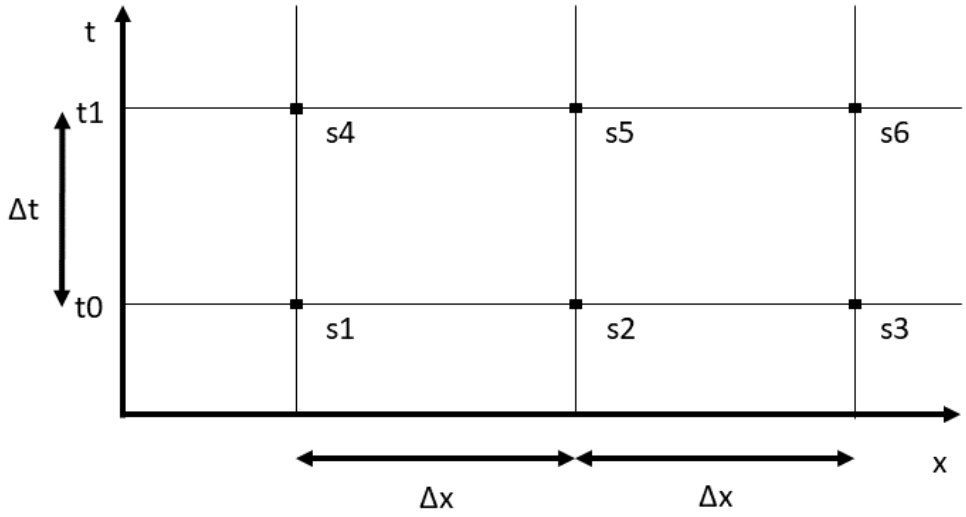

Figure B.1: Six-point implicit finite differences scheme

The operators are defined by:

$$\frac{\Delta s}{\Delta t} = \frac{1}{6\Delta t}(s_4 - s_1 + 4s_5 - 4s_2 + s_6 - s_3) \tag{B.3}$$

$$\frac{\Delta s}{\Delta x} = \frac{1}{4\Delta x}(s_6 - s_4 + s_3 - s_1) \tag{B.4}$$

$$\frac{\Delta^2 s}{\Delta x^2} = \frac{1}{2\Delta x^2}(s_6 - 2s_5 + s_4 + s_3 - 2s_2 + s_1) \tag{B.5}$$

$$s = \frac{1}{12}(s_1 + 4s_2 + s_3 + s_4 + 4s_5 + s_6) \tag{B.6}$$

For every grid point i between the boundary conditions, B.1 - B.6 can be combined into an equation where the known parameters are on the right hand side and the unknown on the left hand side:

$$s_4 a_i + s_5 b_i + s_6 c_i = s_1 d_i + s_2 e_i + s_3 f_i \tag{B.7}$$

with the following x-dependent coefficients:

$$a_i = \frac{1}{6\Delta t} - \frac{D}{2\Delta x^2} - \frac{q}{4\Delta x} \tag{B.8}$$

$$b_i = \frac{2}{3\Delta t} - \frac{D}{\Delta x^2} - \frac{E}{h_0} \tag{B.9}$$

$$c_i = \frac{1}{6\Delta t} - \frac{D}{2\Delta x^2} + \frac{q}{4\Delta x} \tag{B.10}$$

$$d_i = \frac{1}{6\Delta t} + \frac{D}{2\Delta x^2} + \frac{q}{4\Delta x} \tag{B.11}$$

$$e_i = \frac{2}{3\Delta t} - \frac{D}{\Delta x^2} \tag{B.12}$$

$$f_i = \frac{1}{6\Delta t} + \frac{D}{2\Delta x^2} - \frac{q}{4\Delta x} \tag{B.13}$$

The x-dependent coefficients are determined at the start of each time step. Hence, at all but two grid points, each B.7 has three unknowns: s_4, s_5 and s_6. At the two grid points bordering the boundaries of the model, the ocean boundary and the river boundary, the values of s_4 and s_6 are known, the ocean salinity S_0 and river salinity S_f, respectively. Hence B.7 has only two unknowns at the grid points next to the model boundaries.

If there are n grid points between the boundaries, then there are n equations with n unknowns for each time step. The n B.7 can be written in Matrix notation:

$$M \cdot \bar{S} = \bar{K} \tag{B.14}$$

where M is an n by n matrix linking the vector of salinities $\bar{S}$ in the n grid points to the vector $\bar{K}$ of n known right hand sides of B.7. The matrix has only three diagonals consisting of the coefficients a_i, b_i, and c_i; such a matrix is called a tri-diagonal matrix. The system can be readily solved by a Gaussian elimination method, through a "double sweep" method (Carnahan & Wilkes, 1973). In this method, first ocean salinity is substituted in s_4, after which, during the first sweep - in upstream direction - , through consecutive substitutions, s_4 is eliminated from the n equations. In the last equation, the fresh water salinity is substituted in s_6, after which s_5, the salinity in the

grid point bordering the upstream boundary, is obtained. During the second sweep - in downstream direction -, the system is solved by consecutive substitution of the known salinity in s_6.

For the initial salinity distribution required to start up the model, the steady state salinity distribution is used. Hence, the model should run for some time to eliminate the start-up errors.

C DISCHARGE MODEL

For each region in the catchment area (Kedougou and Goudiry), the model approaches the contribution to river flow as follows. When it rains, a certain threshold volume of water needs to be exceeded before the precipitation is contributing to the flow in the river. Depending on the amount of water intercepted by leaves, types of vegetation, types of soil, moisture content in the soil etc. several flows to the river arise. These flows have again a clear distinction. Subsurface flows and groundwater flows are much slower than overland flow but continue for a longer time. To mimic all these hydrological effects and account for the several timescales the model works with a threshold volume that incorporates all resistances before the precipitation reaches the river. Furthermore, multiple timesteps are applied to ensure that groundwater flows are represented well.

The scipy.optimize.minimize function is used to optimize the factors that determine the contribution for each timestep for each region by minimizing the error (formula C.1). The error is the difference between the predicted amount of flow and the measured flow in Gouloumbou. For each timestep and for each region a c is given by the optimization. Since negative flow cannot occur the first negative c determines the number of months that contribute to river flow. This is four months.

$$Error = \sum c_{ij} \cdot P_{ij} - m \tag{C.1}$$

Variable	Character	Dimensions
Weight per timestep	c	-
Precipitation	P	L/T
Time	l	T
Region		j
Measurement of flow	m	L^3/T

Table C.1: Scipy optimization minimize variables

Another complication is the hydropower dam. Part of the generated flow around Kedougou contributes to filling the reservoir behind it and part of it directly feeds into the Gambia river. In personal contact with the FAO it has been shared that half of the flow measured in Gouloumbou is generated in the region which feeds into the reservoir of the hydropower dam. To determine the ideal ratio between the areas around Kedougou and the threshold values for the two regions, an iterative process in excel that maximizes the

R squared value between the measured and predicted flow follows. This process consists of interchangeably changing the threshold values for each region or changing the ratio of contribution, this is done manually. The reason for doing this labor-intensive job manually is simply because perfect solutions are not necessarily the most realistic. Equifinality, the possibility of having multiple best scenarios with different parameter combinations, occurs when having more parameters to optimize than measurements to verify with. The optimization leads to the results presented in table y which meet the flow requirements. The model achieves an R squared value of 86%. The prediction of flow is based on precipitation of previous months and is calculated by following formula C.2. The separation of the flow near Kedougou is calculated with formula C.3.

$$Q = \sum (P - T)_{t_i, r_j} \cdot C_{t_i, r_j} \tag{C.2}$$

$$Q_{river} = (\sum (P - T)_{t_i} \cdot C_{t_i}) \cdot \alpha \tag{C.3}$$

Variable	Character	Dimensions
Discharge	Q	L^3/T
Threshold volume	T	L/T
Ratio of flow generated near Kedougou contributing directly to riverflow	α	-

Table C.2: Variables for equations C.2 and C.3

Variable	Result
Threshold value of Kedougou	60 mm/month
Threshold value Goudiry	55 mm/month
α	26%

Table C.3: Variables for equations C.2 and C.3

D HYDROPOWER DAM OPERATIONAL SCHEMES

Two operational schemes for the hydropower dam have been created. The limited information about the dam lead to some assumptions. This Annex will start with how the reservoir has been modelled and the assumptions made for it. Afterwards both operational schemes are explained in detail. The table containing reservoir and dam characteristics is presented in table D.1.

Characteristics	**Minimum**	**Maximum**
Water level inside reservoir	118 m	200 m
Surface area reservoir	110 km^2	181 km^2
Volume reservoir	2.1 billion m^3	3.8 billion m^3
Useful capacity	-	1.7 billion m^3
Turbine discharge	0 m^3/s	200 m^3/s
Turbine height	75 m	

Table D.1: Reservoir and dam characteristics

D.1 RESERVOIR MODELLING

To know the water level inside the reservoir a relation between the volume and water level needs to be established. The first assumption is that the volume takes the shape of a frustum of a cone between the minimum and maximum water level. Below the minimum water level, a simple cone shape determines the water level to volume relation see figure D.1. The volume present in the reservoir is calculated via a volume balance according to D.1.

$$V_1 = V_0 + (Q_{in} - Q_{out}) \cdot t - E \cdot A \cdot t \tag{D.1}$$

Variable	**Character**	**Dimensions**
Volume	V	L^3
Discharge	Q	L^3/T
Timestep	t	t
Evaporation	E	L/t
Surface area	A	L^2

Table D.2: Variables for equation D.1

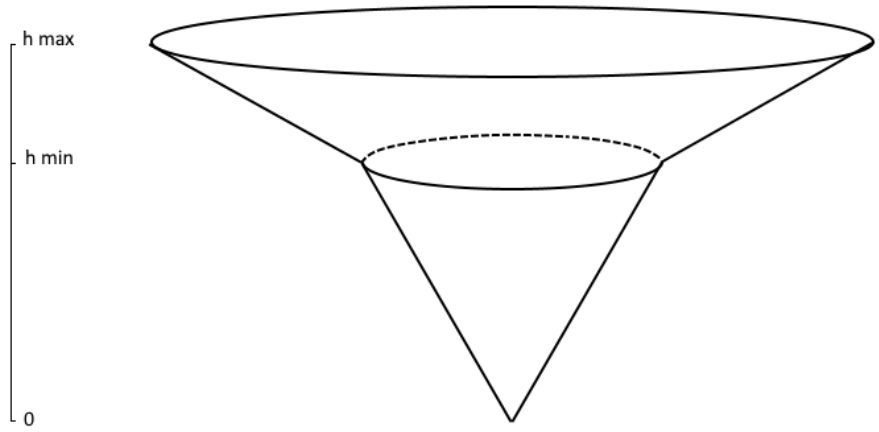

Figure D.1: Frustum of a cone: simple approximation of the reservoir shape

$$V = \frac{1}{3}\pi h \left(r_{max}^2 + r_{max} r_{min} + r_{min}^2\right) \tag{D.2}$$

Variable	Character	Dimensions
Water level	h	L
Radius	r	L

Table D.3: Variables for equation D.2

If here the minimum radius is set equal to zero the volume of a cone is calculated. If r_{max} is subsequently calculated from the minimum operational surface area of the reservoir, this can be rewritten to read.

$$V - V_{min} < 0 \begin{cases} h = \frac{3 \cdot V}{\pi \cdot r_{min}^2} \\ r = \frac{r_{min}}{h_{min}} \cdot h \end{cases} \tag{D.3}$$

For the upper part of the reservoir first formula Y is rewritten such that

$$V = \frac{h}{F_1} \tag{D.4}$$

$$F_1 = \frac{3}{\pi \left(r_{max}^2 \cdot r_{max} r_{min} \cdot r_{min}^2\right)} \tag{D.5}$$

The height of the water level in the reservoir behaves as follows

$$h_t = \Delta h + h_{t-1} = (V_t - h_{t-1}) \cdot F_2 + r_{t-1} \tag{D.6}$$

$$F2 = \frac{r_{max} - r_{min}}{h_{max} - h_{min}} \tag{D.7}$$

$$V - V_{min} \geq 0 \begin{cases} h = (V - V_0) \cdot F_1 + h_{min} \\ r = (h - h_{min}) \cdot F_2 + r_{min} \end{cases} \tag{D.8}$$

Finally, the surface area is calculated for a circle. This results in the same characteristics as in table D.1.

D.2 DAM OPERATIONAL SCHEME A: ECOLOGY FOCUSED FLOW

Dam operational scheme A, ecology focused flow, is based on the environmental study (OMVG, 2014). In this study a basic flow scheme is shown, presented in table D.4. The table contents are open for interpretation, it is not clear when certain discharge turbines are exactly reached. Therefore, the percentages in the annual distribution of production flows have been applied to the water level in the reservoir, which results in increasing discharge when the reservoir level increases. The relations between discharge and reservoir level are presented below in table D.5.

Discharge turbine	**Annual distribution of production flows**	**Comments**
200 m^3/s	8% of the time	Continuously during the wet months of periods of high inputs (such as the years 1954 – 1978 and 1994-2001)
Intermediate flow rates between 64 - 200 m^3/s	8% of the time	
Flow rates close to 60 m^3/s (between 54 - 64 m^3/s)	80% of the time	Continuous supply of guaranteed power, with fluctuations around this average value according to the requirements of the network in certain years, and according to the filling state of the reservoir at the end of the rainy season.
Flow rates between 60 m^3/s and almost zero	4% of the time	In episodes of extreme drought

Table D.4: Translated table from the OMVG study in 2014 with approximate flow characteristics through the hydropower dam

Water level reservoir	**Discharge** $[m^3/s]$
$h \geq h_{max} - 0.08 \cdot \Delta h$	200
$h \geq h_{max} - 0.16 \cdot \Delta h$	$141.666 \cdot h - 27997.3$
$h \geq h_{max} - 0.96 \cdot \Delta h$	$1.0417 \cdot h - 142.333$
$h \geq h_{max} - 1.00 \cdot \Delta h$	$112.5 \cdot h - 21150$
$h < h_{min}$	0

Table D.5: Relations between discharge and reservoir level

It should be noted that in the case of a water level higher than h_{max} the water will be spilled on top of the discharge of 200 m^3/s.

D.3 DAM OPERATIONAL SCHEME B: POWER PRODUCTION FOCUSED

The power production focused flow scheme is based on the maximization of power production (formula D.9). It should be noted that this operational scheme is created for a single scenario in which it was optimized and used on all scenarios that were run with this type of operations. A lower boundary was set by the FAO for ecological minimum flow. This implies that the flow is not allowed to be less than the minimum flow of 18 m^3/s (OMVG & EIES, 2014). Furthermore, the goal is to produce power as constant as possible which increases the reliability of the power grid. To do this the power production is split with the wet and dry season. During the dry season the reservoir slowly drains with a constant discharge while during the wet season the reservoir is filled again.

$$Q_t = \frac{Power}{\rho \cdot g \cdot \Delta h \cdot \eta} \tag{D.9}$$

Variable	Character	Dimensions
Discharge through the turbine	Q_t	L^3/T
Power of the turbine	Power	Watt
Distance between reservoir water level and turbine	Δh	L
Efficiency	η	-

Table D.6: Variables for equation D.9

The maximization of power production has been done manually, which does not guarantee the perfect discharge settings. Nonetheless, the difference between the two different operational schemes show a significant change. The final results for power focused operations lead to the following turbine powers. During the wet season turbines can operate on average with 100 MW while during the wet season turbines operate at 30 MW. It should be noted that the minimum flow condition of 18 m^3/s is always met except for some scenarios in which the reservoir water level reduces too fast (e.g. due to evaporation). In such a moment the reservoir stops flow to retain water. This is because the power production was maximized without some safety factor to ensure such situations do not occur.

A rough estimate of the yearly produced power with these settings would be around 460 GWh, which is higher than the estimates in the environmental flow study.

$$Dryseason : Power \cdot time \approx 30 \cdot 8 \cdot 30 \cdot 24 = 172.8GWh \tag{D.10}$$

$$Wetseason : Power \cdot time \approx 100 \cdot 4 \cdot 30 \cdot 24 = 228GWh \tag{D.11}$$

It is important to realize that the above settings were chosen to show another extreme. For power production a smaller power production ensures that water will always flow according to minimum flow requirements.

E MODEL SCENARIOS

Table E.1 displays an overview of all model scenarios.

Scenario ID:	Sea level rise:	Future weather:	Dam operations	Irrigation development:	Comment:
H	0 m	Historical	No dam	Current	
0.0	0 m	RCP 8.5	No dam	Current	
0.1	0 m	RCP 4.5	No dam	Current	
0.2	0 m	RCP 8.5	No dam	Expected	
1.0	0 m	RCP 8.5	Dam reservoir filling	Expected	2024
1.1	0 m	RCP 8.5	Dam reservoir filling	Expected	2024-2025
2.0	2 m	RCP 8.5	No dam	Current	
2.1	2 m	RCP 8.5	A	Current	
2.2	2 m	RCP 8.5	B	Current	
3.0	0.84 m	RCP 4.5	No dam	Current	
3.1	0.84 m	RCP 8.5	No dam	Current	
3.2	0.84 m	RCP 4.5	A	Current	
3.3	0.84 m	RCP 4.5	B	Current	
3.4	0.84 m	RCP 8.5	A	Current	
3.5	0.84 m	RCP 8.5	B	Current	
4.0	0.84 m	RCP 4.5	A	Expected	
4.1	0.84 m	RCP 4.5	B	Expected	
4.2	0.84 m	RCP 4.5	A	Max	
4.3	0.84 m	RCP 4.5	B	Max	
4.4	0.84 m	RCP 8.5	A	Expected	
4.5	0.84 m	RCP 8.5	B	Expected	
4.6	0.84 m	RCP 8.5	A	Max	
4.7	0.84 m	RCP 8.5	B	Max	
4.8	2 m	RCP 8.5	No dam	Expected	
4.9	2 m	RCP 8.5	No dam	Max	
4.1	2 m	RCP 8.5	A	Expected	
4.11	2 m	RCP 8.5	B	Expected	
4.12	2 m	RCP 8.5	A	Max	
4.13	2 m	RCP 8.5	B	Max	

Table E.1: Overview of all scenarios

F MODEL RESULTS

Table F.2 gives an overview of the model results.

scenario ID	Period:	SLR	FW	DO	ID	CFD-curve				Monthly median min/max				S-x curve	
						F1 [km]	F2 [km]	F3 [-]	F4 [-]	F5 [km]	F6 [km]	F7 [Mos]	F8 [Mos]	F9 [km]	F10 [g/L]
H	1971-2017	0	N/A	N/A	Current	92	316	-0.74	-0.41	124	272	9	6	72	35.6
0.0	2006-2039	0	RCP 8.5	No dam	Current	104	316	-0.88	-0.42	120	274	10	6	92	36
	2040-2069					92	336	-0.79	-0.37	110	282	10	6	128	36.8
	2070-2099					100	368	-0.87	-0.30	114	308	10	6	168	38.3
0.1	2006-2039	0	RCP 4.5	No dam	Current	104	314	-0.94	-0.41	124	280	10	6	98	36.1
	2040-2069					96	308	-0.83	-0.39	112	278	10	6	92	36
	2070-2099					96	328	-0.78	-0.33	110	298	10	6	124	36.6
2.0	2006-2039	2	RCP 8.5	No dam	Current	106	316	-0.84	-0.43	124	276	10	6	86	35.9
	2040-2069					98	452	-0.68	-0.27	128	322	10	6	240	37.7
	2070-2099					122	578	-0.57	-0.18	152	480	11	6	476	62.2
2.1	2006-2039	2	RCP 8.5	A	Current	120	258	-1.07	-1.00	136	206	10	7	50	35.4
	2040-2069					114	344	-1.00	-0.50	138	238	10	6	140	36.4
	2070-2099					134	430	-0.57	-0.22	164	404	11	6	394	54.9
2.2	2006-2039	2	RCP 8.5	B	Current	114	322	-1.16	-0.39	130	282	10	7	86	35.7
	2040-2069					110	454	-1.07	-0.30	134	278	10	7	254	37.8
	2070-2099					134	572	-0.67	-0.17	158	452	11	6	468	59.5
3.0	2006-2039	0.84	RCP 4.5	No dam	Current	108	314	-0.94	-0.41	126	280	10	6	96	36
	2040-2069					100	308	-0.83	-0.41	116	278	10	6	90	35.9
	2070-2099					100	326	-0.78	-0.34	116	298	10	6	116	36.4
3.1	2006-2039	0.84	RCP 8.5	No dam	Current	106	316	-0.84	-0.42	122	276	10	6	90	35.9
	2040-2069					96	336	-0.79	-0.38	114	284	10	6	122	36.6
	2070-2099					104	366	-0.82	-0.31	120	310	10	6	156	37.4
3.2	2006-2039	0.84	RCP 4.5	A	Current	118	258	-1.25	-1.00	140	202	11	7	60	35.6
	2040-2069					112	220	-1.00	-1.00	128	202	10	6	54	35.5
	2070-2099					108	242	-0.98	-0.74	126	216	10	6	74	35.8
3.3	2006-2039	0.84	RCP 4.5	B	Current	116	322	-1.00	-0.39	134	284	10	7	100	36.1
	2040-2069					108	316	-1.00	-0.37	122	264	10	6	86	35.8
	2070-2099					108	328	-1.05	-0.30	122	288	10	6	114	36.4
3.4	2006-2039	0.84	RCP 8.5	A	Current	118	258	-1.07	-1.00	134	202	10	7	52	35.4
	2040-2069					108	242	-0.94	-0.94	124	204	10	6	74	35.9
	2070-2099					112	262	-1.05	-0.59	130	232	11	6	102	36.6
3.5	2006-2039	0.84	RCP 8.5	B	Current	114	322	-1.07	-0.39	128	282	10	7	88	35.7
	2040-2069					106	338	-1.07	-0.31	120	262	10	6	124	36.7
	2070-2099					112	360	-1.05	-0.28	126	282	10	7	158	37.4

4.0	2006-2039	0.84	RCP 4.5	A	Expected	118	258	-1.25	-1.00	142	204	10	7	62	35.6
	2040-2069					112	222	-1.00	-0.94	128	204	10	6	56	35.5
	2070-2099					108	242	-0.98	-0.70	126	218	10	6	74	35.8
4.1	2006-2039	0.84	RCP 4.5	B	Expected	116	330	-1.00	-0.39	134	286	10	7	104	36.2
	2040-2069					108	324	-1.00	-0.36	122	266	10	6	88	35.9
	2070-2099					108	334	-0.98	-0.30	122	288	10	6	118	36.4
4.2	2006-2039	0.84	RCP 4.5	A	Max	118	270	-1.25	-0.94	142	208	11	7	66	35.7
	2040-2069					114	228	-1.00	-0.94	128	210	10	6	60	35.5
	2070-2099					108	250	-1.05	-0.67	126	226	10	6	78	35.9
4.3	2006-2039	0.84	RCP 4.5	B	Max	116	354	-0.94	-0.37	134	294	11	7	114	36.3
	2040-2069					108	352	-1.00	-0.33	124	278	10	6	100	36.1
	2070-2099					108	350	-0.98	-0.27	122	300	10	6	124	36.5
4.4	2006-2039	0.84	RCP 8.5	A	Expected	118	258	-1.07	-1.00	134	204	10	7	52	35.4
	2040-2069					108	244	-0.94	-0.88	124	206	10	6	76	35.9
	2070-2099					112	264	-1.14	-0.59	130	234	11	6	102	36.7
4.5	2006-2039	0.84	RCP 8.5	B	Expected	114	328	-1.07	-0.39	128	282	10	7	92	35.8
	2040-2069					106	342	-1.00	-0.30	120	264	10	6	128	36.7
	2070-2099					112	366	-1.05	-0.28	126	286	10	7	162	37.5
4.6	2006-2039	0.84	RCP 8.5	A	Max	120	258	-1.07	-0.88	136	208	10	7	56	35.5
	2040-2069					110	250	-0.94	-0.79	124	212	10	6	80	36
	2070-2099					112	272	-1.05	-0.57	132	242	11	6	108	36.8
4.7	2006-2039	0.84	RCP 8.5	B	Max	114	352	-1.00	-0.37	128	284	10	7	104	35.9
	2040-2069					106	360	-1.00	-0.28	120	274	10	6	138	36.9
	2070-2099					112	388	-0.98	-0.26	128	296	10	7	176	37.7
4.8	2006-2039	2	RCP 8.5	No dam	Expected	106	320	-0.84	-0.42	124	278	10	6	90	35.9
	2040-2069					98	456	-0.71	-0.27	128	326	10	6	242	37.7
	2070-2099					122	584	-0.55	-0.17	152	486	11	6	480	62.8
4.9	2006-2039	2	RCP 8.5	No dam	Max	106	342	-0.88	-0.41	124	280	10	6	98	35.9
	2040-2069					98	474	-0.71	-0.25	128	344	10	6	266	38.1
	2070-2099					122	602	-0.53	-0.17	154	504	11	6	496	64.5
4.10	2006-2039	2	RCP 8.5	A	Expected	120	258	-1.07	-1.00	136	206	10	7	52	35.4
	2040-2069					114	346	-0.94	-0.48	138	240	10	6	144	36.4
	2070-2099					134	430	-0.59	-0.22	164	406	11	6	394	55.2
4.11	2006-2039	2	RCP 8.5	B	Expected	116	328	-1.07	-0.39	130	282	10	7	88	35.7
	2040-2069					110	460	-1.00	-0.29	134	280	10	6	262	38
	2070-2099					134	578	-0.70	-0.17	158	454	11	6	474	60
4.12	2006-2039	2	RCP 8.5	A	Max	122	258	-1.07	-0.88	110	208	10	7	54	35.4
	2040-2069					114	354	-0.94	-0.45	140	244	10	6	154	36.6
	2070-2099					134	438	-0.55	-0.22	166	412	11	6	396	56
4.13	2006-2039	2	RCP 8.5	B	Max	116	352	-1.00	-0.38	132	284	10	7	100	35.9
	2040-2069					110	484	-0.94	-0.26	136	294	10	6	294	38.5
	2070-2099					134	596	-0.64	-0.16	158	468	11	6	486	61.5

Table F.1: Overview of model results

Scenario ID:			CFD-curve				Monthly median	
	Period:	ID	F1 [km]	F2 [km]	F3 [-]	F4 [-]	F5 [km]	F6 [km]
H	1971-2017	N/A	92	316	-0.41	-0.74	124	272
0	2006-2039	Current	104	316	-0.42	-0.88	120	274
1	2006-2039 [2024]	Expected	104	314	-0.42	-0.92	132	295
1.1	2006-2039 [2024-2025]	Expected	104	324	-0.41	-0.92	132	295

Table F.2: Overview of reservoir filling scenario results